THE UNIVERSITY OF CHICAGO

SPATIOTEMPORAL DYNAMICS OF LARGE-SCALE BRAIN ACTIVITY

A DISSERTATION SUBMITTED TO
THE FACULTY OF THE DIVISION OF THE PHYSICAL SCIENCES
IN CANDIDACY FOR THE DEGREE OF
DOCTOR OF PHILOSOPHY

DEPARTMENT OF PHYSICS

BY
JEREMY NEUMAN

CHICAGO, ILLINOIS
DECEMBER 2015

To my parents, who have always believed in me

"Somewhere, something incredible is waiting to be known."

-Carl Sagan

TABLE OF CONTENTS

LIST OF FIGURES

ACKNOWLEDGMENTS

Like most worthwhile endeavors in life, finishing graduate school has been a long, arduous task which could not have been accomplished without the help of others. It would be nearly impossible to acknowledge everyone that has contributed or guided me along my path to obtaining a Ph.D. but I would like to mention some of them here.

First and foremost, I owe an unbelievable amount of gratitude to my advisors, Jack D. Cowan and Wim van Drongelen. Each one has provided me with a different perspective on neuroscience and the scientific community as a whole. Jack, as a pure theorist, has implanted in my head the necessity for understanding every problem from first principles. He has challenged me to think deeply into the concepts underlying neural networks and ignore the fluff that does not assist us in understanding the task(s) at hand. Wim, as a biophysicist by training, has also directed me to think about what is really going on in the brain but from a more applied perspective, which is vital in its own way. I would have little to no understanding of experimental techniques and data analysis in neuroscience, or epilepsy without him. Simply put, I am forever grateful that, together, both of my advisors have taught me so much about the career of a scientist as well as lessons that span many other aspects of life.

Next, I would like to thank all of my fellow graduate students in the Physics department at the University of Chicago and Wim's lab who have bounced ideas off me ranging from as diverse of areas as string theory, condensed matter physics, neuroscience, mathematics, and computer science.

Not to be outdone, all of my prior math and science teachers have instilled in me a passion for understanding the world using logic and reason to guide my thoughts. My other committee members, David Biron, Daniel Holz, and Michael Rust, have also graciously invested their time in helping me fulfill my goal of obtaining this degree. It is much appreciated.

Lastly, I must thank my family, especially my parents, who have always supported me in my academic journey.

ABSTRACT

Understanding the dynamics of large-scale brain activity is a tough challenge. One reason for this is the presence of an incredible amount of complexity arising from having roughly 100 billion neurons connected via 100 trillion synapses. Because of the extremely high number of degrees of freedom in the nervous system, the question of how the brain manages to properly function and remain stable, yet also be adaptable, must be posed. Neuroscientists have identified many ways the nervous system makes this possible, of which synaptic plasticity is possibly the most notable one. On the other hand, it is vital to understand how the nervous system also loses stability, resulting in neuropathological diseases such as epilepsy, a disease which affects 1% of the population.

In the following work, we seek to answer some of these questions from two different perspectives. The first uses mean-field theory applied to neuronal populations, where the variables of interest are the percentages of active excitatory and inhibitory neurons in a network, to consider how the nervous system responds to external stimuli, self-organizes and generates epileptiform activity. The second method uses statistical field theory, in the framework of single neurons on a lattice, to study the concept of criticality, an idea borrowed from physics which posits that in some regime the brain operates in a collectively stable or marginally stable manner. This will be examined in two different neuronal networks with self-organized criticality serving as the overarching theme for the union of both perspectives.

One of the biggest problems in neuroscience is the question of to what extent certain details are significant to the functioning of the brain. These details give rise to various spatiotemporal properties that at the smallest of scales explain the interaction of single neurons and synapses and at the largest of scales describe, for example, behaviors and sensations. In what follows, we will shed some light on this issue.

CHAPTER 1

INTRODUCTION

1.1 The neuroscience problem

Without question, the mammalian cortex is one of nature's greatest unsolved mysteries. At first glance, the fact that one hundred billion neurons connected to each other via one hundred trillion synapses, resulting in a configuration space on the order of 10^{37}, renders understanding it hopeless. To put that last number in perspective, consider that there are only roughly about 10^{29} stars in the entire known universe. We would need one hundred million universes, each with the same number of stars as our own, to equal the number of ways our brain can be configured and generate activity patterns. However difficult this may seem though, we do not need to know the details of every single neuron or synapse to understand the brain's large-scale important properties in the same way that, to understand the thermodynamics of a liquid or gas, clearly macroscopic quantities, we do not need to know what every atom or molecule is doing.

If we continue along with the analogy of atoms in a gas, it becomes obvious that another significant issue arises. At what length scale do we start to keep track of important variables? If we acknowledge that every single neuron and/or synapse isn't important, where do we draw the line? The philosophy of science is to answer every question possible and that every question has an answer. However, with such a complex system and such limited knowledge of it, where at this moment in history we are chiefly interested in how the brain generally adapts and codes information, the first step in any theoretical model is to provide an axiomatic answer these questions. This shall be our starting point.

1.2 Spatiotemporal models

In the following chapters, our starting point for analyzing neocortical properties will be to consider neurons as simple switches, which are either firing an action potential or are quiescent. These neurons will be connected to each other electrically via gap junctions or chemically via synapses whose strengths will be free parameters and may or may not change depending on the model. From here, we build our network, keeping track of the percentage of active excitatory or inhibitory neurons, the reason of which will be explained in the following chapter. The simplest (and influential) equations governing a network of only 1 type of excitatory and inhibitory neurons to date are the Wilson-Cowan equations, [125] and [126]

$$\begin{aligned} \tau_E \frac{dE}{dt} &= -E + (1-E)S_e[w_{EE}E - w_{EI}I + P] \\ \tau_I \frac{dI}{dt} &= -I + (1-I)S_i[w_{IE}E - w_{II}I + Q] \end{aligned} \tag{1.1}$$

where E and I represent the fraction of active neurons for each respective population, τ_E and τ_I are time constants, S_e and S_i are firing functions, w_{ij} are the inter- and intra-population connection strengths, and P and Q are arbitrary external inputs. At this point we will leave most of the significant details of these equations for later. All we need to mention here is that these equations and their spatially inhomogeneous extension will be used heavily to model spatiotemporal dynamics such as damped traveling waves, localized behavior and then self-organization and epileptiform activity.

In the derivation of Equation 1.1, Wilson and Cowan time-course grained the activity to eliminate fluctuations present in the full integro-differential equations. In other words, the variables E and I are deterministic quantities i.e. we can calculate $E(t)$ and $I(t)$ exactly if given initial conditions. However, it is obvious from neurophysiological recordings that noise plays a crucial role in describing certain neural dynamics. Hence, in order to capture these effects, we need to introduce a stochastic, modified Wilson-Cowan model to capture the

inherent randomness in neurons. As will also be expanded upon in further chapters, neurons in this adjusted framework represent two-state Markov particles on a lattice with transition rates between firing and quiescence. Thus, our second model is no longer deterministic and, as with all non-deterministic theories, the important quantity to find is now a probability distribution. The reason for this is because outcomes are no longer defined for all time by just initial conditions. Rather, an outcome is described by a probability. We will see that the probability distribution for all of the 10^{37} neural configurations is solved via what is known as a master equation. While E and I maintain their same meaning as before, they are now averaged quantities (with respect to the probability distribution). The master equation and its implications will be discussed in ensuing chapters.

1.3 Properties of neocortical activity and the purpose of this study

With the two models mentioned above, in this thesis, we study a range of properties of neural networks, all of which shed light on how the cortex might maintain stability. We first consider, in Chapter 2, the general modes of behavior for resting and driven activity. Many of these behaviors have been previously studied and we show how both models can be used to provide a quantitative account of the dynamics of this activity. We first begin with the original Wilson-Cowan equations and then describe how the Markov model provides an alternative examination of similar behavior. Our new contribution is to show that the deterministic model can account for recent data indicating that there are two distinct modes of response to stimuli: damped traveling waves resulting from weak inputs and localized activity associated with strong stimuli. This is an interesting problem because it indicates the brain is able to remain incredibly stable for large inputs, but loses much of its coding ability unless the drive is small.

Next, Chapter 3 will introduce the idea of self-organized criticality, a property of cer-

tain systems which can intrinsically tune their dynamics towards a critical point where the system becomes stable or marginally stable and displays spatiotemporal scale invariance. We first show that two connected excitatory populations with a synaptically-plastic connection strength self-organizes to one of these locations and the statistical properties appear to be that of a directed percolation phase transition seen in models of forest fires, reaction-diffusion processes, etc. We show that an array of E and I populations can also self-organize to a weakly stable node located near a similar critical point. However, because the $E-I$ network never actually reaches the critical point, we refer to the process as self-organized near-criticality. Both examples touch on a topic of considerable theoretical interest in the neuroscience community, namely whether the brain has developed its own fine-tuning mechanism over years of evolution to allow itself to constantly change but still remain stable under normal circumstances.

After investigating self-organized criticality, Chapter 4 in this thesis concerns epilepsy, the neurological disease characterized by repeated seizures. While approximately 1% of the population has epilepsy, its cause is still very much unknown and, unfortunately, modern medication has not aided much in treatment. What is understood is that epileptiform activity is a manifestation of the unstable neocortex. In particular, the activity patterns are large-amplitude traveling waves. To get this spreading behavior, we noted that experimental data taken during actual human seizures and also evoked epileptic activity suggest that neurons saturate, resulting in a redefinition of the familiar firing functions used in Chapters 2-3. We introduce this new framework in the Wilson-Cowan formalism and investigate a spatially continuous 1-dimensional $E-I$ network to model epileptic waves. One of the outstanding results of this work is that spreading inhibition precedes excitation, which is not possible in the deterministic Wilson-Cowan model without taking saturation effects into account. Because of the resulting spatiotemporal dynamics, it is clear how, theoretically, the brain might lose stability. However, it is still unclear why the network properties that allow this behavior to happen are present in the first place.

In the final chapter, we make closing remarks regarding neocortical activity and many of the spatiotemporal properties discussed in previous chapters. Some philosophical comments will be posed as well in light of what the preceding chapters have examined. Lastly, with an emphasis on the implications of this work's analysis, the overall theme will be summarized and future directions will be mentioned.

CHAPTER 2

WILSON-COWAN EQUATIONS AND NEOCORTICAL DYNAMICS

2.1 Introduction

The analysis of large-scale brain activity is a difficult problem. Of the roughly 100 billion neurons in the cortex of the human brain, 80% are excitatory and the remaining 20% are inhibitory. Each neuron has about seven thousand axon terminals from other neurons, but there is some redundancy in the connectivity so that it has effective connections from about 80 other neurons, mostly nearest neighbors. Each neuron is actually a complex switching device, but here, we introduce only the simplest cellular model in which neurons are binary switches, either quiescent or activated. It follows that there are approximately 10^{37} configurations of activated or quiescent neurons. Such a large configuration space suggests the need to use statistical methods to analyze large-scale brain activity. In addition there is some degree of microscopic randomness in neural connectivity, and there are also random fluctuations of neural activity, both of which support the need for a statistical treatment, as noted by Sholl in 1956, [100].

2.2 Experimental data on large-scale brain activity

There is a large body of data on large-scale brain activity, including electroencephalographic (EEG) recordings with large electrodes from the surface of the scalp, functional magnetic resonance (fMRI) measurements of blood flow in different brain regions (also large-scale), local field potentials (LFP) recorded with smaller electrodes, microelectrode recordings from or near individual neurons, or (currently) microelectrode arrays (MEA) which can record the simultaneous activity of many neighboring neurons. Currently, there are also new techniques for forming optical images of local brain activity using voltage sensitive dyes (VSD). All such

recordings can be classified as measuring either *spontaneous* (or *resting*) activity, or stimulus-driven *evoked* activity.

2.2.1 Resting activity

We first consider the resting brain activity of unanaesthetized animals first observed in animals by Caton in 1875, [28], and in humans by Berger in 1924, [14]. Recordings from the human scalp are referred to as electroencephalographs (EEG) and are measured via electrodes on the unshaven scalp. The voltage differences measured between such electrode pairs are about 50 μV. Figure 2.1 shows a typical EEG recording.

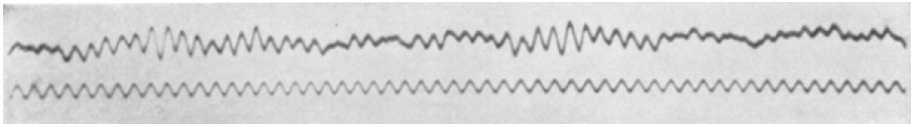

Figure 2.1: The upper trace is the first recording of spontaneous electrical activity from the human scalp. The lower trace is a 10 Hz oscillation. Reproduced from [14].

It will be seen that there are intermittent bursts of 10 Hz oscillations in the scalp activity. These oscillations comprise the *alpha* rhythm, seen in awake relaxed humans, mainly in the occipital region of the brain which processes visual signals from the eyes. Figure 2.2 shows the power spectrum of such activity.

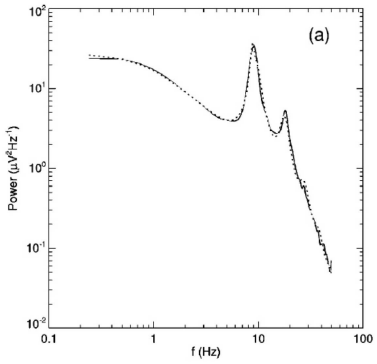

Figure 2.2: The power spectrum of the occipital EEG of a resting, awake human. Reproduced from [94].

It will be seen that there is a pronounced peak in the power spectrum at around 10 Hz and a secondary peak around 20 Hz. This peak is said to be in the range of the *beta* rhythm of occipital EEG activity. Interestingly if the contributions of such peaks are eliminated, what is left can be fitted with the function $a/(b + f^2)$, where a and b are constants, and f is the frequency in Hz. Figure 2.3 shows such a function and its fit to the EEG power spectrum.

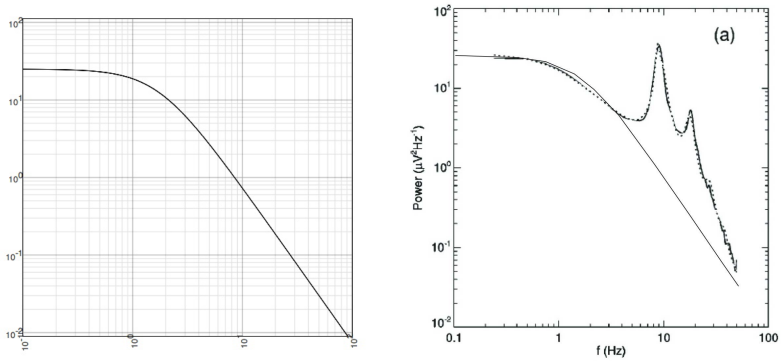

Figure 2.3: The left panel shows the function $75/(3+f^2)$, the right panel the fit of such a function to the EEG power spectrum shown in Figure 2.2.

It is important to note that this power spectrum fit is that of Brownian motion, which suggests that resting brain activity is largely *desynchronized* and *random*.

Other measurements of resting brain activity have been carried out on lightly anesthetized animals using local field potential recordings of spiking neuron activity, or else via fMRI measurements of blood flows in the brain that accompany unanesthetized brain activity. Figure 2.4 shows examples.

Note the fit of the Brownian motion power spectrum $125/(5 + f^2)$ to the resting LFP.

Isolated neocortex

But the most detailed studies, and the most information about the nature of spontaneous activity, has been obtained from studies of isolated neocortical slabs. The first detailed studies were carried out in the early 1950s by B. DeLisle Burns, on isolated slabs of parietal

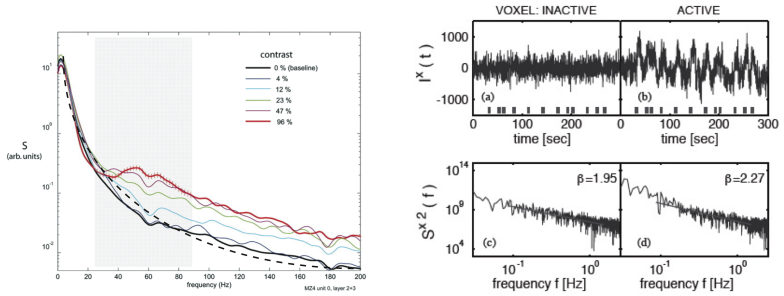

Figure 2.4: The left panel shows the power spectra of LFP recordings from cat visual cortex in response to sine-wave modulated grating patterns. Reproduced from [55]. The right panel shows fMRI recordings of both resting and stimulated human brain activity, and their associated power spectra. Reproduced from [110].

neocortex, [22] and [23]. The main relevant result was that very lightly anesthetized slabs spontaneously generated *bursts* of propagating activity from a number of randomly occurring sites. Any variation of the level of anesthesia, either up or down, abolished the activity.

However, it was not until 2003 that a systematic study of such burst activity was carried out by Beggs and Plenz, [9], using isolated slabs of rat somatosensory cortex, either in mature tissue cultures, or else in slices. The tissue cultures exhibited spontaneous bursts of propagating activity in the form of local field potentials recorded at microelectrodes. The slices, however, were silent until stimulated with NMDA, a glutamate-receptor agonist, in combination with a dopamine D_1-receptor agonist. In contrast to DeLisle Burns, Beggs and Plenz used an 8×8 microelectrode array to record local field potentials (LFPs) in the slab. The main result of their experiments is summarized in Figures 2.5 and 2.6.

Beggs and Plenz's conclusion is that such bursts of activity are *avalanches* defined as follows: the configuration of active electrodes in the array during one time bin of width Δt is termed a frame, and a sequence of frames preceded and followed by blank frames, is called an avalanche. However successive frames are not highly correlated, so the activity is not wave-like: it is in fact *self-similar*, and in addition, the avalanche size distribution follows the power law $P[n] \propto n^{\alpha}$. In addition the exponent α is approximately -1.5. This is the mean-field exponent of a critical branching process, [5]. This result was a step beyond

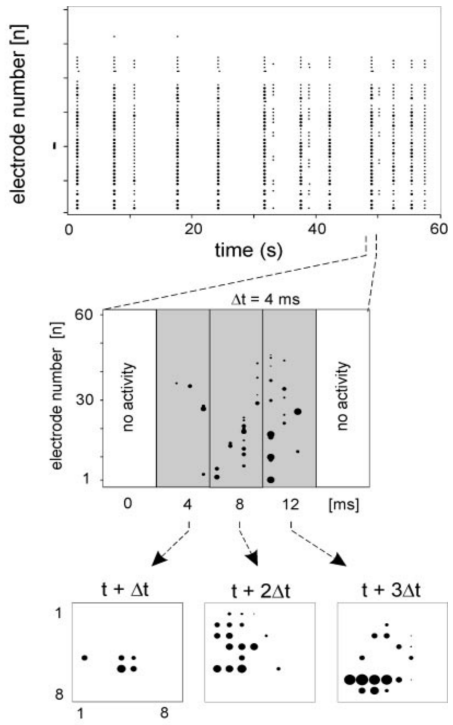

Figure 2.5: Electrode data from slices of rat neocortex. The top graph is a raster plot of electrode activation times. They seem synchronous, but closer examination reveals that the times exhibit self-similarity. The bottom graphs show a sequence of electrode activations in the original array. Reproduced from [9].

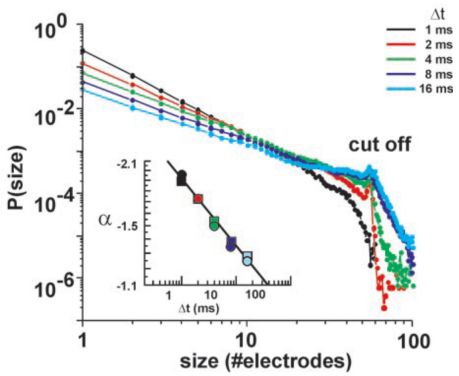

Figure 2.6: Probability distribution of burst sizes at different bin widths Δt. Inset: Dependence of slope exponent α on bin width. Reproduced from [9].

that of Softky and Koch, [103], who found Poisson-like spiking activity in individual cortical neurons, and introduced the possibility of criticality in brain dynamics. In fact this mean-field exponent turns up in several kinds of *percolation* processes on random graphs, including both isotropic and directed percolation. But branching and annihilating random walks are equivalent to directed percolation, so it is possible that what Beggs & Plenz observed in cortical slices was a form of directed percolation. We will return to this topic later.

2.2.2 Driven or stimulated activity

In case there is an external stimulus, neocortical dynamics indicates a very different picture. It turns out that there is a big difference in the responses to weak stimuli, compared to those triggered by stronger stimuli. In addition correlations between pairs of neurons in driven neocortex have a shorter length scale than those found in spontaneous activity.

Weak stimuli

The basic result for weak stimuli is that the cortical response is a *propagating wave* whose amplitude decays exponentially with distance. Figure 2.7 shows the cortical responses to low amplitude stimuli in the form of spikes, recorded by an implanted microelectrode array in three monkey visual cortices by Nauhaus *et al*, [82]. Each row shows data from the spike triggered local field potentials (LFP) from a single location. The first column shows the dependence of time to peak of the LFP as a function of the cortical distance from the triggering electrode, and estimated propagation velocities. The second column shows the propagating wave, both as a pseudo-colored Image, and as a plot of wave amplitude vs distance from the triggering electrode, together with estimates of the space-constants of the decaying waves. The third column shows average LFP waveforms at three locations from the triggering spike.

It will be seen that the response is indeed a traveling LFP, whose velocity is about $25-30$ cm/sec. In addition the LFP amplitude decays exponentially, with a decay constant λ of

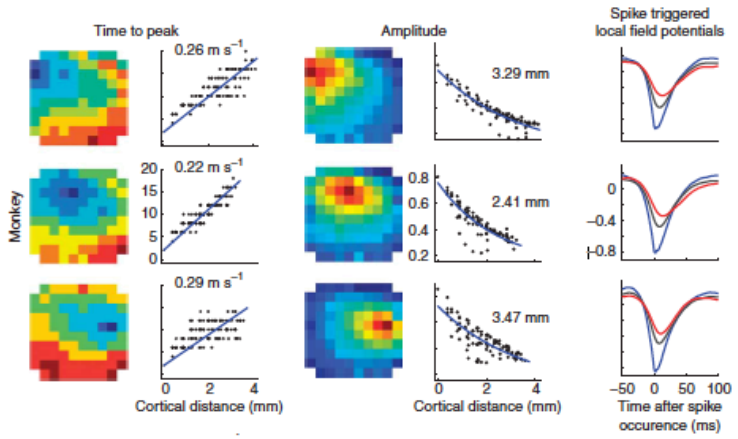

Figure 2.7: Spikes of low amplitude initiate traveling waves of LFP in the cortex. See text for details. Reproduced from [82].

about 3 mm.

Strong stimuli

In contrast the basic result for strong stimuli is that cortical responses to such stimuli are much more *localized*. Figure 2.8 shows a comparison of cortical responses to weak and strong stimuli, [82]. It will be seen that responses to larger stimuli remain essentially *localized*. These observations immediately suggest a role for inhibition in localizing such responses.

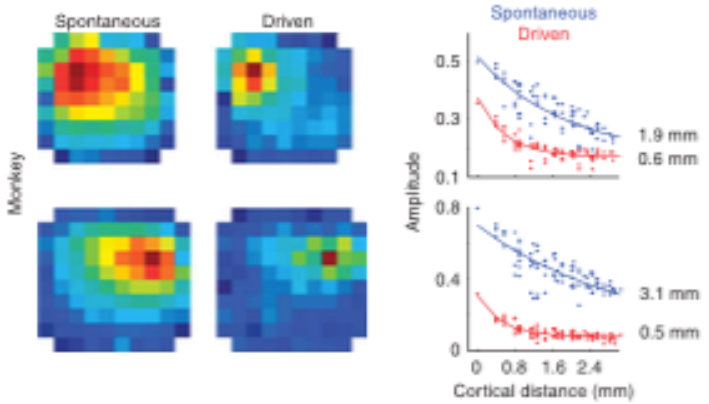

Figure 2.8: Spikes of larger amplitude initiate standing waves of LFP in the cortex. See text for details. Reproduced from [82].

Correlations

The basic result for correlations is that correlations between pairs of LFP fall off with separation distance, and such a falloff is much greater for strong stimuli than for weaker ones, see Figure 2.9. Thus strong stimuli weaken the intrinsic pair correlations that exist in spontaneous activity. See Lampl *et al* and others ([30], [67], [72], and [98]). These observations also suggest a role for inhibition.

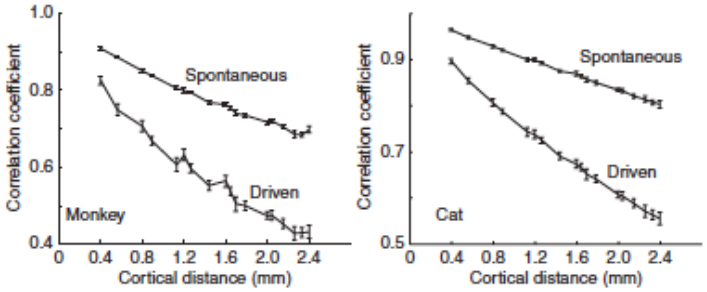

Figure 2.9: Fall of with distance of cortical pair correlations. See text for details. Reproduced from [82].

To explain all these observations we need to understand the competing roles of neural excitation and inhibition in neural population dynamics. We therefore give a short account of the history and development of the Wilson-Cowan neural population equations.

2.3 Neural population equations

2.3.1 Introduction

Following early work by Shimbel & Rapaport [99], Beurle focused, not on the activity of single neurons, but on the proportion of neurons activated per unit time in a given volume element of a slice or slab of neocortex, denoted by $n(\mathbf{x}, t)$, [15]. For all practical purposes this can be taken to be equivalent to the spike-triggered LFP and VSD described earlier.

Beurle introduced the update equation

$$n(\mathbf{x}, t+\tau) = q(\mathbf{x}, t)\, f[n(\mathbf{x}, t)] \tag{2.1}$$

where $q(\mathbf{x}, t)$ is the density of quiescent neurons in the given volume element, and $f[n(\mathbf{x}, t)]$ the proportion of neurons receiving *exactly* threshold excitation. [There is an implicit assumption that individual neurons are of the integrate-and-fire variety.]

There are three points to note here.

1. By assuming that $n(t+\tau) = q(t)f[n(t)]$ Beurle ignored the effects of fluctuations and correlations on the dynamics. It is not true that q and $f[n]$ are statistically independent quantities, as was first pointed out in [102].

2. The update equation is incorrect. $f[n]$ should be the proportion of neurons receiving *at least* threshold excitation, as was first noted by Uttley [113].

This proportion can be expressed [126] as:

$$f[n] = \int_{-\infty}^{n} P(n_{\mathrm{TH}}) dn_{\mathrm{TH}} = \int_{-\infty}^{\infty} \vartheta[n - n_{\mathrm{TH}}] P(n_{\mathrm{TH}}) dn_{\mathrm{TH}} = \langle \vartheta[n] \rangle \tag{2.2}$$

where $\vartheta[n]$ is the Heaviside step function and $\langle \vartheta[n] \rangle$ is the average of $\vartheta[n]$ over the probability distribution of thresholds $P(n_{\mathrm{TH}})$.

This implies that the function $f[n]$ should have the form of a probability distribution function, not a probability density. In Cowan, [32], the logistic or *sigmoid* form:

$$f[n] = [1 + \exp[-n]]^{-1} = \frac{1}{2}[1 + \tanh(\frac{n}{2})] \tag{2.3}$$

was introduced, as an analytic approximation to the Heaviside step function used in McCulloch-Pitts neurons, [76]. This indicates that the required continuum equations should represent the dynamics of a population of integrate-and-fire neurons in which there is a random distribution of thresholds.

The corrected version of Beurle's takes the form:

$$\begin{aligned} n(\mathbf{x}, t+\tau) &= q(\mathbf{x}, t) f[n(\mathbf{x}, t)] \\ &= q(\mathbf{x}, t) f\left[\int_{-\infty}^{t} dt' \int_{-\infty}^{\infty} d\mathbf{x}' \alpha(t-t')[\beta(\mathbf{x}-\mathbf{x}') n(\mathbf{x}', t') + h(\mathbf{x}, t')]\right] \end{aligned} \tag{2.4}$$

where

$$q(\mathbf{x}, t) = 1 - \int_{t-r}^{t} n(\mathbf{x}, t) \tag{2.5}$$

$r = 1$ ms is the (absolute) refractory period or width of the action potential, and

$$\alpha(t-t') = \alpha_0 e^{-(t-t')/\tau}, \quad \beta(\mathbf{x}-\mathbf{x}') = b e^{-|\mathbf{x}-\mathbf{x}'|/\sigma} \tag{2.6}$$

are the impulse response function and spatially homogeneous weighting function of the continuum model, with membrane time constant $\tau \sim 10$ ms, and space constant $\sigma \sim 100$ μm.

3. Beurle's formulation does not explicitly incorporate a role for inhibitory neurons.

2.3.2 The Wilson-Cowan equations

Wilson and Cowan corrected and extended Beurle's work and introduced equations for the population dynamics of a spatially homogeneous population of coupled excitatory and inhibitory binary neurons [126], and its extension to spatially inhomogeneous populations [125]. These equations take the forms:

$$\begin{aligned} \tau \frac{dE}{dt} &= -E(t) + (1 - rE(t))\, f_E\left[w_{EE} E - w_{EI} I + h_E(t)\right] \\ \tau \frac{dI}{dt} &= -I(t) + (1 - rI(t))\, f_I\left[w_{IE} E - w_{II} I + h_I(t)\right] \end{aligned} \tag{2.7}$$

for the spatially homogeneous case, and

$$\begin{aligned}
&\tau\frac{\partial E(\mathbf{x},t)}{\partial t} = -E(\mathbf{x},t) + (1 - rE(\mathbf{x},t)) \times \\
&f_E\left[\int_{-\infty}^{\infty}\rho_E d\mathbf{x}'\beta_{EE}(\mathbf{x}-\mathbf{x}')E(\mathbf{x}',t) - \int_{-\infty}^{\infty}\rho_I d\mathbf{x}'\beta_{EI}(\mathbf{x}-\mathbf{x}')I(\mathbf{x}',t) + h_E(\mathbf{x},t)\right] \\
&\tau\frac{\partial I(\mathbf{x},t)}{\partial t} = -I(\mathbf{x},t) + (1 - rI(\mathbf{x},t)) \times \\
&f_I\left[\int_{-\infty}^{\infty}\rho_E d\mathbf{x}'\beta_{IE}(\mathbf{x}-\mathbf{x}')E(\mathbf{x}',t) - \int_{-\infty}^{\infty}\rho_I d\mathbf{x}'\beta_{II}(\mathbf{x}-\mathbf{x}')I(\mathbf{x}',t) + h_I(\mathbf{x},t)\right]
\end{aligned} \tag{2.8}$$

for the continuum form of the spatial case, in which ρ_E, and ρ_I are, respectively, the packing densities of excitatory and inhibitory cells in the cortical slab. Note that $f_E[n]$ and $f_I[n]$ are modified versions of the firing rate function $f[n]$ introduced in Equation 2.3, such that $f_E[0] = f_I[0] = 0$. Note also that the variables $E(\mathbf{x},t)$ and $I(\mathbf{x},t)$ are time coarse-grained, i.e.

$$E(\mathbf{x},t) = \int_{-\infty}^{t} dt'\alpha(t-t')n_E(\mathbf{x},t'), \quad I(\mathbf{x},t) = \int_{-\infty}^{t} dt'\alpha(t-t')n_I(\mathbf{x},t') \tag{2.9}$$

where $n_E(\mathbf{x},t)$ and $n_I(\mathbf{x},t)$ are the proportions of excitatory and inhibitory neurons activated per unit time. It follows from Equation 2.4 that $\alpha(t)$ acts as a low-pass filter, and therefore that $E(\mathbf{x},t)$ and $I(\mathbf{x},t)$ are low-pass filtered version of $n_E(\mathbf{x},t')$ and $n_I(\mathbf{x},t')$, respectively. The net effect of such a coarse-graining is to remove oscillatory components of neural population responses greater than 100 Hz.

2.3.3 Attractor dynamics

A major feature of Equation 2.7 is that it supports different kinds of asymptotically stable equilibria. Figure 2.10 shows two such equilibrium patterns: There is also another phase plane portrait in which the equilibrium is a damped oscillation, i.e., a stable *focus*. In fact by varying the synaptic weights w_{EH} and w_{IH} or $a = w_{EE}w_{II}$ and $b = w_{IE}w_{EI}$ we can move from one portrait to another. It turns out that there is a substantial literature dealing

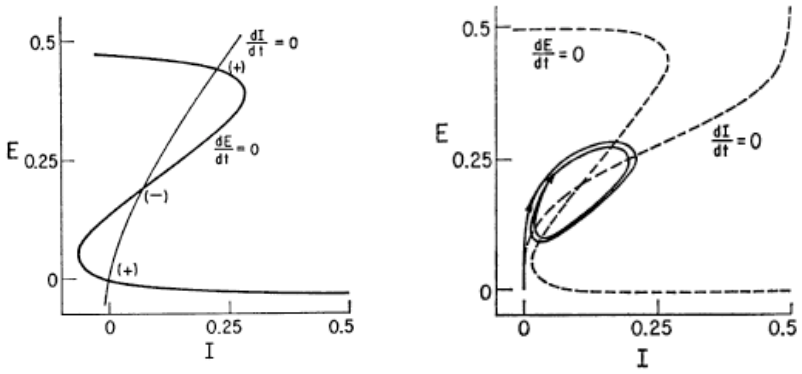

Figure 2.10: The left panel shows the E-I phase plane and null clines of Equation 2.7. The intersections of the two null clines are equilibrium or fixed points of the equations. Those labelled + are stable, those labelled − are unstable. Parameters: $w_{EE} = 12, w_{EI} = 4$, $w_{IE} = 13, w_{II} = 11, n_H = 0$. The stable fixed points are *nodes*. The right panel shows an equilibrium which is periodic in time. Parameters: $w_{EE} = 16, w_{EI} = 12, w_{IE} = 15$, $w_{II} = 3, n_H = 1.25$. In this case the equilibrium is a *limit cycle*. Redrawn from [126].

with the way in which such changes occur, The mathematical technique for analyzing these transformations is bifurcation theory, and it was first applied to neural problems 54 years ago by Fitzhugh, [46], but first applied systematically by Ermentrout and Cowan in [42], [43], and [44] in a series of papers on the dynamics of the mean-field Wilson-Cowan equations. Subsequent studies by Borisyuk and Kirillov, [17], and Hoppenstaedt and Izhikevich, [58], have greatly extended this analysis.

The left panel of Figure 2.11 shows the detailed structure around such bifurcations. Evidently the saddle-node and Andronov-Hopf bifurcations lie near the Bogdanov-Takens bifurcation. Thus, all the bifurcations described in the spatially homogeneous Wilson-Cowan equations lie close to such a bifurcation in the $(\mathbf{a}, \mathbf{b})$-plane. The Bogdanov-Takens bifurcation depends on two control parameters $\mathbf{a}$ and $\mathbf{b}$, and is therefore of *codimension* 2. In such a bifurcation an equilibrium point can simultaneously become a marginally stable saddle and an Andronov-Hopf point. So at the bifurcation point the eigenvalues of its stability matrix have zero real parts. In addition the right panel of Figure 2.11 shows how the fast E-nullcline and the slow I-nullcline intersect. The first point of contact of the two nullclines is the Bogdanov-Takens bifurcation point. The two nullclines remain close together over

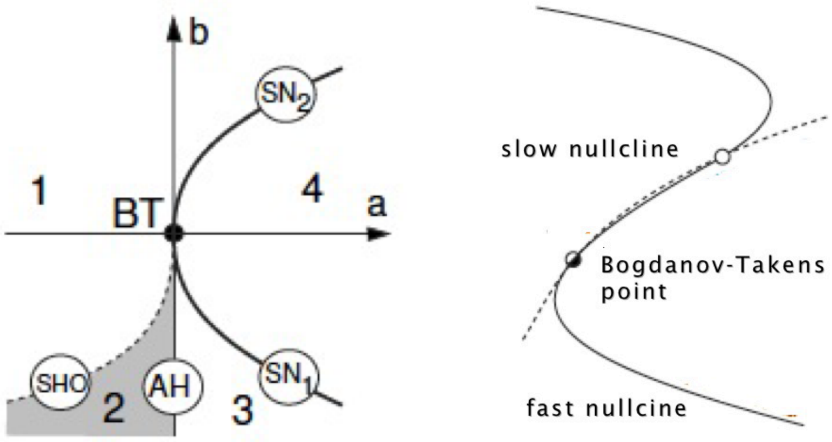

Figure 2.11: The left panel shows bifurcations of Equation 2.7 in the spatially homogeneous case, organized around the Bogdanov-Takens (BT) bifurcation. SN1 and SN2 are saddle-node bifurcations. AH is an Andronov-Hopf bifurcation, and SHO is a saddle homoclinic-orbit bifurcation. Note that a and b are bifurcation parameters in the canonical model for the BT bifurcation [60]. The right panel shows the nullcline structure of a Bogdanov-Takens bifurcation. At the Bogdanov-Takens point, a stable node (open circle) coalesces with an unstable point. Redrawn from [60].

a large part of the subsequent E-I phase space before diverging. As we will later discuss, this property of the nullclines is closely connected with the existence of a *balance* between excitatory and inhibitory currents in the network described by the Wilson-Cowan equations, and therefore with the existence of *avalanches* in stochastic Wilson-Cowan equations, [11].

2.4 Stochastic neural dynamics

2.4.1 Introduction

To develop such equations we need to reformulate neural population dynamics as a Markov process. We first consider the representation of the dynamics of a cortical sheet or slab comprising a single spatially homogeneous network of N excitatory binary neurons. Such neurons transition from a quiescent state q to an activated state a at the rate f and back again to the quiescent state q at the rate α, as shown in Figure 2.12.

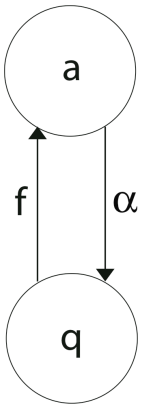

Figure 2.12: Neural state transitions. a is the activated state of a neuron. q is the quiescent state. α is a decay constant, but f depends on the number of activated neurons connected to the neuron, and on an external stimulus h.

2.4.2 A master equation for a network of excitatory neurons

The first step is to formulate a master equation describing the evolution of the probability distribution of neural activity $P_n(t)$ in such a network. Consider first n activated neurons, each becoming quiescent at the rate α. This produces a flow out of the state n at rate α, proportional to $p_n(t)$, hence a term in the master equation of the form $-\alpha n P_n(t)$. Similarly the flow into n from the state $n+1$ produces a term $\alpha(n+1)P_{n+1}(t)$. The net effect is the term

$$\alpha\left[(n+1)P_{n+1}(t) - nP_n(t)\right]. \tag{2.10}$$

Now consider the $N-n$ quiescent neurons in state n, each prepared to spike at rate $f[s_E(n)]$, leading to the term $-(N-n)f[s_E(n)]P_n(t)$, in which the total input is $s_E(n) = I(n)/I_{\mathrm{TH}} = (w_{EE}n + h_E)/I_{\mathrm{TH}}$, and $f[s_E(n)]$ is the function shown in Figure 2.13, a low-noise version of Equation 2.3.

The flow into the state n from the state $n-1$ is therefore $(N-n+1)f[s_E(n-1)]P_{n-1}(t)$, and the total contribution from excitatory spikes is then

$$(N-n+1)f[s_E(n-1)]P_{n-1}(t) - (N-n)f[s_E(n)]P_n(t) \tag{2.11}$$

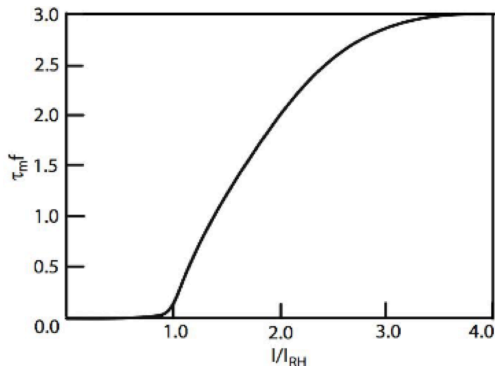

Figure 2.13: The firing rate function $f[s_E(n)]$, $\tau_m = 1/\alpha = 3$ ms is the neural membrane time constant, I is the input current, and $I_{\rm RH}$ is the *rheobase* or threshold current.

It follows that the probability $P_n(t)$ evolves according to the Master equation

$$\begin{aligned} \frac{dP_n(t)}{dt} &= \alpha\left[(n+1)P_{n+1}(t) - nP_n(t)\right] \\ &+ (N-n+1)f[s_E(n-1)]P_{n-1}(t) - (N-n)f[s_E(n)]P_n(t) \end{aligned} \tag{2.12}$$

It is easy to derive an evolution equation for $\langle n(t)\rangle$, the average number of active neurons in the network, using standard methods. The equation takes the form

$$\frac{d\langle n(t)\rangle}{dt} = -\alpha\langle n(t)\rangle + (N - \langle n(t)\rangle)f[\langle s_E(n)\rangle] \tag{2.13}$$

where $\langle s_E(n)\rangle = w_{EE}\langle n\rangle + h_{EE}$, and is the simplest form of Equation 2.7 for a single excitatory population. Such a mean field equation can be obtained in a number of different ways, in particular by using the van Kampen "system-size expansion" of Equation 2.12 about a locally stable equilibrium, [116]. However, as is well known, this expansion breaks down at a marginally stable critical point, e.g. at a Bogdanov-Takens point, and a different method must be used to analyze such a situation.

Before proceeding we note that these equations can be extended to cover the situation introduced in Equation 2.7 which incorporates spatial effects. The variable $n(t)/N$ is extended to $n(\mathbf{x}, t)$ representing the *density* of active neurons at the cortical location $\mathbf{x}$ at time

t, and the total input current $I(n)$ becomes the current density

$$I(n(\mathbf{x})) = \int d^d x' w_{EE}(\mathbf{x} - \mathbf{x}') n(\mathbf{x}') + h_E(\mathbf{x}) \tag{2.14}$$

2.4.3 A master equation for a network of excitatory and inhibitory neurons

Since about 1/5 th of all cortical neurons are inhibitory, it is important to include the effects of such inhibition. We therefore extend Equation 2.10 to include inhibitory neurons. The result is the Master equation:

$$\begin{aligned}
\frac{dP(n_E, n_I, t)}{dt} &= \alpha_E \left[(n_E + 1)P(n_E + 1, n_I, t) - n_E P(n_E, n_I, t)\right] \\
&+ \left[(N_E - n_E + 1) f_E[s_E(n_E - 1, n_I)] P(n_E - 1, n_I, t)\right. \\
&- \left.(N_E - n_E) f_E[s_E(n_E, n_I)] P(n_E, n_I, t)\right] \\
&+ \alpha_I \left[(n_I + 1)P(n_E, n_I + 1, t) - n_I P(n_E, n_I, t)\right] \\
&+ \left[(N_I - n_I + 1) f_I[s_I(n_E, n_I - 1)] P(n_E, n_I - 1, t)\right. \\
&- \left.(N_I - n_I) f_I[s_I(n_E, n_I)] P(n_E, n_I, t)\right]
\end{aligned} \tag{2.15}$$

See Benayoun *et al*, [11], for a derivation of this equation. It is easy to derive Equation 2.7 from this master equation. However there is much more information about stochastic neural dynamics contained in Equation 2.15 than is contained in such an equation. We refer, of course, to the effects of intrinsic fluctuations and of correlations.

2.5 Analyzing intrinsic fluctuations

To analyze such effects we need to look more closely at the attractor dynamics of Equation 2.7. There are two cases to consider. In case 1, the attractor is either an asymptotically stable node or focus, or it is a limit cycle. In case 2, the attractor is only marginally stable. In nonlinear dynamics, this is a bifurcation point, e.g. a Bogdanov-Takens point, or a Saddle

Node or Andronov-Hopf point. In statistical mechanics this is the critical point of a phase transition.

2.5.1 The system-size expansion

The System-Size Expansion was introduced by van Kampen, [116], to analyze the effects of intrinsic fluctuations in case 1. The intuition behind this approach comes from the idea that if neurons are independently activated, then the total activity in a excitatory neural network in such a case is Gaussian distributed, with mean activity $\langle n_E(t) \rangle$ proportional to N, the total number of neurons in the network, and standard distribution proportional to $\sqrt{N}$. So the number of neurons activated at a given time can be represented by the variable

$$k = Nn_E + \sqrt{N}\xi_E \tag{2.16}$$

where ξ_E is a Gaussian random perturbation.

The deterministic term satisfies Equation 2.7, the random variable satisfies the linear Langevin equation

$$\frac{d\xi_E}{dt} = A\xi_E + \sqrt{\alpha_E n_E + (1 - n_E) f_E[s_E(n_E)]}\eta_E \tag{2.17}$$

to order $N^{-1/2}$, where A is a constant and η_E is an independent white noise variable, whose amplitudes are calculated from Equation 2.7.

An early version of this application of the System-Size expansion can be found in Ohira and Cowan, [88]. The extension to the excitatory and inhibitory neural network introduced in Equation 2.7 is to be found in Benayoun *et al*, [11]. This paper is notable for its use of the Gillespie algorithm, [49]. In this algorithm, the simulation time is advanced only when the network's state is updated, and the time intervals dt are random variables dependent upon the network state. The simulation is carried out for a network in which certain symmetry

conditions are introduced. These conditions are

$$w_{IE} = w_{EE} = w_E; \quad w_{EI} = w_{II} = w_I; \quad w_E - w_I = w_0 \tag{2.18}$$

where w_0 is kept constant. Figures 2.14-2.17 show the results.

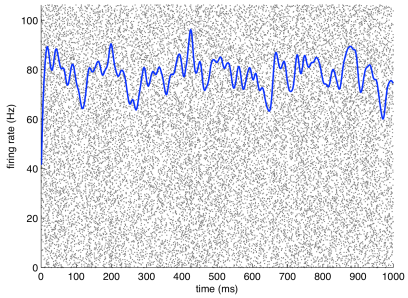

Figure 2.14: Raster plot of the spiking patterns in a network of $N = 800$ excitatory neurons. Each black dot represents a neural spike. The mean activity $\langle n_E(t) \rangle$ is represented by the blue trace. Simulation using the Gillespie algorithm with parameter values $h_E = h_I = 0.001$, $w_0 = w_E - w_I = 0.2$, and $w_E + w_I = 0.8$. Redrawn from [11].

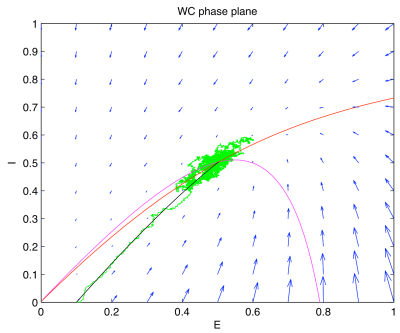

Figure 2.15: Phase plane plots of the activity shown in Figure 2.14 showing the vector field (blue) and nullclines $\dot{E} = 0$ (magenta) and $\dot{I} = 0$ (red), of Equation 2.1 and plots of a deterministic (black) and a stochastic (green) trajectory starting from identical initial conditions. Redrawn from [11].

It should be evident from a study of these figures that the location of the fixed point of Equation 2.7 remains unchanged as $w_E + w_I$ increases from 0.8 to 13.8, but the stochastic trajectory (green) becomes increasingly spread out as the nullclines become more parallel. Such a feature is also evident in the right panel of Figure 2.11 in which the nullcline structure

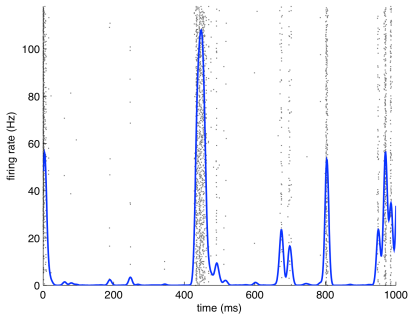

Figure 2.16: Raster plot of the spiking patterns in a network of $N = 800$ excitatory neurons. Each black dot represents a neural spike. The mean activity $\langle n_E(t) \rangle$ is represented by the blue trace. Simulation using the Gillespie algorithm with parameter values $h_E = h_I = 0.001$, $w_0 = w_E - w_I = 0.2$, and $w_E + w_I = 13.8$. Redrawn from [11].

of the Bogdanov-Takens bifurcation is shown. It is also evident that a qualitative change has taken place in the nature of the activity: it has changed from random fluctuations to random bursts. Figures 2.18 and 2.19 make this clear.

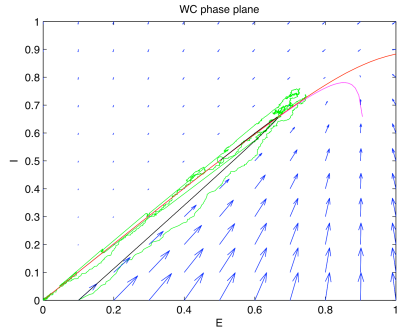

Figure 2.17: Phase plane plots of the activity shown in Figure 2.16 showing the vector field (blue) and nullclines $\dot{E} = 0$ (magenta) and $\dot{I} = 0$ (red), of Equation 2.1 and plots of a deterministic (black) and a stochastic (green) trajectory starting from identical initial conditions. Redrawn from [11].

2.5.2 Symmetries and power laws

It will be seen that the simulations described above, in which the network symmetry represented in Equation 2.17 is present, have uncovered an important property, namely that a stochastic version of Equation 2.7 incorporating such a symmetry can spontaneously gener-

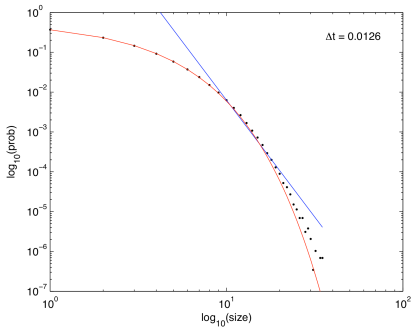

Figure 2.18: Network Burst Distribution in number of spikes, together with Geometric (red) and Power Law (blue) fit; Δt, the mean inter-spike interval, is the time bin used to calculate the distribution, and $\beta = -1.62$ is the slope exponent of the fit. Simulation using the Gillespie algorithm with parameter values $h_E = h_I = 0.001$, $w_0 = w_E - w_I = 0.2$, and $w_E + w_I = 0.8$. [Redrawn from [11].

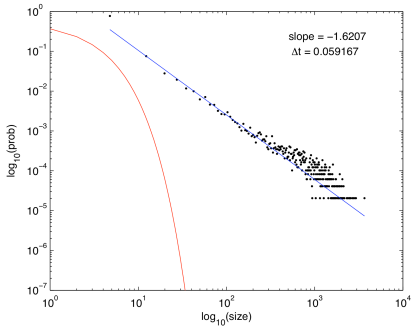

Figure 2.19: Network Burst Distribution in number of spikes, together with Geometric (red) and Power Law (blue) fit; Δt, the mean inter-spike interval, is the time bin used to calculate the distribution, and β is the slope exponent of the fit. Simulation using the Gillespie algorithm with parameter values $h_E = h_I = 0.001$, $w_0 = w_E - w_I = 0.2$, and $w_E + w_I = 13.8$. Redrawn from [11].

ate random activity in the form of bursts, whose statistical distribution is a power law. The other important property concerns the basic network dynamics generating such bursts.

We first note the experimental data provided by DeLisle Burns, [22], and Beggs & Plenz, [9], described in the introduction, and then we discuss the underlying neurodynamics. The main result of the Beggs-Plenz observations is that isolated slices generate bursting behavior similar to that found in the simulations, with a Power Law burst distribution with slope exponent of $\beta = -1.5$. This should be compared with the simulation data shown in Figure 2.18 in which $\beta = -1.62$. Note however that the geometry of our network simulation is not comparable with that of a cortical slice. It remains to carry out simulations of the stochastic version of Equation 2.7 on a 2-dimensional lattice. Work on this is currently ongoing. In any event, the Beggs-Plenz paper generated a great deal of interest in the possibility of critical behavior in the sense of statistical physics existing in stochastic neural dynamics, including the possibility that brain dynamics exhibits self-organized criticality. In the later parts of this chapter, we briefly address this possibility.

Random bursting

We turn now to the neuro-dynamics underlying random bursting. We first note that the fixed point of the dynamics remains unchanged as $w_E + w_I$ increases from $0.8 \to 13.8$, and $n_E = n_I$. We also recall Equation 2.18 that $w_E - w_I = w_0 = 0.2$, so that as the network begins to fire in random bursts,

$$w_0 \ll w_E + w_I \tag{2.19}$$

This inequality has a number of consequences. (see [11] and [81] for details.) Most importantly, it allows a particular change of variables in Equation 2.12 extended to include

inhibition.

$$\begin{aligned} \frac{d\langle n_E(t)\rangle}{dt} &= -\alpha\langle n_E(t)\rangle + (1 - \langle n_E(t)\rangle) f[\langle s\rangle] \\ \frac{d\langle n_I(t)\rangle}{dt} &= -\alpha\langle n_I(t)\rangle + (1 - \langle n_I(t)\rangle) f[\langle s\rangle] \end{aligned} \tag{2.20}$$

where $\langle s\rangle = w_E n_E - w_I n_I + h$, and $\langle n_E\rangle$ and $\langle n_I\rangle$ are interpreted as the mean fractions of activated neurons in the network. Now introduce the change of variables

$$\Sigma = \frac{1}{2}(n_E + n_I), \quad \Delta = \frac{1}{2}(n_E - n_I) \tag{2.21}$$

so that Equation 2.20 transforms into the equation

$$\begin{aligned} \frac{d\langle \Sigma(t)\rangle}{dt} &= -\alpha\langle \Sigma(t)\rangle + (1 - \langle \Sigma(t)\rangle) f[\langle s\rangle] \\ \frac{d\langle \Delta(t)\rangle}{dt} &= -\langle \Delta(t)\rangle(\alpha + f[\langle s\rangle]) \end{aligned} \tag{2.22}$$

Such a transformation was introduced into neural dynamics by Murphy and Miller, [81], and used by Benayoun *et al*, [11]. But it was introduced much earlier by Janssen, [61], in a study of the statistical mechanics of stochastic Lotka-Volterra population equations on lattices, which are known to be closely related to stochastic neural population equations on lattices, [31].

The important point about the transformed equations is that they are *decoupled*, with the unique stable solution $(\Sigma_0, 0)$, which is equivalent to $n_E = n_I$ in the original variables. This is precisely the stable fixed point used in the simulations. Note also that in the new variables Σ and Δ, the fixed point current is

$$s = w_0\Sigma + (w_E + w_I)\Delta + h \tag{2.23}$$

So at the stable fixed point $(\Sigma_0, 0)$, $s = w_0\Sigma_0 + h$. Near such a fixed point, Δ is only weakly

sensitive to changes in Σ, and Σ_0 is unchanged when varying $w_E + w_I$ for constant w_0. Murphy & Miller called Equation 2.20 an *effective feedforward system* exhibiting a balance between excitatory and inhibitory currents, and a *balanced amplification* of a stimulus h.

We can now perform a system-size expansion of the associated master equations, as in [11], to obtain a two component linear Langevin equation for small Gausssian fluctuations about the stable fixed point $(\Sigma_0, 0)$. This takes the form

$$\frac{d}{dt}\begin{pmatrix} \xi_\Sigma \\ \xi_\Delta \end{pmatrix} = \begin{pmatrix} -\lambda_1 & w_{\text{ff}} \\ 0 & -\lambda_2 \end{pmatrix}\begin{pmatrix} \xi_\Sigma \\ \xi_\Delta \end{pmatrix} + \sqrt{\alpha\Sigma_0}\begin{pmatrix} \eta_\Sigma \\ \eta_\Delta \end{pmatrix} \tag{2.24}$$

where the eigenvalues are $\lambda_1 = (\alpha + f[s_0]) + (1 - \Sigma_0)w_0 f'[s_0]$ and $\lambda_2 = (\alpha + f[s_0])$, and $w_{\text{ff}} = (1 - \Sigma_0)(w_E + w_I)f'[s_0]$. The Jacobian matrix

$$A = \begin{pmatrix} -\lambda_1 & w_{\text{ff}} \\ 0 & -\lambda_2 \end{pmatrix}$$

is upper triangular and has eigenvalues $-\lambda_1$ and $-\lambda_2$. It follows that when w_0 is small and positive, then so are the eigenvalue magnitudes λ_1 and λ_2. So, the eigenvalues are small and negative and the fixed point $(\Sigma_0, 0)$ is weakly stable. Evidently A lies close to the matrix

$$B = \begin{pmatrix} 0 & w_{\text{ff}} \\ 0 & 0 \end{pmatrix} = \begin{pmatrix} 0 & 1 \\ 0 & 0 \end{pmatrix} w_{\text{ff}} = \bar{B} w_{\text{ff}}$$

But, the matrix $\bar{B}$ is the signature of the *normal form* of the Bogdanov-Takens bifurcation, [58]. Thus, the weakly stable node lies close to a Bogdanov-Takens bifurcation, as we have suggested.

2.5.3 Intrinsic fluctuations at a marginally stable fixed point

We now turn to case 2, in which the network dynamics is at a marginally stable fixed point. As we showed earlier, such a fixed point is a Bogdanov-Takens point. We cannot use the system-size expansion at such a point, but we can use the methodology and formalism of statistical field theory found in [20], [21], [33]. For the neural dynamics considered in this chapter, case 1 applies: the resting and driven activities are all at or near a weakly stable fixed point. Despite this, the fact that the fixed point is only weakly stable indicates that the resting and weakly-driven states lie in what has been called the *fluctuation-driven* region near the marginally stable fixed point, [26]. Thus, we need to outline some of the results of the analysis of case 2. The reader is referred to the details in Chapter 3 and Appendix A of this text or the article by Cowan *et al*, [34].

The basic result is that the stochastic equivalent of the Bogdanov-Takens bifurcation is the critical point of a *directed percolation* phase transition, or DP, [56]. In DP, there are two stable states, separated by a marginally stable critical point. One of these is an *absorbing* state, corresponding to the neural population state in which all neurons are quiescent, so that the mean number of activated states or *order parameter* $\langle n \rangle = 0$. The other is one in which many neurons are activated, so that $\langle n \rangle \neq 0$ in the *activated* state. At a critical point, the quiescent state becomes marginally stable and is driven by fluctuations into the activated state.

What is important for the present study is that in the neighborhood of such a critical point, i.e. in the fluctuation-driven regime, there are two significant features of the activity which relate to the experimental data we have described: (a) the resting behavior shows random burst behavior whose statistical signature is consistent with DP, i.e., the distribution of bursts follows a power law with slope exponent -1.5, which is the slope of several forms of random percolation, including what is called mean-field DP as in [9] and [5]; (b) intrinsic *correlations* are large, and pair-correlations extend over significant cortical distances, [98].

2.6 Modeling the experimental data

2.6.1 Resting activity

Random burst activity

Assuming that the resting state occurs in the neighborhood of a weakly stable node or focus, to start with, we can use the results of the system-size expansion of the E-I master equation described earlier. The conclusion we reach is that when there is a *balance* between excitation and inhibition, so that the network is at a weakly stable node, or possibly a focus, then random burst behavior with a power law slope exponent close to -1.5 is seen, [11]. This is the result shown in Figures 2.14-2.19, and of course the result is also completely consistent with the Beggs-Plenz data plotted in Figures 2.5-2.6. We also note that these results are completely consistent with our recent analysis, Cowan *et al*, [34] and [35], and with recent experimental data that demonstrates the sub-criticality of the resting state by Priesemann *et al*, [93].

Pair correlations

With regards to pair correlations associated with resting or spontaneous activity, we refer to Figure 2.9 in which the measured resting pair correlations fall off with separation distance between electrodes, in both cats and monkeys. This finding can be replicated within the theoretical framework we have established in two differing ways. (a) We first make use of Equation 2.7, the mean-field Wilson-Cowan equations for the 1D-spatial case, and simply add δ-correlated Gaussian noise to the equations. The resulting pair correlation function for resting activity is shown in the left panel of Figure 2.20. (b) We then use the stochastic Wilson-Cowan master equation introduced in Equation 2.12, extended to the spatial case. In such a case, the noise is multiplicative and intrinsic. To simulate the Markov process derived from this model, we used the Gillespie algorithm, [49]. These simulations of the behavior of

Wilson-Cowan equations replicate, very accurately, the pair correlation behavior shown in Figure 2.9, reported in [82], both for resting activity, and for driven activity.

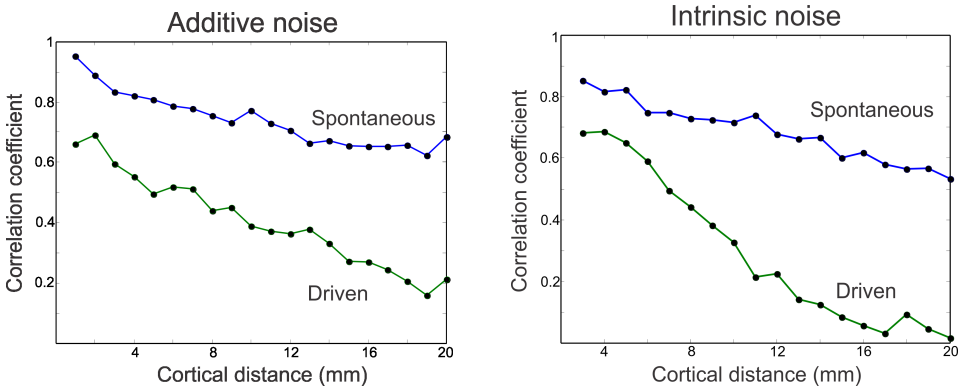

Figure 2.20: The left panel shows the pair correlation function for resting and driven activity with additive Gaussian noise. The right panel shows the pair correlation function for resting and driven activity with intrinsic noise, averaged over many simulations using the Gillespie algorithm [49].

2.6.2 Driven activity

A plot of the results for varying strengths of the external stimulus is found in Figure 2.21. Notice that we find multiple thresholds, the first of which is the bifurcation from no active transient behavior to damped traveling activity. A simulation of this mode is seen in the left panels of Figure 2.22. Increasing the input strength, we find another threshold where the damped traveling waves extend to the boundary of the 1-dimensional lattice. Here, it is likely that edge effects cause the wave to decay. Because of this uncertainty, we cannot be positive that the wave takes the same analytic form as it does for smaller input strengths. The final threshold appears when the strong stimulus disrupts the functional connectivity, a point we will discuss later, and eliminates traveling behavior. The result is a localized response as seen in the right panels of Figure 2.22.

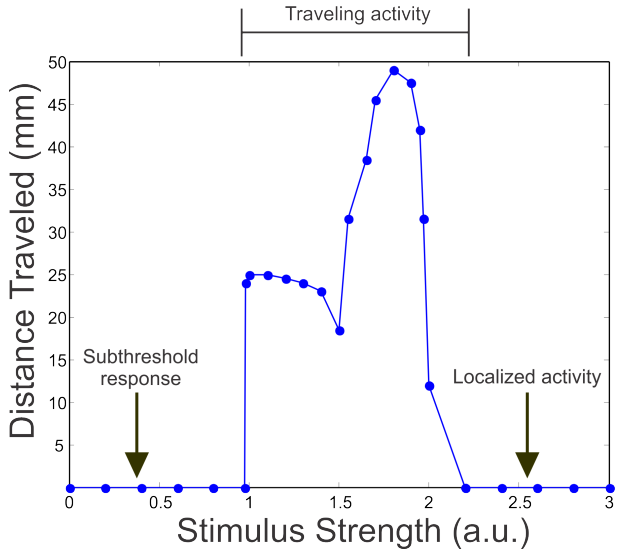

Figure 2.21: Plot of the distance traveled of activity as a function of input strength. It is clear that around a stimulus strength of 1 (arbitrary units) spreading occurs. If the stimulus strength increases further, the traveling wave eventually extends out to the end of the lattice before localization occurs. For all values larger than ≈ 2.2 the response does not spread.

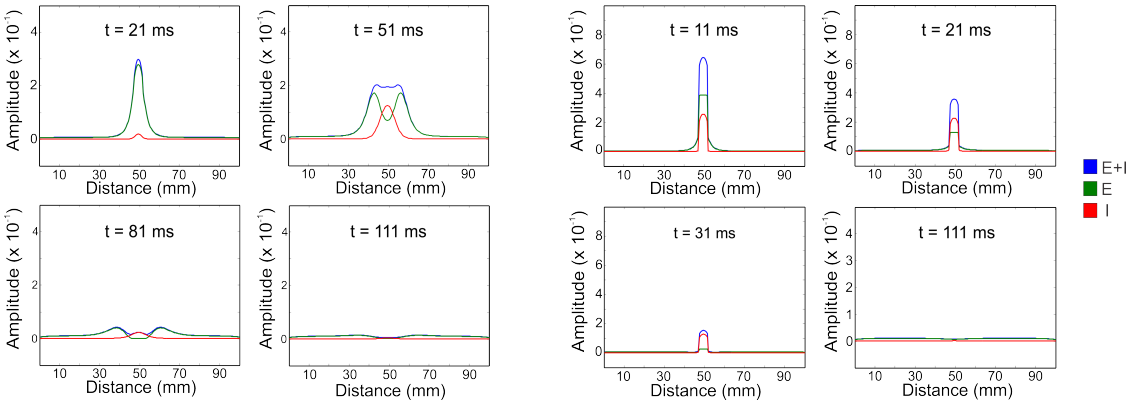

Figure 2.22: The left panel shows a damped traveling wave at four different snapshots with a stimulus strength of 1.2 a.u. The wave propagates approximately 2 times the spatial profile of the wave. The right panel shows localized behavior with no spreading and a stimulus strength of 2.8 a.u. Notice in the second time plot that inhibition has overtaken excitation and the activity remains localized.

Weak stimuli

We now investigate the results reported by Carandini *et al*, such as [12], [82], and [83], of traveling, decaying waves seen in LFP, shown in Figures 2.7-2.8; and by Muller & Destexhe, [79], in VSD recordings, in response to brief weak current pulses. These results can be replicated quite precisely in simulations of Equation 2.8, in which the network dynamics is near the balanced state in which $E \approx I$. Again, the left panels of Figure 2.22 and top row of Figure 2.23 show a simulation of this behavior. These results should be compared with those plotted in Figure 2.7. One important point to mention is that when activity spreads, on the propagating wavefront, excitation (green in Figure 2.22) is much larger than inhibition (red in Figure 2.22), but behind it, inhibition is large enough to cause the wave to dampen. Without this effect, damped traveling waves cannot occur because they would either not spread at all or would travel to infinity. From the simulations shown here, it should be clear that we can replicate the Carandini *et al* data very closely.

Strong stimuli

The other result reported by Carandini *et al* is that for strong stimuli the resulting LFP does *not* propagate very far, and remains localized. This property was actually reported in Wilson & Cowan's 1973 paper, [125]. The right panels of Figure 2.22 and bottom row of Figure 2.23 show a simulation of this dynamical mode, again in which the network state is approximately balanced. It is clear that the response does not move at all, owing to the fact that inhibition overtakes excitation at an early time, preventing any traveling behavior.

2.6.3 Explaining the differing effects of weak and strong stimuli

It is evident that there are big differences between the effects produced by weak and strong stimuli. What is the cause of such differences? Given that the only parameter in the Wilson-Cowan equations that is varied in the two cases is the stimulus intensity, this suggests that

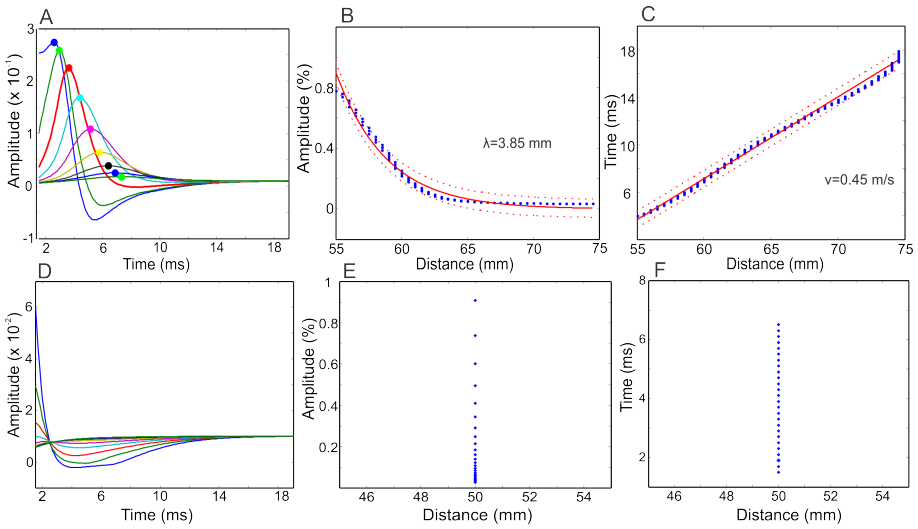

Figure 2.23: A. Variation in the LFP amplitude of decaying waves. The largest amplitude is the initial response to a brief weak current pulse. B. The exponential decay of the LFP amplitude, as a function of distance traveled. C. Time-Distance plot of the peak amplitude indicating that the velocity of wave propagation is constant at about 0.45 m $\sec^{-1}$. D. Localized LFP in response to a strong current pulse. E. Rapid decay of the amplitude which does not move F. No propagation of the LFP.

the property which causes the different responses is the level of inhibition. It must, therefore, be the case that the threshold for inhibitory activity is set high enough that weak stimuli do not trigger inhibitory effects, whereas strong enough stimuli do trigger such effects. Thus, it's clear that inhibition is the key to explaining why propagation gets blocked in LFP and VSD recordings. Put another way, external stimuli disrupt the functional connectivity of a network via activation of the inhibitory neurons, which prevent the excitatory ones from generating traveling waves. Indeed, this is one of the possibilites suggested by Carandini *et al* in their papers.

This possibility is also consistent with the effects of stimuli on pair correlations. We predict that the pair correlation function should falloff more slowly in the case of resting or weakly driven activity, than in the case of stronger stimuli. As of now, preliminary results from simulations do show this effect. Such a conclusion would be consistent with the suggestions of Churchland *et al*, [30], that one effect of stimuli is to lower noise levels.

2.7 Discussion

The main results described in this chapter concern the use of the the Wilson-Cowan equations to analyze the dynamics of large populations of interconnected neurons. Early workers, including Shimbel and Rapaport, [99], and Beurle, [15], appreciated the need to use a statistical formulation of such dynamics, but lacked the techniques to go beyond mean-field theory. The Wilson-Cowan equations, [125] and [126], were the first major attempt at a statistical theory, but still lacked a treatment of 2nd and higher moments. However, what the equations did describe was mathematical conditions for *attractor* dynamics. Further work by Ermentrout and Cowan, found in [42], [43], and [44], by Borisyuk and Kirillov, [17], and by Hoppenstaedt and Izhikevich, in [58] and [60], used the mathematical techniques of bifurcation theory to more fully analysis such dynamics. The main result was that neural population dynamics is organized around a Bogdanov-Takens bifurcation point, in the neighborhood of which (in a phase space of two control parameters) are Saddle-Node and Andronov-Hopf bifurcations. Thus neural network dynamics contains locally stable equilibria in the form of stationary and oscillatory attractors.

The problem of going beyond the mean-field regime proved to be very difficult. Some progress was made by Ohira and Cowan, [88], formulating stochastic neural dynamics in the neighborhood of a stable stationary equilibrium as a random Markov process and using the Van Kampen system-size expansion, [116]. Further progress along these lines was made by Benayoun *et al*, [11], who formulated Equation 2.7 as a random Markov process. But Benayoun *et al* went further, by incorporating some symmetries into Equation 2.7 discovered by Murphy and Miller, [81], which, in retrospect, located the stationary equilibrium of the equations near a Bogdanov-Takens point. The result was that the stochastic version of Equation 2.7 generates the random bursts of activity we now refer to as *avalanches*. In addition, the avalanche distribution was that of a power law, with a slope exponent of $\beta = 1.6$. This value is close to that observed by Beggs and Plenz, [9], in their observations of neural activity in an isolated cortical slab, of avalanche distributions with a slope exponent

of $\beta = 1.5$.

There remained the problem of developing a statistical theory for the fluctuations about a marginally stable critical point, such as a Bogdanov-Takens point. This problem was formulated by Cowan, [33], and solved by Buice & Cowan in [20] and [21]. This is a major result since it connects the theory of stochastic neural populations at a critical point, with many well studied examples of other populations of interconnected units. Examples include percolation in random graphs, branching and annihilating random walks, catalytic reactions, interacting particles, contact processes, nuclear physics, and bacterial colonies. Many of these processes are subject to a phase transition, known as a directed percolation phase transition (DP). and all these processes have the same statistical properties, including the appearance of random bursts or avalanches.

However, although the statistical theory is relevant to the pair-correlation problem, it is the mean-field Wilson-Cowan equations that proved to be necessary and sufficient to analyze neocortical responses to brief stimuli, both weak and strong.

CHAPTER 3

SELF-ORGANIZED CRITICALITY AND NEAR CRITICALITY IN NEURAL NETWORKS

3.1 Introduction

Ideas about criticality in non-equilibrium dynamical systems have been around for at least fifty years or more. Criticality refers to the fact that nonlinear dynamical systems can have local equilibria that are stable, in which case the system remains there, or marginally stable, so that small perturbations can drive the system away from the local equilibria towards one of several locally stable equilibria. In physical systems such marginally stable states manifest in several ways, in particular if the system is spatially as well as temporally organized, then long-range correlations in both space and time can occur, the statistics of the accompanying fluctuating activity becomes non-Gaussian, and in fact is self-similar in its structure, and therefore follows a power law. Bak *et al*, [8], introduced a mechanism whereby such a dynamical system could self-organize to a marginally stable critical point, which they called *self-organized criticality*. Their paper immediately triggered an avalanche of papers on the topic, not the least of which was a connection with $1/f$ or scale-free noise. However it was not until another paper appeared, by [48], which greatly clarified the dynamical prerequisites for achieving SOC, that a real understanding developed with the essential requirements for SOC: (1) an *order-parameter* equation for a dynamical system with a time-constant τ_o, with stable states separated by a threshold, (2) a *control-parameter* equation with a time-constant τ_c which tunes the system, and (3) a steady *driving force*. In Bak *et al*'s classic example, the sand-pile model, the order parameter is the rate of flow of sand grains down a sand-pile, the control parameter is the sand-pile's slope, and the driving force is a steady flow of grains of sand onto the top of the pile. Gil and Sornette showed that if $\tau_o \ll \tau_c$ then the resulting avalanches of sand down the pile would have a scale-free distribution, whereas if $\tau_o \gg \tau_c$ then the distribution would also exhibit one or more large avalanches.

In this chapter, we analyze two neural network models. The first is in one-to-one correspondence with the Gil-Sornette SOC-model, and therefore also exhibits SOC. The second is more complex and instead of SOC it self-organizes to a weakly stable local equilibrium near a marginally stable critical point. We therefore refer to this mechanism as *self-organized near-criticality*, or SONC.

3.2 Neural network dynamics

Consider first the mathematical representation for the dynamics of a neocortical slab, comprising of N excitatory neurons in a single spatially homogeneous network. Such neurons make transitions from a quiescent state q to an activated state a at the rate f and back again to the quiescent state q at the rate α, as shown in Figure 3.1.

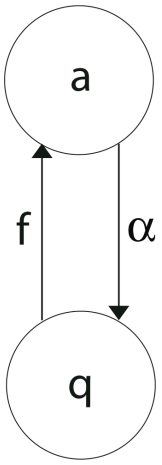

Figure 3.1: Neural state transitions. a is the activated state of a neuron, q is the inactivated or quiescent state, α is a decay constant, f depends on the number of activated neurons connected to the nth neuron, and on an external stimulus h.

From here, it is straight-forward to write down a master equation describing the evolution of the probability distribution of neural activity $P_n(t)$ in such a network. We consider n active excitatory neurons, each becoming inactive at rate α. This causes a flow of rate α out of the state, which we call n, proportional to $P_n(t)$, hence a term $-\alpha n P_n(t)$. Similarly, the flow into state n from state $n+1$, caused by one of $n+1$ active excitatory neurons becoming

inactive at rate α, gives a term $\alpha(n+1)P_{n+1}(t)$. The net effect is a contribution

$$\alpha\left[(n+1)P_{n+1}(t) - nP_n(t)\right]. \tag{3.1}$$

In state n, there are $N-n$ quiescent excitatory neurons, each prepared to spike at the rate $f\left(s_E(n)\right)$, leading to a term $-(N-n)f\left(s_E(n)\right)P_n(t)$, where the total input is

$$s_E(n) = I(n)/I_{\mathrm{RH}} = \Sigma_i(\Sigma_j w_{ij} n_j + h_{E,i})/I_{\mathrm{RH}} \tag{3.2}$$

and $f(s_E(n))$ is the function shown in Figure 3.2.

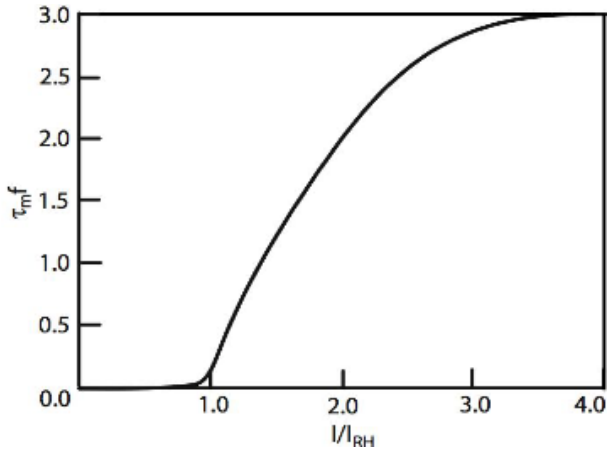

Figure 3.2: Graph of the firing rate function $f[s(I)]$. $\tau_m = 1/\alpha = 3$ is the membrane time constant (in ms) and $s(I) = I/I_{\mathrm{TH}}$ is the input current, where $I_{\mathrm{TH}} \equiv I_{\mathrm{RH}}$ is the threshold or *rheobase* current.

Correspondingly, the flow into the state n from $n-1$ due to an excitatory spike is given by $(N-(n-1))f\left(s_E(n-1)\right)P_{n-1}(t)$. The total contribution to the master equation from excitatory spikes is then

$$(N-n+1)f\left(s_E(n-1)\right)P_{n-1}(t) - (N-n)f\left(s_E(n)\right)P_n(t). \tag{3.3}$$

Putting all this together, the probability $P_n(t)$ evolves according to the master equation

$$\begin{aligned}\frac{dP_n(t)}{dt} &= \alpha\left[(n+1)P_{n+1}(t) - nP_n(t)\right] \\ &+ \left[(N-n+1)f\left(s_E(n-1)\right)P_{n-1}(t) - (N-n)f\left(s_E(n)\right)P_n(t)\right] \end{aligned} \tag{3.4}$$

Using standard methods it is easy to derive an equation for the evolution of the average number $\langle n(t)\rangle$ of active neurons in the network. The resulting equation takes the form

$$\frac{d\langle n(t)\rangle}{dt} = -\alpha\langle n(t)\rangle + (N - \langle n(t)\rangle)f\left(\langle s_E(n)\rangle\right) \tag{3.5}$$

where $\langle s_E(n)\rangle = w_{EE}\langle n\rangle + h_E$, and Equation 3.5 is the simplest form of the Wilson-Cowan equations, [126]. This mean-field equation can be obtained in several ways, in particular it can be obtained using the van Kampen "system-size expansion", mentioned in the previous chapter, of the master equation about a locally stable equilibrium or fixed point of the dynamics, [116]. However such an expansion breaks down at a marginally stable fixed point, which is the situation to be analyzed in detail in this chapter, and a different method must be used to analyze such a situation.

Before proceeding further we note that it is straightforward to extend these equations to deal with spatial effects. In such a case the variable $n(t)/N$ is extended to $n(\mathbf{x}, t)$ which represents the *density* of active neurons at the location $\mathbf{x}$ at time t, and the total input $s_E(n)$ becomes the current density

$$s_E(n(\mathbf{x})) = \int d^d x' w_{EE}(\mathbf{x} - \mathbf{x}')n(\mathbf{x}') + h_E(\mathbf{x}) \tag{3.6}$$

3.2.1 Stochastic effects near a critical point

To deal with the effects of fluctuations near criticality we use the methods of statistical field theory. Essentially we rewrite the solution of the spatial master equation in the form

of a Wiener path integral. We then apply the Renormalization Group method [127], to calculate the statistical dynamics of the network at the marginally stable (or critical) points. The details of this procedure can be found in [34]. The main result is that the random fluctuations about such a critical point have the statistical signature of a certain kind of percolation process on a discrete lattice, called *directed percolation*. Such a random process is similar to isotropic percolation which occurs in the random formation of chemical bonds, except that there is a direction, which in the neural network case is time, to the process. The statistical signature of directed percolation occurs in a large class of systems, is independent of many of their various dynamical details and therefore taken to define a *universality class*. It is found in random contact processes, branching and annihilating random walks, predator-prey interactions in population dynamics, [56], and even in bacterial colonies growing in Petri dishes, [68]. Thus stochastic neural networks described by the simple Markov process we depicted in Figure 3.1 exhibit a non-equilibrium phase transition whose statistical signature is that of directed percolation, [19].

In what follows we describe how these methods and results can be used to provide insights into the nature of fluctuating neural activity found in fMRI, EEG and local field potentials both in cortical slices and slabs and in the intact neocortex.

3.2.2 Annihilation and creation operators

We begin by defining an $N = 0$ network vector to be

$$|\text{Network with 0 neurons}\rangle = |0\rangle \tag{3.7}$$

We next introduce Fock space *annihilation* and *creation* operators satisfying boson commu-

tation rules

$$
\begin{aligned}
[a_i, a_j^\dagger] &= [q_i, q_j^\dagger] = \delta_{ij} \\
[a_i, a_j] &= [a_i^\dagger a^\dagger{}_j] = 0 \\
[q_i, q_j] &= [q_i^\dagger, q_j^\dagger] = 0
\end{aligned} \tag{3.8}
$$

Such operators act on a Fock space state vector $|n_i\rangle$ representing n_i activated neurons at the ith site, and its dual, so that

$$
\begin{aligned}
a_i^\dagger |n_i\rangle &= |n_i + 1\rangle, \quad a|n_i\rangle = n_i |n_i - 1\rangle \\
\langle n_i | a_i^\dagger &= \langle n_i - 1 | n_i, \quad \langle n_i | a = \langle n_i + 1|
\end{aligned} \tag{3.9}
$$

These operate on the *vacuum* vector $|0\rangle$ to generate vectors comprising activated or quiescent neurons. The configuration space vector $|\nu\rangle$ is thus generated as

$$
|\nu\rangle = \Pi_{i=1}^{2^N} \Phi^\dagger_{\nu_i i} |0\rangle \tag{3.10}
$$

where

$$
\Phi^\dagger_{\nu_i i} = \begin{cases} a_i^\dagger & \text{if } \nu_i = 1 \\ q_i^\dagger & \text{if } \nu_i = 0 \end{cases} \tag{3.11}
$$

and the dual configuration space vector $\langle\nu|$ is generated as

$$
\langle\nu| = \Pi_{i=1}^{2^N} \langle 0 | \Phi_{\nu_i i} \tag{3.12}
$$

where

$$
\Phi_{\nu_i i} = \begin{cases} a_i & \text{if } \nu_i = 1 \\ q_i & \text{if } \nu_i = 0 \end{cases} \tag{3.13}
$$

Inner products in the resulting vector space are generated by $\langle 0|0\rangle = 1$ and the commutation

relations in Equation 3.8.

3.2.3 A neural state vector and expectation values

We now define a network state vector as the weighted sum over all configurations, where the weight is the probability distribution given in the master equation,

$$|\phi(t)\rangle = \sum_{\nu} P(\nu, t)|\nu\rangle \tag{3.14}$$

Let

$$|p\rangle = \exp\left(\sum_{i=1}^{N} a_i^\dagger\right)|0\rangle \tag{3.15}$$

If we apply the dual vector $\langle p|$ to the state $|\phi(t)\rangle$ we obtain

$$\langle p|\phi(t)\rangle = \sum_{\nu} P(\nu, t) = 1, \quad \text{and} \quad \langle p|\partial_t|\phi(t)\rangle = -\langle p|\hat{H}|\phi(t)\rangle = 0$$

which is a restatement of probability conservation.

We note that applying the operator $a_i^\dagger a_i$ to the configuration vector $|\nu\rangle$ asks the question: is the ith neuron activated? If the answer is positive the operator leaves the ith state untouched, if negative the answer is 0. Thus, the operator $\sum_i a_i^\dagger a_i$ *counts* the number of activated neurons in $|\nu\rangle$. Similarly, the operator $\sum_i q_i^\dagger q_i$ counts the number of quiescent neurons in $|\nu\rangle$.

We can use the projection technique to calculate the expected number of activated neurons at the ith site using the number operator $a_i^\dagger a_i$. Let p_i be the probability that the ith neuron is activated. Then

$$\langle p|a_i^\dagger a_i|\phi(t)\rangle = \sum_{\nu} n_i P(\nu, t) = \langle n_i\rangle = p_i \tag{3.16}$$

In similar fashion

$$\langle p|a_i^\dagger a_i a_j^\dagger a_j|\phi(t)\rangle = \sum_\nu n_i n_j P(\nu,t) = \langle n_i n_j\rangle = p_{ij} \tag{3.17}$$

In the model considered here n_i and n_j are restricted to the values 0 and 1. This restriction is achieved using the microscopic occupancy condition,

$$a_i^\dagger a_i + q_i^\dagger q_i = 1 \tag{3.18}$$

All configurations in the vector space $|\nu\rangle$ are thus restricted, and are called *physical* states.

Finally, we note that we can use the commutation rules introduced in Equation 3.8 to commute $\exp(\sum_i a_i^\dagger)$ all the way to the right in expectation values, so that they take the form of a *vacuum expectation* value $\langle A\rangle = \langle 0|A|0\rangle$. It can be shown that this is equivalent to the shift $a_i^\dagger \to a_i^\dagger + 1$, so that $a_i^\dagger a_i \to a_i^\dagger a_i + a_i$. We will employ this shift shortly.

3.2.4 A neural master equation

We now construct a neural master equation using the operators introduced above, as

$$\frac{d}{dt}|\phi(t)\rangle = \sum_i \left[\alpha(1-a_i^\dagger)a_i + (a_i^\dagger - 1)(1-a_i^\dagger a_i) f[s(I_i)]\right]|\phi(t)\rangle \tag{3.19}$$

or formally as

$$\frac{d}{dt}|\phi(t)\rangle = -\hat{H}|\phi(t)\rangle \tag{3.20}$$

where

$$-\hat{H} = \sum_i \left[\alpha(1-a_i^\dagger)a_i + (a_i^\dagger - 1)(1-a_i^\dagger a_i) f[s(I_i)]\right] \tag{3.21}$$

is the *quasi-Hamiltonian* operator.

This operator is constructed by noting that

$$\left[\alpha(1-a_i^\dagger)a_i + (a_i^\dagger - 1)(1-a_i^\dagger a_i)f[a_i^\dagger a_i]\right]|\nu_i\rangle \tag{3.22}$$

only gives a non-zero contribution from the first term when $\nu_i = 1$ and a contribution from the second term when $\nu_i = 0$. Thus it correctly represents the transitions between quiescence and activation in the neuron at the site i, and the factor $1-a_i^\dagger a_i = q_i^\dagger q_i$ eliminates the q-state variable from the expression, by using Equation 3.18 to limit occupancy at the site i to one state. (See [117] and [109].)

3.2.5 From bosons to coherent states

Equation 3.20 is a linear operator equation with formal solution

$$|\phi(t)\rangle = \exp\left[-\hat{H}(t-t_0)\right]|\phi(t_0)\rangle$$

We need to re-express this solution in terms of complex numbers rather than operators in order to solve for the probability distribution. This can be achieved by introducing *coherent states*. These were introduced by Schrödinger [97] and first used extensively in coherent optics by Glauber [52]. We therefore introduce such states $|\varphi_i\rangle$ in the form

$$|\varphi_i\rangle = \exp[-\frac{1}{2}\varphi_i^\star\varphi_i + \varphi_i a_i^\dagger]|0_i\rangle \tag{3.23}$$

where φ_i is the right eigenvalue of a_i, i.e. $a_i|\phi_i\rangle = \varphi_i|\phi_i\rangle$. There is also a coherent state representation of q_i in the form $|\vartheta_i\rangle$ such that the right eigenvalue of q_i is ϑ_i, i.e. $q_i|\vartheta_i\rangle = \vartheta_i|\vartheta_i\rangle$. In similar fashion $\langle\varphi_i|a_i^\dagger = \langle\varphi_i|\tilde{\varphi}_i$ where $\tilde{\varphi}_i$, the complex conjugate of φ, is the left eigenvalue of $a_i^\dagger$, and similarly $\langle\vartheta_i|q_i^\dagger = \langle\vartheta_i|\tilde{\vartheta}_i$, i.e. $\tilde{\vartheta}_i$ is the left eigenvalue of $q_i^\dagger$. It follows that

$$\langle\varphi_i|a_i^\dagger a_i|\varphi_i\rangle = \langle\varphi_i|\tilde{\varphi}_i\varphi_i|\varphi_i\rangle = \tilde{\varphi}_i\varphi_i \tag{3.24}$$

All this suggests that the operator quasi-Hamiltonian has a coherent state representation in the form

$$-\mathcal{H} = \sum_i [\alpha(1-\tilde{\varphi}_i)\varphi_i + (\tilde{\varphi}_i - 1)(1-\tilde{\varphi}_i\varphi_i)f[s(I_i)]] \tag{3.25}$$

where

$$s(I_i) \propto \sum_j w_{ij}\tilde{\varphi}_j\varphi_j + \tilde{h}_i h_i \tag{3.26}$$

We note that in transforming to the coherent state representation we must again use the commutation rules to ensure that all creation operators $a_i^\dagger$ precede the annihilation operators a_i, to produce the *normal ordered* form. Thus the normal ordered form of $a_i^\dagger a_i a_i^\dagger$ is written as $:a_i^\dagger a_i a_i^\dagger: = (a_i^\dagger)^2 a_i + a_i^\dagger$. It follows from this that we need to expand the function $f[s(a^\dagger, a)]$ in powers of $s(a^\dagger, a)$ in order to produce the normal ordered form of $\mathcal{H}$. We do this in Appendix A, but will defer including the results in the main body of the chapter until later.

3.2.6 The continuum limit of $\mathcal{H}$

The final preliminary step of this formulation is to take the *continuum limit* of the expression for $\mathcal{H}$ in Equation 3.25, so that

$$\mathcal{H} = \int d^d x\, [\alpha\tilde{\varphi}\varphi - \tilde{\varphi}(\rho - \tilde{\varphi}\varphi - \varphi)f[s(\tilde{\varphi}\varphi + \varphi)]] \tag{3.27}$$

in which $\varphi_i \to \rho\varphi(\mathbf{x}, t) \equiv \varphi$ etc., where ρ is the packing density of neurons in the neocortex, and the conjugate coherent state $\tilde{\varphi}$ has been shifted to $\tilde{\varphi} + 1$.

Note that in taking the continuum limit we make the assumption that the cortex is translation symmetric on the relevant length scales of mm to cm. This requires that we assume that $w_{ij} \to w_{i-j}$, so that in the continuum limit $w_{ij} \to w(\mathbf{x} - \mathbf{x}')$ and $\sum_j w_{ij} \to w\star$, where $\star$ is the convolution operator $\int d^d x' w(\mathbf{x} - \mathbf{x}')$.

3.2.7 Dimensions and the density representation

Before proceeding further, in order to use Renormalization Group techniques later on, we need to assign a dimension to each variable in Equation 3.27. To do so we use a modified version of the convention used in particle physics so that $[x] = L^{-1}$, $[t] = L^{-2}$, where L is the length scale used, whence $[x^2/t] = L^0$. Thus, a diffusion constant would be dimensionless; this generates a scaling commonly found in Markov random walks and related processes such as stochastic neural activity like we have here. Then, $[\alpha] = L^2$, $[\varphi] = L^d$, $[\tilde{\varphi}] = L^0$, $[\tilde{\varphi}\varphi] = L^d$, $[f[s]] = [\alpha] = L^2$. This last value of $[f[s]]$ implies that the input current function $s(\tilde{\varphi}\varphi + \varphi) = s(I) = kI$ where the constant k has the dimensions of inverse current density, so that $[s] = L^0$. The net effect of such a choice leads to the required result that $[\mathcal{H}] = L^2$.

To emphasize this choice we further transform the coherent state quasi-Hamiltonian by introducing the *density representation*,

$$\tilde{\varphi} + 1 \to e^{\tilde{n}}, \varphi \to ne^{-\tilde{n}} \tag{3.28}$$

where $n(\mathbf{x}, t)$ is the local density of activated neurons. Then, Equation 3.27 transforms into

$$\mathcal{H} = \int d^d x \, [\alpha(1 - \exp(-\tilde{n}))n - (\exp(\tilde{n}) - 1)(\rho - n)f[s(w \star n + h)]] \tag{3.29}$$

3.2.8 From the quasi-Hamiltonian to a neural path integral

Using standard methods (see [39] and [90]), Buice and Cowan [19] incorporated the quasi-Hamiltonian into the action of a Wiener path integral. This action takes the form

$$S(n, \tilde{n}) = \int \int d^d x \, dt \left[\tilde{n}\,\partial_t n + \alpha(1 - e^{-\tilde{n}})n - (e^{\tilde{n}} - 1)(\rho - n)f[s(w \star n + h)]\right] \tag{3.30}$$

The significance of this action is that it can be used to construct a generating functional for statistical moments of the probability density $P[\nu, t]$ such as the mean spike count at the location $\mathbf{x}$ at the instant t, $\langle n(\mathbf{x}, t)\rangle$, and the correlation function $\langle n(\mathbf{x}, t)\tilde{n}(\mathbf{x}', t')\rangle$, etc.

This generating functional is the path integral

$$\mathbb{Z}\left[\tilde{J}(\mathbf{x},t),J(\mathbf{x},t)\right]=\int\int\mathcal{D}n\,\mathcal{D}\tilde{n}\,e^{-\mathcal{S}(n,\tilde{n})+\tilde{J}\cdot n+J\cdot\tilde{n}}\equiv\left\langle\exp[\tilde{J}\cdot n+J\cdot\tilde{n}]\right\rangle \tag{3.31}$$

where $\mathcal{D}n\ \mathcal{D}\tilde{n}$ is the Wiener measure, and $\tilde{J}\cdot n=\int d^d\mathbf{x}\tilde{J}(\mathbf{x},t)n(\mathbf{x},t)$, etc. Functional differentiation of this and related expressions with respect to J and $\tilde{J}$, subject to the conditions $J,\tilde{J}=0$, generates the various moments and moment equations. In particular, we obtain the first moment or mean-field Wilson-Cowan equations, [125],

$$\partial_t\langle n\rangle=-\alpha\langle n\rangle+(\rho-\langle n\rangle)f[s(w\star\langle n\rangle+\langle h\rangle)] \tag{3.32}$$

Thus, the Wilson-Cowan equation is a nonlinear integro-differential equation. The derivation given here presents one way to extend these equations to a stochastic formulation that can be analyzed by the techniques of statistical field theory.

We further note that if the population activity is sparse, then $\rho-n\to\rho$ in Equation 3.30 and $1-a_i^\dagger a_i\to 1$ in Equation 3.21. These equations then become, respectively, the action and master equation for the *spiking* model described in [19] and [20], except that n_i is now interpreted as the number of spikes emitted by the ith neuron.

3.3 The dynamics of synaptic plasticity

Now that we have analyzed a network of intrinsically stochastic neurons, we turn our attention to the mathematical representation of synaptic plasticity and consider first a single excitatory neuron e_i embedded in a network E of excitatory neurons. Such a neuron receives input currents from neurons in the network, and also from a population H of other neurons outside the network as seen in Figure 3.3.

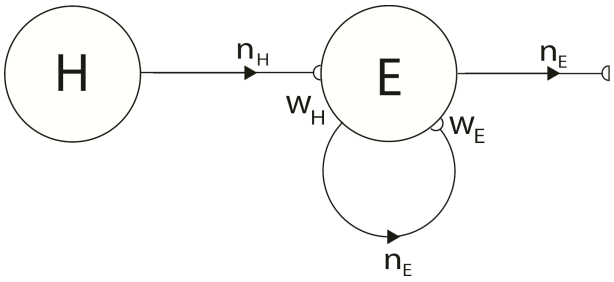

Figure 3.3: A network consisting of a recurrent excitatory population driven by the input population H, acting in a feedforward fashion through the synaptic weight w_H.

Equation 3.2 now reads

$$s(I_i) = k_i \left(\sum_j w_{ij}^E n_i + \sum_k w_{ik}^H n_k \right) \tag{3.33}$$

We consider a single input n'_k from H, acting on e_i through the synapse $w_{ik'}^H$. We can implement this by letting $w_{ik}^H \to w_{ik}^H \delta_{kk'}$, so that $\sum_k w_{ik}^H n_k \to w_{ik'}^H n_{k'}$. The continuum limit of the expression for the current from H therefore takes the form

$$\int d^d x' w_H(\mathbf{x}, \mathbf{x}') n_H(\mathbf{x}') \to \int d^d x' b_H(\mathbf{x}) \delta^d(\mathbf{x} - \mathbf{x}') n_H(\mathbf{x}') = b_H(\mathbf{x}) n_H(\mathbf{x}) \tag{3.34}$$

The synaptic weight $b_H(\mathbf{x})$ is *modifiable*. In Appendix A, we derive its mean-field equation, which takes the form

$$\frac{d\langle b_H(\mathbf{x})\rangle}{dt} = -\beta g_E(\mathbf{x}) \left(\frac{\langle n_E(\mathbf{x})\rangle}{\rho_S} - \frac{\langle n_{E,0}(\mathbf{x})\rangle}{\rho_S} - \kappa_{E,S} \langle b_H(\mathbf{x})\rangle \right) \frac{\langle n_H(\mathbf{x})\rangle}{\rho_S} \tag{3.35}$$

where β is the rate constant for weight changes, ρ_S is the density of synapses at $\mathbf{x}$, and g_E is the state-dependent function:

$$g_E(\mathbf{x}) \approx \frac{k(\mathbf{x}) F'}{1/\rho - k(\mathbf{x}) F' w_0} \tag{3.36}$$

where $F = \rho f/(\alpha + f)$, $\langle n_{E,0}(\mathbf{x})\rangle$ is a constant neural activity, w_0 is the total synaptic

weight per neuron (see Appendix A), and $\kappa_{E,S} = L(0) < 0$ is a constant derived from the *window function* $L(\Delta t)$ of spike-time dependent plasticity (STDP) used in [118]. The ratios $\langle n_E(\mathbf{x})\rangle/\rho_S$, $\langle n_{E,0}(\mathbf{x})\rangle/\rho_S$, $\langle n_H(\mathbf{x})\rangle/\rho_S$ have dimension L^0, and represent the *mean numbers of spikes* in the populations and the target rate. The expression for $g_E(\mathbf{x})$ is approximate in the sense that for values of the rate constant $\alpha \ll \beta$ it requires corrections that are nontrivial to calculate. However, experimental data suggests this range of values is not common and most of our simulations in the following sections reflect that.

In Equation 3.35 the synaptic weight $b_H(\mathbf{x})$ is depressed by an *anti-Hebbian* mechanism ($\kappa_{E,S} < 0$), and potentiated by the input activity n_H. Such an equation was first introduced in [118] for a purely feedforward circuit with no loops, and a linear firing rate function f, in which the synapse was inhibitory rather than excitatory, and Hebbian rather than anti-Hebbian. The Vogels formulation has an important property: the equation can be shown to implement gradient descent to find the minimum of an energy function, the effect of which is to balance incoming excitatory and inhibitory currents to the output neuron. This $E-I$ balance in neural networks is believed to explain a wide variety of dynamics including asynchronous network activity (see [112]). Equation 3.35 is an extension of the Vogels equation to the case of circuits with feedback loops, and a nonlinear firing rate function f, and incorporates modifiable synapses that are excitatory and anti-Hebbian. In fact, there is experimental evidence to support both kinds of synapses (see [66] and [54]). It remains to formulate an action for the master equation that generates this mean-field equation.

3.3.1 Developing an action for synaptic plasticity

To derive an action for synaptic plasticity we follow the same procedure as before. We first formulate the changes in b_H as a Markov process with discrete states in continuous time. We therefore assume that b_H is *quantized* in units of synaptic weight, and similarly for b_E. (Note: we could formulate the changes in b_H as a Markov process with continuous states and use duality to obtain a bosonic action for a discrete state Markov process [89]. Here we

proceed in the opposite direction.)

We first introduce bosonic annihilation and creation operators for b_{ik}^H. Let such operators be denoted by $b_{ik}^\dagger$ and b_{ik} respectively, and let $|b_{ik}^H\rangle$ be a column vector representing the synaptic weight b_{ik}^H such that

$$b_{ik}^\dagger|b_{ik}^H\rangle = |b_{ik}^H + 1\rangle, \quad b_{ik}|b_{ik}^H\rangle = b_{ik}^H|b_{ik}^H - 1\rangle \tag{3.37}$$

Such operators act on a configuration space built from a null synapse, i.e. a synapse with weight $b_{ik}^H = 0$. Let this be represented, again, by the vacuum vector $|0\rangle$. The configuration space vector $|\zeta\rangle$ then ranges from $b_{ik}^H = 0$ to $b_{ik}^H = (b_{ik}^H)_{\mathrm{MAX}} = M_i$ where M_i is the maximum synaptic weight per neuron, which is a limit imposed by the finite surface area of any individual neuron's membrane. Let S be the number of (effective) synapses per neuron. Then

$$|\zeta\rangle = \Pi_{i=1}^N \Pi_{k=1}^S (b^H)_{ik}^\dagger |0\rangle \tag{3.38}$$

The dual vector $\langle\zeta|$ can be defined in similar fashion, and a synaptic state vector

$$|\theta(t)\rangle = \sum_\zeta P(\zeta, t)|\zeta\rangle \tag{3.39}$$

can be introduced. The rest of the development (almost) completely parallels that for neural activity introduced earlier.

We next look at the steps necessary to construct a quasi-Hamiltonian for synaptic plasticity. The first thing to do is to model the synaptic state transitions $b_{ik}^H + 1 \to b_{ik}^H$ and $b_{ik}^H \to b_{ik}^H + 1$ as a Markov process. Following the formulation of the neural quasi-Hamiltonian in Equation 3.22 we construct a provisional synaptic quasi-Hamiltonian in the form

$$-\hat{H}_b = \sum_i \Big[\lambda(1 - b_{ik'}^\dagger)b_{ik'} + \mu(b_{ik'}^\dagger - 1)\Big] \tag{3.40}$$

where λ and μ are state-dependent rate functions. Comparison with Equation 3.35 indicates that we require

$$\lambda = \beta g_{E,i} |\kappa_{E,S}| \frac{n_{H,k'}}{\rho_S}, \quad \mu = \beta g_{E,i} \frac{(n_{E,0,i} - n_{E,i})}{\rho_S} \frac{n_{H,k'}}{\rho_S} \tag{3.41}$$

to correctly generate the mean-field equation.

Thus, we can write the quasi-Hamiltonian in the form

$$-\hat{H}_b = \sum_i \left[\beta g_{E,i} |\kappa_{E,S}| \frac{n_{H,k'}}{\rho_S} (1 - b^\dagger_{ik'}) b_{ik'} + \beta g_{E,i} \frac{(n_{E,0,i} - n_{E,i})}{\rho_S} \frac{n_{H,k'}}{\rho_S} (b^\dagger_{ik'} - 1) \right] \tag{3.42}$$

We note an important difference between this $\hat{H}_b$ and the neural quasi-Hamiltonian $\hat{H}$, apart from the fact that they work on different configuration spaces. There is no restricted occupancy condition in $\hat{H}_b$, and it is now a simple matter to introduce a coherent state representation of $\hat{H}_b$, shift to the density representation and construct the action for synaptic plasticity $S(b_H)$, and take the continuum limit. We refer the reader to Appendix A for the details. The result is

$$S(b_H) = \iint d^d x \, dt \left[\tilde{b}_H \partial_t b_H + \beta g_E |\kappa_{E,S}| \frac{n_H}{\rho_S} (1 - e^{-\tilde{b}_H}) b_H - \beta g_E (n_{E,0} - n_E) \frac{n_H}{\rho_S} (e^{\tilde{b}_H} - 1) \right] \tag{3.43}$$

where $b_H \to \rho_S b_H = b_H(\mathbf{x})$, a *weight density*, $g_{E,i} \to g_E(\mathbf{x})$, etc. Using variational techniques we can derive Equation 3.35 from $S(b_H)$.

3.4 Combining the actions

It follows from this formulation that the full action for the coupled system of equations for the evolution of n_E and b_H can be obtained simply by adding the actions $S(n_E)$ and $S(b_H)$

together. The combined action therefore takes the form

$$S(n_E, b_H) = \iint d^d x\, dt \Big[\tilde{n}_E\, \partial_t n_E + \alpha(1 - e^{-\tilde{n}_E}) n_E - (e^{\tilde{n}_E} - 1)(\rho - n) f[s(n_E)] \\ + \tilde{b}_H\, \partial_t b_H + \beta g_E |\kappa_{E,S}| \frac{n_H}{\rho_S}(1 - e^{-\tilde{b}_H}) b_H - \beta g_E (n_{E,0} - n_E) \frac{n_H}{\rho_S}(e^{\tilde{b}_H} - 1) \Big] \quad (3.44)$$

where the current $s(n_E) = k(w \star n_E + b_H \delta^d \star n_H)$. Note that the time scale of the growth and decay of neural activity is set by the constant α, whereas that of the growth and decay of synaptic plasticity is set by βg_E, which is both state and position dependent. Thus the ratio $\alpha/\beta g_E$ is an important parameter.

3.4.1 A simulation of the behavior of the combined mean-field equations

The first variation of Equation 3.44 generates the mean-field equations for n_E and b_H in the form

$$\begin{aligned} \frac{\partial_t \langle n_E(\mathbf{x}) \rangle}{\partial t} &= -\alpha \langle n_E(\mathbf{x}) \rangle + (\rho - \langle n_E(\mathbf{x}) \rangle) f[s(\langle I_E \rangle)] \\ \frac{\partial \langle b_H(\mathbf{x}) \rangle}{\partial t} &= -\beta g_E \left(\langle n_E(\mathbf{x}) \rangle - \langle n_{E,0}(\mathbf{x}) \rangle - \kappa_{E,S} \langle b_H(\mathbf{x}) \rangle \right) \frac{\langle n_H(\mathbf{x}) \rangle}{\rho_S} \end{aligned} \quad (3.45)$$

where

$$s_E(\langle I_E \rangle) = k \left(w_E \star \langle n_E \rangle + \langle b_H \rangle \langle n_H \rangle \right) \quad (3.46)$$

These equations can be simulated. The results are shown in Figure 3.4. It will be seen that in the 'ground-state' or DOWN state of low values of $N^\star = n_E^\star$ the synaptic weight b_H increases until it reaches a critical point (a saddle-node bifurcation), at which point $N^\star$ becomes unstable and the system switches to the 'excited-state' or UP state. But then the anti-Hebbian term in the synaptic plasticity dynamics kicks in, and b_H declines until the excited-state fixed-point becomes unstable at the upper critical point, (also a saddle-node bifurcation), and switches back to the ground-state fixed point, following which the hysteresis cycle starts over. This is an exact representation of the sand-pile model's behavior. The

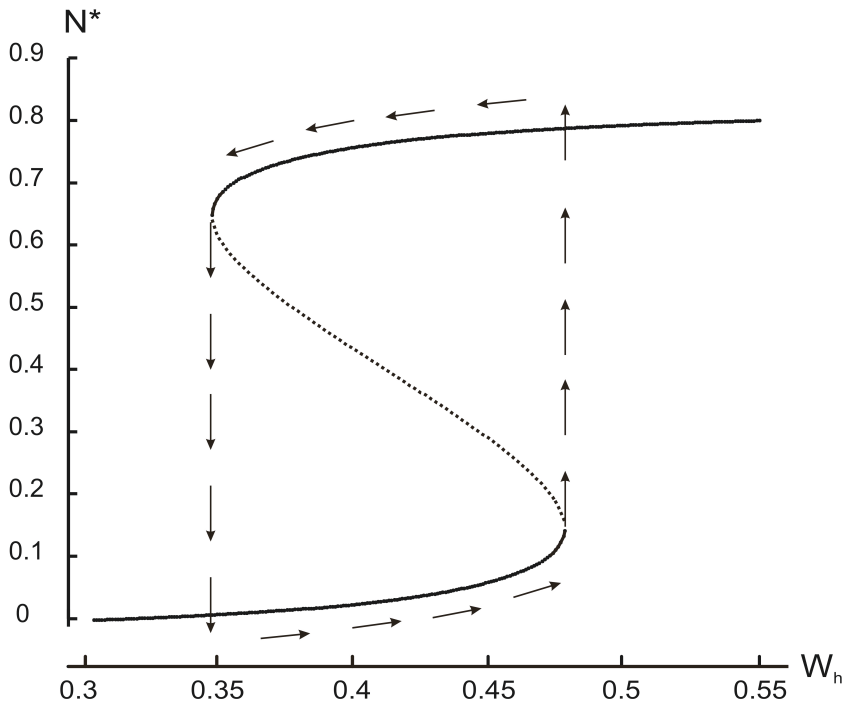

Figure 3.4: Neural state transitions between a ground state and an excited state. Parameter values: $m_E = 3, n_H = 3; \alpha = 0.2$. $N^\star$ is the fixed-point value of n_E, and W_h is the magnitude of the anti-Hebbian synapse in the input path.

reader should compare this with the synaptic mechanisms described in [73] and in [78].

3.4.2 Fluctuations around stable and marginally stable fixed points

The mean-field behavior we have described fits the Bak *et al* setup for achieving SOC very well. However, such an analysis does not account for the effects of fluctuations. We need the stochastic formulation for such a project. There are two situations to consider: (a) when the fixed point values $N^\star$ of the neural activity are stable, and (b) when $N^\star$ becomes marginally stable. In case (a) we can use the van Kampen system-size expansion [116] to develop a linear Fokker-Planck equation, and its associated linear Langevin equation to describe the fluctuations about $N^\star$. The reader is referred to [11] for an example of such a treatment in a network comprising coupled excitatory and inhibitory neurons.

3.4.3 Renormalizing the neural action

Case (b) requires a renormalization group treatment. All the details of such a treatment are described in Appendix A. We first renormalize the neural action given in Equation 3.44 in the case where the external stimulus $n_H = 0$, so that the resulting spontaneous activity is driven only by internal fluctuations.

The result is

$$S(s_E) = \int\int d^dx\, dt \left[\tilde{s}_E(\partial_t + \mu_E - D_E\nabla^2)s_E + u_E\tilde{s}_E(s_E - \tilde{s}_E)s_E\right] \tag{3.47}$$

This action is well-known: it is called Reggeon field theory, and is found in directed percolation (DP) in random graphs, in contact processes, in high-energy nuclear physics, and in bacterial colonies, all of which exhibit the characteristic properties of what is called a *universality class*, a group of mathematical models in which only certain dynamical details of the system become relevant as a specific scaling limit is reached. It also shows up in branching and annihilating random walks, catalytic reactions, and interacting particles. Thus, we

have mapped the mathematics of large-scale neural activity in a single homogeneous neural population into a percolation problem in random graphs, or equivalently into a branching and annihilating random walk. A first version of this work was presented in [19]. A more extensive paper with many applications to neuroscience was presented in [20].

Note that $\tilde{s}_E$ and s_E are scaled versions of $\tilde{n}_E$ and n_E, where the latter is no longer interpreted to be the density of activated neurons at a given location, but the *fluctuation* in n_E about the mean value $\langle n_E \rangle = n_{\mathrm{E,cl}}$, as detailed in Appendix A.2.

It is also important to note that in DP there are essentially two stable states separated by a marginally stable critical point. One of these states is an *absorbing* state, corresponding to a neural population state in which all neurons are quiescent, $\langle n \rangle = 0$ (e.g. they are all subject to an inhibitory or *hyperpolarizing* current), or a sub-threshold excitatory current. The other state is one in which many of the neurons are activated, so that $\langle n \rangle \neq 0$, i.e. the order parameter is close to zero in the lower stable state, and is non-zero in the upper stable state. At a critical point (corresponding to a saddle-node bifurcation in the mean-field analysis), the lower state with $\langle n \rangle = 0$ becomes marginally stable, and so is driven by fluctuations into the upper stable state.

Here, we note that there is an *upper critical dimension* at which directed percolation crosses over to mean-field behavior. This upper critical dimension is $d = 4$. What is the dimension of the neocortex? To answer this question we note that the neocortex can be unfolded and flattened into a slab with the dimensions 1 m $\times$ 1 m $\times$ 3 mm $= 3 \times 10^6$ mm^3. Since there are an estimated 1×10^{11} neurons in the neocortex, their packing density is $\rho = 3.33 \times 10^4$ mm^{-3}. It has been estimated that there are about 4×10^3 synaptic contacts per neuron [105]. Since about $50 - 100$ such contacts belong to a single axon, the number of neighbors per neuron is about $40 - 200$. Nevertheless, the essential physical property of the neocortex is that it is two-dimensional. Thus, the critical exponents characterizing the neural phase transition are the $d = 2$ exponents of directed percolation. These appear in the linear response of the neocortical model to an impulsive stimulus, known to mathematicians as the

Green's function and to physicists as the *propagator*, and can be calculated. Following [1], [2], and [6], this takes the general form

$$G(x,t) \overset{\substack{x^2,t\to\infty \\ \mu\to 0}}{\sim} |\mu|^{\nu(\frac{1}{2}dz-\eta)}\Phi(|\mu|^{\nu}t, |\mu|^{\nu z}x^2) \tag{3.48}$$

where $x = x_2 - x_1$, $t = t_2 - t_1$, $\mu = \mu_E$, and ν, η, and z are critical exponents that depend only on the dimension d. Φ is a universal scaling function that takes on various forms depending on whether μ is greater than or less than $\mu = 0$, the critical value.

When the network is subcritical ($\mu > 0$),

$$G(x,t) \sim g^2 t^{-d/2} e^{(-x^2/4\alpha' t - \Delta t)} \tag{3.49}$$

where $\Delta \sim |\mu|^{\nu}, \alpha' = |\mu|^{-\nu(z-1)}$, and $g^2 \sim |\mu|^{\nu(\frac{1}{2}d(z-1)-\eta)}$. We can also calculate the *susceptibility*, given by

$$\chi = \int\int d^d x\, dt\, G(x,t) \sim |\mu|^{-\gamma} \tag{3.50}$$

where $\gamma = \nu(1+\eta)$.

When the network is supercritical ($\mu < 0$),

$$G(x,t) \sim M^2 \theta(vt - |x|) \tag{3.51}$$

where $M \sim |\mu|^{\beta}, v \sim |\mu|^{\nu(1-\frac{1}{2}z)}$, and $\beta = \frac{1}{2}\nu(\frac{1}{2}dz - \eta)$. $\theta(x)$ is the Heaviside step function.

When the network is critical ($\mu = 0$),

$$G(x,t) = t^{-(\frac{1}{2}dz-\eta)}[\Phi_c(x^2/t^2) + O(t^{-\lambda})] \tag{3.52}$$

where λ is another critical exponent which describes the approach to scaling [47] and Φ_c is a scaling function calculated using a one-loop approximation. (For more details, see [3], [27], [80], and [56].)

3.4.4 Renormalizing the driven neural action

We now assume that $n_H(\mathbf{x}, t) \neq 0$, so that the function s_E now takes the form

$$s(n_E, n_H) = k(Ln_E + b_H \frac{n_H}{\rho_S}) \tag{3.53}$$

The extra term in the current $s(n_E, n_H)$ adds extra terms to the neural action. However, we show in Appendix A that all but one of the additional terms do not survive the renormalization group process, so that the renormalized action for this case takes the simpler form

$$S(s_E, s_H) = \iint d^d x\, dt[\tilde{s}_E(\partial_t + \mu_E - D_E\nabla^2)s_E + u_E\tilde{s}_E(s_E - \tilde{s}_E)s_E + v_E\tilde{s}_E s_H m_H] \tag{3.54}$$

where m_H is a scaled version of n_H.

We see that the additional term acts as a source to drive the dynamics away from the absorbing state $n_E = 0$. However, we assume that n_H is small in our network, so that the lowest value reached is $n_E \approx 0$. In other words, the character of the neural activity remains close to DP.

3.4.5 Renormalizing the synaptic plasticity action

In similar fashion the action for neural plasticity given in Equation 3.43 can be renormalized. The result derived in Appendix A is:

$$S(s_H) = \int\int d^d x\, dt\, \left[\tilde{s}_H \partial_t s_H + u_H \tilde{s}_H s_H m_H + v_H \tilde{s}_H (s_E - s_{E,0}) m_H\right] \tag{3.55}$$

The result indicates that the renormalized synaptic weight fluctuation s_H is driven by m_H and depresses or potentiates, depending on the sign of the renormalized neural activity term $s_E - s_{E,0}$. By itself, this behavior suggests that the fixed points of s_H oscillate between an upper and a lower state.

3.4.6 Renormalizing the combined action

Renormalization of the combined action is now simple. We just add together the renormalized actions for the driven neural action and the synaptic plasticity. The result is

$$S(s_E, s_H) = \iint d^d x\, dt[\tilde{s}_E(\partial_t + \mu_E - D_E\nabla^2)s_E + u_E\tilde{s}_E(s_E - \tilde{s}_E)s_E + v_E\tilde{s}_E s_H m_H + u_H\tilde{s}_H\partial_t s_H + u_H\tilde{s}_H s_H m_H + v_H\tilde{s}_H(s_E - s_{E,0})m_H] \quad (3.56)$$

We note that the last term acts as a source or sink term for s_H, depending on the sign of $s_E - s_{E,0}$. It is not clear how this term affects the nature of the fluctuations in s_E.

3.5 Simulating the effects of fluctuations

In order to gain some insight into the behavior of the network dynamics beyond the mean-field regime, we simulated the full system of coupled stochastic equations for a two-dimensional network comprising 60 x 60 excitatory neurons connected with nearest neighbor connections and toroidal boundary conditions, with each neuron receiving current pulses from all four neighbors, and also from an external cell through a modifiable synapse with weight function $w_H(\mathbf{x}, \mathbf{x}') = b_H\delta^d(\mathbf{x} - \mathbf{x}')$ such that $\int d^d\mathbf{x}' w_H \propto b_H$.

The simulations were run using the Gillespie algorithm for Markov processes (see [11]). The results are shown in Figure 3.5. It will be seen that the population behavior shown in panel (A) replicates qualitatively that shown in the phase-plane of Figure 3.4, and that the mean synpatic weight shows the oscillation-like character of the activity. Panel (B) shows the burst or avalanche-size distributions of the underlying spiking activity. Note that the fluctuations in spiking activity about the lower nullcline, or 'DOWN' state, show a power-law distribution with a slope of about -1.51, whereas those about the higher nullcline, or 'UP' state, also show a power-law distribution with a slope of about -1.31. This property is not seen in studies of the behavior of stochastic Wilson-Cowan equations for coupled $E - I$ networks with fixed synpases, reported in [11], in which the 'DOWN' state shows power-law

statistics, and the 'UP' state shows Poisson statistics. This is just the opposite of the results reported in [73] and [78], in which the 'UP' states show power-law behavior, and 'DOWN' states show Poisson behavior.

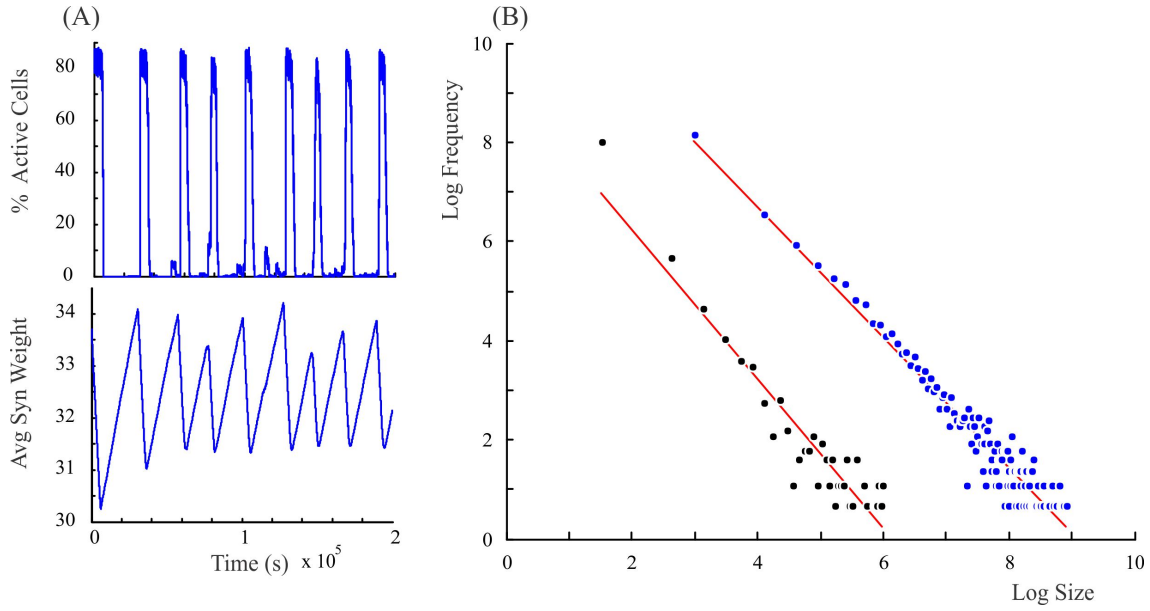

Figure 3.5: Neural state transitions between a ground state and an excited state in a two-dimensional network of 60 x 60 excitatory neurons with nearest neighbor connections. (A) Population activity and mean synaptic weight as a function of time. Activity levels display cyclic behavior, oscillating between 'UP' and 'DOWN' states. (B) Avalanche distribution of 'DOWN' states (black dots) and 'UP' states (blue dots). Parameter values: $\kappa_{E,S} = -0.001$, $n_{E,0} = 0.2$, $w_E = 4$, $\alpha = 0.2$, $\beta = 0.002$, $g_E = 1$, and $I_{RH} = 1$. $f(x)$ is the function introduced in Figure 3.2.

However, we note that the results of this simulation differ in certain respects from those obtained by Gil and Sornette [48]. In their paper, they introduced simulations performed with a choice of time constants corresponding to the ratios $\alpha/\beta = 0.01$ and 100. Both simulations produced similar power-laws for small avalanche sizes, but the latter also produced an isolated large system-size avalanche, 1.25 orders of magnitude greater than the smaller avalanches. In the simulation considered here, the ratio used is $\alpha/(\beta g_E) = 100$. The result we find is that there are two branches of power-law distributed avalanches, corresponding to the 'UP' and 'DOWN' mean-field states. The 'UP' avalanches are approximately three orders of magnitude greater than the 'DOWN' ones.

3.6 Excitatory and inhibitory neural network dynamics

Now that we have studied the case of network of excitatory neurons, we need to introduce inhibitory neurons, given that about 20% of all neurons in the neocortex are inhibitory and that the effect of such inhibition greatly changes the nature of neocortical dynamics. Thus, we now investigate a coupled $E-I$ network as seen in Figure 3.6. We need to generalize the excitatory master equation, Equation 3.4 to include inhibitory neurons. This can be done and the result is the master equation

$$\begin{aligned}
\frac{dP(n_E,n_I,t)}{dt} &= \alpha_E\left[(n_E+1)P(n_E+1,n_I,t)-n_EP(n_E,n_I,t)\right] \\
&+ \left[(N_E-n_E+1)f_E[s_E(n_E-1,n_I)]P(n_E-1,n_I,t)\right. \\
&- \left.(N_E-n_E)f_E[s_E(n_E,n_I)]P(n_E,n_I,t)\right] \\
&+ \alpha_I\left[(n_I+1)P(n_E,n_I+1,t)-n_IP(n_E,n_I,t)\right] \\
&+ \left[(N_I-n_I+1)f_I[s_I(n_E,n_I-1)]P(n_E,n_I-1,t)\right. \\
&- \left.(N_I-n_I)f_I[s_I(n_E,n_I)]P(n_E,n_I,t)\right] \qquad (3.57)
\end{aligned}$$

See [11] for a derivation of this equation.

From this, following the same steps that were used to derive Equation 3.5, it is easy to find the mean-field $E-I$ equations, which take the form

$$\begin{aligned}
\frac{d\langle n_E(t)\rangle}{dt} &= -\alpha_E\langle n_E(t)\rangle+(N_E-\langle n_E(t)\rangle)f_E\left[\langle s_E(n_E)\rangle\right] \\
\frac{d\langle n_I(t)\rangle}{dt} &= -\alpha_I\langle n_I(t)\rangle+(N_I-\langle n_I(t)\rangle)f_I\left[\langle s_I(n_I)\rangle\right] \qquad (3.58)
\end{aligned}$$

where $\langle s_E(n_E)\rangle = \langle I_E\rangle/I_{\rm RH}$, $\langle I_E\rangle = w_{EE}\langle n_E\rangle - w_{EI}\langle n_I\rangle + w_{EH}\langle n_H\rangle$, $\langle s_I(n_I)\rangle = \langle I_I\rangle/I_{\rm RH}$, and $\langle I_I\rangle = w_{IE}\langle n_E\rangle - w_{II}\langle n_I\rangle + w_{IH}\langle n_H\rangle$. These are the familiar mean-field Wilson-Cowan equations we've seen in Chapter 2 and derived in [126] and [125].

3.7 An $E-I$ neural network exhibiting self-organized near criticality

We now directly study the neural patch or module shown in in Figure 3.6. Again we note that this module is spatially homogeneous. We model the neocortical sheet as a two-dimensional network or array of such circuits. In such an array, note that the neighboring excitation provides the recurrent excitatory connection. This requires $\mu_j^E = 1/4$, so that the recurrent excitatory connection shown in Figure 3.6 (not labeled) has strength w_{EE}. The recurrent inhibitory connection (also unlabeled) takes the value w_{II}. The basic equations for the array thus take the form of Equations 3.57 and 3.58, except that the activities n_E and n_I are now functions of position, as are the excitatory and inhibitory currents I_E and I_i^I which are given by the expressions

$$I_i^E = \frac{1}{4}\sum_j w_{ij}^{EE} n_j^E - w_{ii}^{EI} n_i^I + w_{ii}^{EH} n_{ii}^H, \quad I_i^I = w_{ii}^{IE} n_i^E - w_{ii}^{II} n_i^I + w_{ii}^{IH} n_{ii}^H$$

where $\sum_j$ runs over all nearest neighbor patches.

Note also that the density of inter-patch $E \to I$, $I \to E$, and intra-patch $I \to I$ connections is very small relative to that of $E \to E$ connections, so we have neglected them in calculating the excitatory and inhibitory currents I_i^E and I_i^I.

3.7.1 Modifiable synapses

We now introduce generalized Vogels' equations, the derivation of which follow the same steps as for the E network discussed earlier, for the four internal synaptic weights in each patch, $w_{ii}^{EE}, w_{ii}^{IE}, w_{ii}^{EI}$ and w_{ii}^{II}. The excitatory synapses w_{ii}^{EE} and w_{ii}^{IE} are assumed to be *anti-Hebbian*, and the inhibitory synapses w_{ii}^{EI} and w_{ii}^{II} *Hebbian*. Mean field equations for

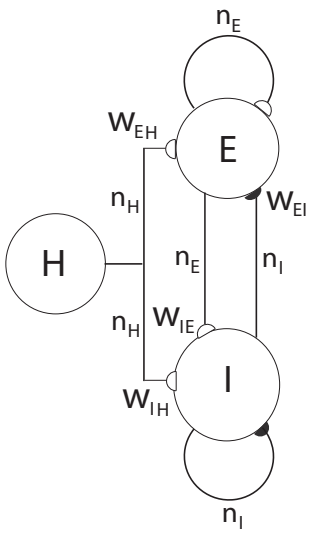

Figure 3.6: A recurrent E-I network module driven by the input H, acting through the synaptic weight w_{EH} and w_{IH}.

these weights take the form:

$$\frac{d\langle w^{\alpha\beta}\rangle}{dt} = \lambda_{\alpha\beta} - \mu_{\alpha\beta}\langle w^{\alpha\beta}\rangle \tag{3.59}$$

where α and β run over the set $\{E, I\}$, and the coefficients $\lambda_{\alpha,\beta}$ and $\mu_{\alpha,\beta}$ give the transitions rates for the Markov processes governing the four weights. These take the form

$$\lambda_{\alpha E} = \beta_E g_\alpha n_{\alpha,0} n_E; \quad \mu_{\alpha E} = \beta_E g_\alpha \left(\frac{n_\alpha}{w^{\alpha E}} + |\kappa_{E,S}|\right) n_E \tag{3.60}$$

for the excitatory anti-Hebbian weights, and

$$\lambda_{\alpha I} = \beta_I g_\alpha n_\alpha n_I; \quad \mu_{\alpha I} = \beta_I g_\alpha \left(\frac{n_{\alpha,0}}{w^{\alpha E}} + \kappa_{I,S}\right) n_I \tag{3.61}$$

for the inhibitory Hebbian weights. Note that for such weights $\kappa_{E,S} < 0$ and $\kappa_{I,S} > 0$, respectively. In the continuum limit these equations take the form

$$\frac{d\langle w_{\alpha E}(\mathbf{x})\rangle}{dt} = -\beta_E g_\alpha(\mathbf{x}) \left(\frac{\langle n_\alpha(\mathbf{x})\rangle - n_{\alpha,0}(\mathbf{x})}{\rho_S} + |\kappa_{E,S}|\langle w_{\alpha E}(\mathbf{x})\rangle \right) \frac{\langle n_E(\mathbf{x})\rangle}{\rho_S} \tag{3.62}$$

for excitatory weights, and

$$\frac{d\langle w_{\alpha I}(\mathbf{x})\rangle}{dt} = \beta_I g_\alpha(\mathbf{x}) \left(\frac{\langle n_\alpha(\mathbf{x})\rangle - n_{\alpha,0}(\mathbf{x})}{\rho_S} - \kappa_{I,S}\langle w_{\alpha I}(\mathbf{x})\rangle \right) \frac{\langle n_I(\mathbf{x})\rangle}{\rho_S} \tag{3.63}$$

for inhibitory weights.

3.7.2 A simulation of the combined mean field $E-I$ equations

The complete set of mean field equations for an $E-I$ patch with modifiable weights comprises the Wilson-Cowan equations together with the generalized Vogels equations 3.62 and 3.63, supplemented by the modified current equations given above, for the full two-dimensional array. Such a system of equations can be simulated, and the results are shown in Figure 3.7. It will be seen that a single patch self-organizes from one stable fixed point defined by the initial conditions to another stable fixed point at which $n_E = n_{E,0}, n_I = n_{I,0}$ as expected. Hence, the activity has reached its target rates. We note that in the case the initial conditions are constrained so that $w_{EE} = w_{IE} = w_E$ and $w_{EI} = w_{II} = w_I$, and all the fixed parameters of the E population equal those of the I population, then the final state is also similarly constrained. We refer to this as a *symmetry* of the system. Given such a symmetry and the target condition $n_{E,0} = n_{I,0}$ it follows that $w_E - w_I \to 0$, so that

$$w_0 = w_E - w_I \ll w_E + w_I$$

Thus the combined system is *homeostatic*. It self-organizes so that the strengths of all the synaptic weights stay with a certain range. The homeostatic properties of anti-Hebbian

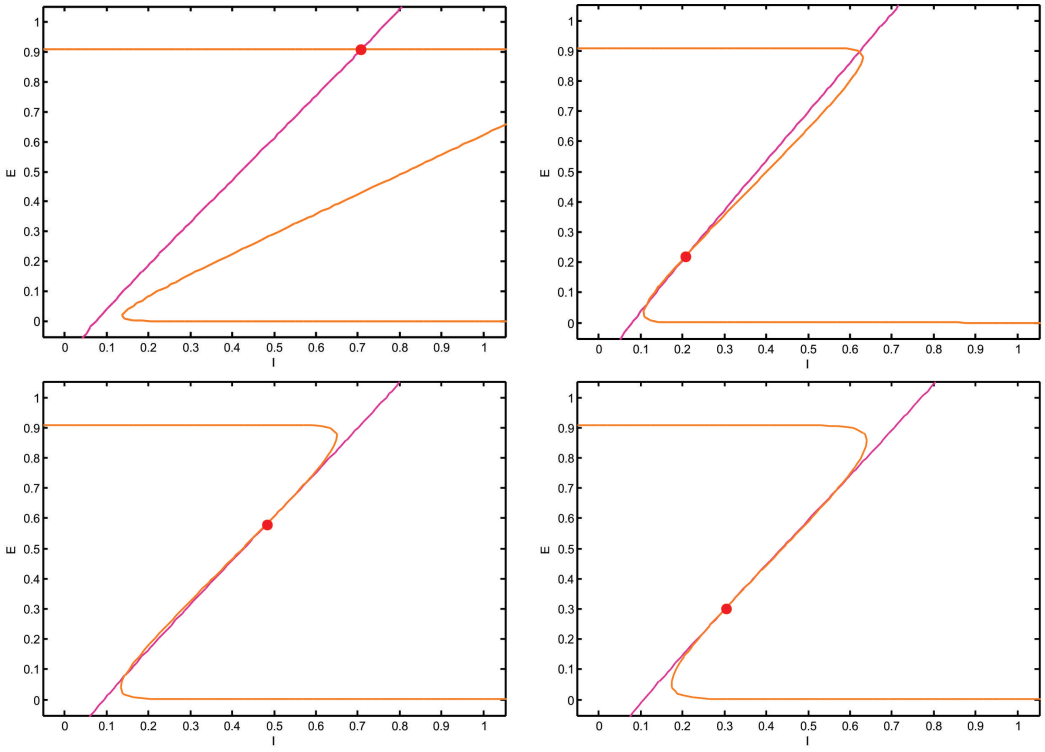

Figure 3.7: $E - I$ phase plane and null clines of the mean-field Wilson-Cowan equations. The intersections of the two null clines in each panel are equilibrium or fixed points of the equations. The upper left panel shows the initial state at $t = 0$ s with weights $w_{EE} = 36$, $w_{IE} = 25$, $w_{EI} = 22$, and $w_{II} = 33$. There is a stable fixed point at $n_E \approx 0.9$, $n_I \approx 0.7$. The upper right panel shows the state at $t = 1.25 \times 10^5$ s with weights $w_{EE} = 20.05$, $w_{IE} = 20.17$, $w_{EI} = 24.78$, and $w_{II} = 30.45$. There is now a saddle-point at $n_E \approx 0.2$, $n_I \approx 0.2$. The lower left panel shows the state at $t = 2.5 \times 10^5$ s with weights $w_{EE} = 16.09$, $w_{IE} = 18.63$, $w_{EI} = 18.72$,and $w_{II} = 24.86$, and a saddle point at $n_E \approx 0.6$, $n_I \approx 0.6$. The lower right panel shows the final state at $t = 1 \times 10^6$ s with weights $w_{EE} = 11.80$, $w_{IE} = 15.63$, $w_{EI} = 13.22$, and $w_{II} = 20.83$, with a stable fixed point at $n_E = 0.3$, $n_I = 0.3$. The remaining fixed parameters are $w_{EH} = w_{IH} = 0$, $\beta_E = 1$, and $\beta_I = 1.5$.

synapses were previously noted by [95].

3.8 Discussion

We have demonstrated the following properties of stochastic Wilson-Cowan equations: (a) a simple two-dimensional array comprising patches of excitatory neurons driven by a weak external stimulus acting through a modifiable anti–Hebbian synapse self-organizes into an oscillation between two stable states, an UP state of high neural activity, and a DOWN state of low activity, each of which loses its stability at the critical point of a non-equilibrium phase transition in the universality class of directed percolation. Such noisy oscillations generate bursts or avalanches of neural activity whose avalanche distributions are consistent with such a phase transition. (b) We then analyzed the properties of a array comprising patches of both excitatory and inhibitory neurons, with excitatory anti-Hebbian, and inhibitory Hebbian synapses. We found that the spontaneous fluctuation driven activity of a single patch self-organizes to a weakly stable fixed point. However such a fixed point lies close to a marginally stable fixed point. Thus we conclude that the effect of Hebbian inhibition is to *stabilize* the dynamics of the patch, but that the statistical dynamics of the patch remains within the fluctuation driven regime surrounding the critical point of a non-equilibrium phase transition, which again is in the universality class of directed percolation. In the future, we would like to write a paper containing a detailed analysis of this situation using renormalization group techniques, along the lines of Täuber's analysis of stochastic Lotka-Volterra equations. (c) We have also seen, as explained in Chapter 2, that the mean-field dynamics of an E/I network can be analyzed around the Bogdanov-Takens bifurcation, and that the generalized Vogel's equations for Hebbian and anti-Hebbian plasticity drive the patch dynamics to a weakly stable node near such a bifurcation, and in doing so reduce the E/I dynamics to the E dynamics of a single E patch.

In summary, we conclude that an array of E-patches will self-organize around critical points of the directed percolation phase transition, and when driven by a weak stimulus

will oscillate between an UP state and a DOWN state each of which generates avalanches consistent with directed percolation. The array therefore exhibits self-organized criticality and replicates the behavior of the original sandpile model of [8]. We also can conclude that an array of E/I patches will also self-organize to a weakly stable node located near the critical point of a directed percolation phase transition, so that fluctuations about the weakly stable node will also follow a power slope with a slope characteristic of directed percolation. We refer to this as self-organized near criticality. We note that there is some experimental evidence to support this conclusion such as [53] and [106]. Lastly, it should be said that if the conclusions mentioned above are correct, it indicates that the approach we have outlined in this chapter may prove to be of some value in the analysis of stochastic effects in neural networks.

CHAPTER 4

MODELING FOCAL EPILEPTIC ACTIVITY IN THE WILSON-COWAN MODEL WITH DEPOLARIZATION BLOCK

4.1 Introduction

Epilepsy is a neurological disease characterized by recurrent spontaneous seizures, i.e. episodes of unstable, abnormal excessive brain activity. Although epilepsy is one of the most prevalent neural diseases, affecting about 1% of the world population, the mechanisms governing seizure activity are not well understood and consequently treatment is unsuccessful for a significant fraction (33%) of patients [71]. According to the clinical classification, epilepsy is a heterogeneous disease [13]. In spite of this heterogeneity in the pathology, there is also commonality between different seizure events suggesting that a variety of mechanisms may lead to a final common process, the seizure, [63]. For example, in studies of brain slices it was demonstrated that seizure-like activity is characterized by spatial propagation, defined as failure of an inhibitory veto in neocortex, [111], or failure of a dentate gate function in case of hippocampal driven events, [107]. This shows that, in addition to a temporal evolution of a developing seizure, its spatial component at this mesoscopic level may be critically important. In fact, recently described microelectrode array recordings in patients with epilepsy confirmed that propagation of neural activity occurs at a spatial scale below the size of a conventional cortical or scalp electroencephalogram (EEG) electrode, [96]. At the microscopic level, intracellular measurements in human brain slices during evoked seizure activity show that neurons go into a depolarization block, i.e. they saturate, e.g. [75]. A recent report, [4], describes an important role of the depolarization block in inhibitory cells in human cortical areas where seizures propagate, leading to the failed inhibition scenario described by, [111]. In addition, it can be expected that under these high levels of activity, synaptic resources deplete, also contributing to a saturation effect. These data indicate that during high levels of seizure activity, hyperactive neurons may operate close to what can be described as an

upper-threshold of its input-output relationship. Such an epileptiform state would be in contrast to normal physiological operation of neuronal networks where the neurons operate around a lower activation threshold.

The goal of this chapter is to examine focal seizures propagating in cortex employing a modeling approach that includes details of the network under the EEG electrode. The tissue under the EEG electrode can be modeled by coupled neuronal populations. (see [37], [125], and [126].) Each population consists of an excitatory and inhibitory component. Many previous experimental, [59], and theoretical studies, such as [45], [91], and [125], have shown that disinhibition can lead to traveling wave activity via blocking inhibition, assuming no synaptic inhibition or including a non-specific afferent affecting the inhibitory current. An important component in these studies is the sigmoidal activation function that describes the nonlinear relationship between the population's input current reflected partially in the local field potential (LFP) and its output firing rate. In this study, motivated by neuronal saturation, we modified the equations to include a Gaussian firing rate function to reflect an upper-threshold phenomenon specific to the epileptiform network state. In Section 2, we present experimental evidence that such a function exists during seizures in the human cortex, and we incorporate this into the existing Wilson-Cowan formalism. In Section 3, we investigate the introduction of a new activation function from a theoretical point of view and then discuss the network and report simulation results showing the effect of the altered activation function on the dynamics. In Section 4, we discuss the relevance of our new findings to our understanding of seizure propagation.

4.2 Experimental observations

4.2.1 Observations during human seizures

Both in vitro and in vivo electrophysiologic measurements suggest using an alternative to the commonly employed sigmoidal activation function in the Wilson-Cowan equations, [126]

and [125], in our seizure model. One experimental component supporting this alternative function stems from single cell recordings obtained from human brain tissue resected from patients with drug-resistant epilepsy. During evoked seizures in cortical slices prepared from this brain tissue, single neurons show a strong paroxysmal depolarization, indicating an arrest of neuronal firing after high-level synaptic input exceeds an (upper-)threshold. (see [75] for details.)

A technique, recently approved for use in humans, allows application of micro-electrode recordings, during seizure activity, [96]. Study participants consisted of adults with pharmaco-resistant focal epilepsy who underwent chronic invasive EEG studies to help identify the epileptogenic zone for subsequent removal. A 96, 4 mm x 4 mm, micro-electrode array (also known as Utah array) was implanted along with subdural electrodes with the goal of recording from seizure onset sites; see Figure 4.1A. The study was approved by the Institutional Review Board of the Columbia University Medical Center, and informed consent was obtained from each patient prior to implantation. Signals from the microelectrode array were acquired continuously at 30 kHz per channel (0.3 Hz-7.5 kHz bandpass, 16-bit precision, range $\pm$ 8 mV). The reference was either subdural or epidural, chosen dynamically based on recording quality. See also [96] for details of study enrollment, surgical procedures and signal recording.

The signals in Figure 4.1B were recorded from a single microelectrode around seizure onset in a patient with intractable epilepsy. This in vivo recording shows the local field potential (LFP) that represents the weighted space-averaged electrical activity surrounding the electrode. The broadband signal from the microelectrode can be filtered to examine its low frequency component (L-LFP, 2-50 Hz) as well as the multi-unit spike activity (300-3000 Hz). We have examined the relationship between L-LFP and spike activity to study the population's activation function. An index of the overall activity (firing rate index, FRI) was obtained by rectifying and integrating the spike traces (Figure 4.1B, two bottom traces), [114]. The leaky integrator's time constant employed here is 50 ms, which was chosen

because it is close to the time constant of a cortical pyramidal cell, [104]. We found that during seizure activity in focal areas where seizures are initiated, a plot of the FRI versus L-LFP is not a standard sigmoidal relationship, but rather is a mixture of sigmoid and Gaussian with a clear maximum, see Figure 4.1C. To interpret this relationship properly, it should be noted that by convention, the L-LFP polarity is reversed, i.e. negative, relative to intracellular depolarization (positive). This relationship reflects contributions from inhibitory and excitatory neurons. We assume the small inhibitory cells are saturated at high L-LFP levels which would explain the maximum.

The comparison between activation function and spike activity versus L-LFP is an approximation, based on a number of assumptions. First, the L-LFP is generated by multiple types of cellular current, [25]. However, it is reasonable to assume that during the high-levels of activity during seizures, the synaptic component will be the principal contributor. (see [64], [96], and [111].) In addition, a significant part of the non-synaptic sources of the L-LFP will be proportional to synaptic activity. In this context, it should be noted that such a relationship between synaptic activity and field potential has been the basis of many models of the electroencephalogram (EEG) as well, e.g. [87]. Next, we use the spike signal as a metric for network output while the multi-unit spike activity in a micro-electrode recording contains both input as well as output spikes of the local population. This is plausible since, due to geometry, the probability of picking up an output spike from an active neuron is much higher than recording from a thin afferent axon. Furthermore, if we assume the input spikes are proportional to the synaptic potentials they generate, they could only destroy the Gaussian-like result that we obtained in Figure 4.1C. Another significant fact is that we only found Gaussian-like functions as in Figure 4.1C within the epileptic core and not outside that area. This suggests that (inhibitory) cells reach depolarization block only within the core. Thus, although the relationship between L-LFP and multi-unit activity is not an exact measure of the population's activation function, it is a reasonable proxy for it.

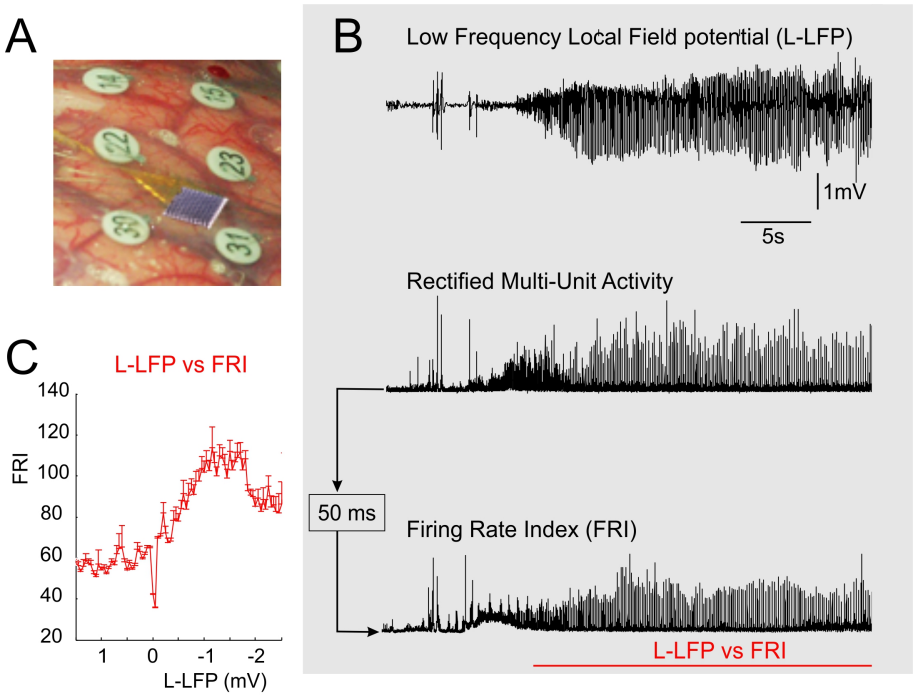

Figure 4.1: Experimental data supporting the use of a Gaussian population response function during human seizure activity. A: Recording setup depicting the multi-electrode array situated in between the standard electrocorticography electrodes numbered 22, 23, 30, and 31. B: Example recordings of the low frequency component of the local field potential (2-50Hz, L-LFP, upper trace), the rectified signal filtered for spikes (300-3000Hz, middle trace), and the integrated version thereof, using a leaky integrator with a 50ms time constant (bottom trace) generating a firing rate index (FRI) for the multi-unit spike activity. The relationship between L-LFP and FRI is plotted in panel C; the error bars indicate SEM values.

4.2.2 Behavior of single cells during seizures and in biophysically plausible models

The activation function turns synaptic activity into a population firing rate, and is therefore also referred to as the firing rate function. Cells within a population have a slightly different firing threshold. In this simplified approach, we assume that the number of spikes does not depend on the input current, i.e. each cell has a Heaviside firing function. Summing all individual contributions, the jitter in thresholds leads to a sigmoidal function, see Figure 4.2. In this regard, neurons do not only have a minimal value for the input current to spike, but also a maximal value where the membrane potential experiences a depolarization block. See,

for instance, a dynamical systems explanation in [60], where it is called excitation block. Likewise, the precise critical value for the block will differ from cell to cell. Hence, for every cell, there is a finite range of input currents that results in spikes. Summing over the whole population leads to a Gaussian population activation function. This fundamental reasoning, based on the observation that the depolarization block occurring during evoked seizures represents an upper-threshold for neuronal firing, also supports replacing a sigmoidal nonlinearity by a Gaussian-like activation function. There is some early work, [102], supporting such a procedure.

The range of thresholds differs between cell types. For example, due to differences in the size, inhibitory neurons are activated by relatively small depolarizing inputs, whereas larger pyramidal neurons have a higher threshold. As inhibitory neurons are smaller, they have a propensity to reach depolarization block earlier than larger excitatory neurons during seizure activity. This is reflected in our choice of thresholds E_θ, I_θ and standard deviations E_{sd}, I_{sd}, see also Figure 4.2.

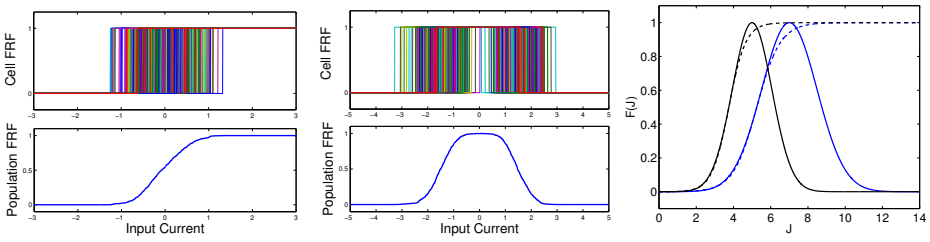

Figure 4.2: Constructing sigmoidal and Gaussian firing rate functions. Left: Heterogeneity in firing onset for individual cells leads to a sigmoidal population activation function. Middle: Including the effect of heterogeneous thresholds for depolarization block leads to a population activation function with a maximum. Right: The activation functions used in this chapter: Gaussian (solid) and sigmoid (dashed) for excitatory (blue) and inhibitory (black) populations.

We noted above that there is a range of thresholds associated with both the excitatory and inhibitory populations. In the first Wilson-Cowan paper, it was assumed that these threshold distributions were either Poisson-like, or Gaussian. It then followed that the integrals of such curves would lead to an expression for the firing rate curves as the fraction of neurons receiving at least threshold excitation. In the distributions cited above, both

integrals give rise to sigmoidal firing rate curves. Within this approach, it follows that a legitimate way of deriving a non-monotonic firing rate curve involves an additional threshold mechanism to express the effects of depolarization block.

4.3 Modeling epileptiform activity

4.3.1 Theory of population activation functions

As mentioned in the Section 1, the canonical population models, the Wilson-Cowan equations, [125] and [126], were introduced as a way to describe the activity of interacting isotropic excitatory and inhibitory neuronal populations. Ignoring space, which can easily be put back into the formalism, their dynamical behavior is captured by the variables $E(t)$ and $I(t)$, the proportion of excitatory or inhibitory cells firing per unit time at time t, where single neurons are active above a threshold, θ. In [126], they derive the following set of coupled integro-differential equations:

$$E(t+\tau) = [1 - \int_{t-r}^{t} E(t')dt']S_e(\int_{-\infty}^{t} \alpha(t-t')(c_1E(t') - c_2I(t') + P(t'))dt) \tag{4.1}$$

$$I(t+\tau') = [1 - \int_{t-r}^{t} I(t')dt']S_e(\int_{-\infty}^{t} \alpha(t-t')(c_3E(t') - c_4I(t') + Q(t'))dt) \tag{4.2}$$

where τ is a time increment, the first term on the right represents the number of non-refractory neurons and the second is the proportion of neurons receiving at least threshold input (the integrands) per unit time i.e. the population response or activation function. The second term can be written as:

$$S(x(t)) = \int_{-\infty}^{x(t)} D(\theta)d\theta \tag{4.3}$$

where $x(t)$ is the total input to a population (assuming all neurons receive on average the same excitation and inhibition) and $D(\theta)$ is the probability distribution function of the lone

threshold, assumed to be Gaussian as the law of large numbers predicts. Clearly, $S(x(t))$ will be a monotonically increasing function on the interval $[0, 1]$ with an inflection point at θ if $D(\theta)$ is unimodal ($S''(\theta) = D'(\theta) = 0$). In other words, $S(x)$ is the cumulative distribution function of $D(\theta)$ i.e. $S(x) = P(\theta \leq x)$.

Now let us consider the situation where single neurons have two thresholds, one for activation (θ_1) and one for deactivation (θ_2) where $\theta_2 > \theta_1$. Figure 4.3 illustrates a single neuron with this consideration. If, again, we assume that neuronal thresholds are stochastic variables with probability distribution functions $D_1(\theta)$ and $D_2(\theta)$ (examples in Figure 4.4), each threshold has an associated cumulative distribution, $S_1(x(t))$ and $S_2(x(t))$, respectively. See Figure 4.5.

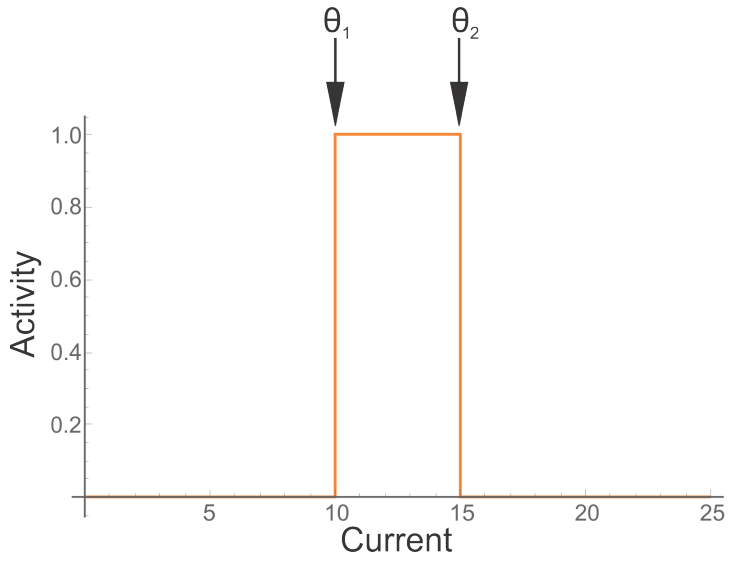

Figure 4.3: An example neuron with activation and deactivation thresholds given by $\theta_1 = 10$ and $\theta_2 = 15$, respectively.

However, due to the deactivation threshold, we must redefine the population response function, $S(x(t))$, to be the proportion of cells which receive at least activation input but less than deactivation input. In terms of probabilities, we have $S(x(t)) = P(\theta_1 \leq x(t) \leq \theta_2)$. Thus, our redefined response function is no longer a cumulative distribution function. Also, it is clear that $S(x(t))$ has a global maximum. We can see this by noting that $S(-\infty) = S(\infty) = 0$ and $S(x(t)) > 0$ for some $\theta_1 < x(t) < \theta_2$ because of the nature of probability

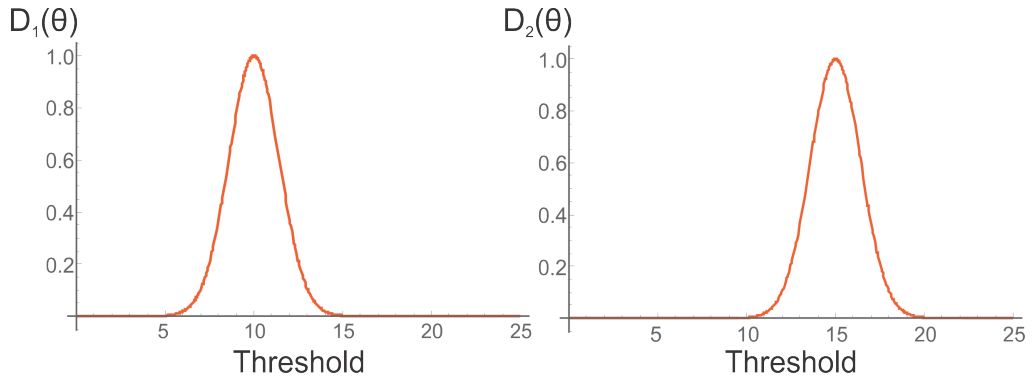

Figure 4.4: Example distribution functions of activation (left) and deactivation (right) thresholds, respectively. Note that these have not been normalized.

distribution functions. This condition holds with no knowledge of the statistical dependence of the thresholds. If we restrict the two thresholds to be independent, it follows that:

$$\begin{aligned} S(x) &= P(\theta_1 \le x \le \theta_2) = P(\theta_1 \le x)P(\theta_2 \ge x) = P(\theta_1 \le x)(1 - P(\theta_2 \le x)) \\ &= \Big(\int_{-\infty}^{x(t)} D_1(\theta)d\theta\Big)\Big(1 - \int_{-\infty}^{x(t)} D_2(\theta)d\theta\Big) = S_1(x)(1 - S_2(x)) \ge 0 \\ S'(x) &= D_1(x)(1 - S_2(x)) - S_1(x)D_2(x) \\ S''(x) &= D_1'(x)(1 - S_2(x)) - S_1(x)D_2'(x) - 2D_1(x)D_2(x) \end{aligned}$$

Figure 4.6 shows examples of $S_1(x)$, $1-S_2(x)$ and $S(x)$. If we also assume neuronal thresholds are approximately Gaussian-distributed, which the law of large numbers predicts, with equal variances (as in Figure 4.4), $D_i(\theta) = \frac{1}{\sqrt{2\pi\sigma^2}} e^{-(\theta-\theta_i)^2/2\sigma^2}$, $S_i(x) = \frac{1}{2}(1 + \text{erf}(\frac{x-\theta_1}{\sigma\sqrt{2}}))$, $S(x)$ has a single maximum near $x = (\theta_1 + \theta_2)/2$ and inflection points near θ_1 and θ_2. Thus, it is reasonable to model the Wilson-Cowan equations with the same integro-differential equations where the only replacement is now that $S_e(x(t))$ and $S_i(x(t))$ are Gaussians (green curve in Figure 4.6). It should be noted that this approximation breaks down if the two thresholds are spaced far apart.

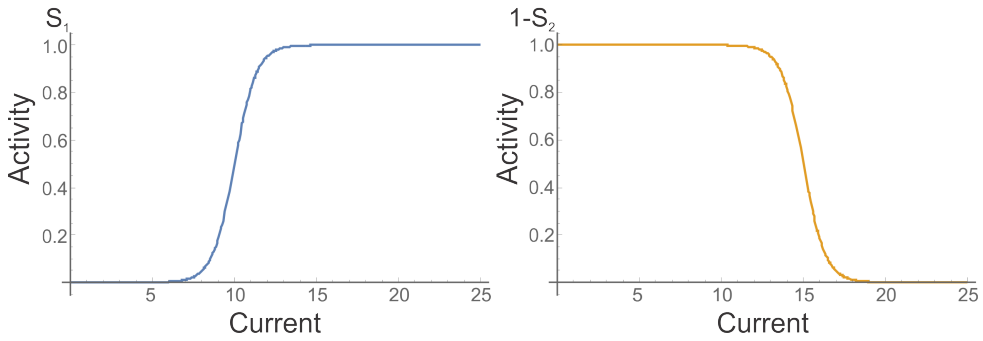

Figure 4.5: Threshold activation (left) and deactivation (right) curves. The former is the CDF of $D_1(\theta)$ and the latter is the survival function of $D_2(\theta)$.

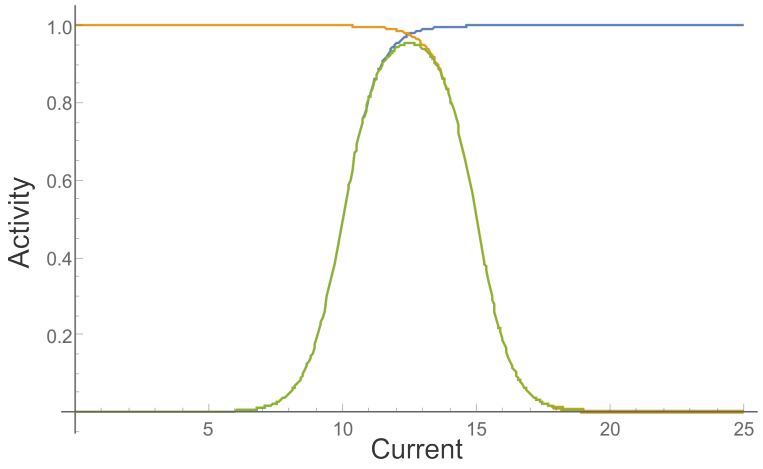

Figure 4.6: Threshold activation (blue) and deactivation (yellow) curves and redefined population response function (green). The first is the CDF of $D_1(\theta)$, the second is the survival function of $D_2(\theta)$, and the third is their product.

4.3.2 Network details

Since we have motivated the use of a Gaussian activation function, in order to understand epileptiform wave dynamics, we consider a spatially-extended model where $E(y,t)$ and $I(y,t)$ represent the activity of our excitatory and inhibitory populations, $y \in [0, L]$ and $L = 1000\ \mu$m. See Figure 4.7. Using the same form as in [125], we have

$$\begin{aligned}
\tau_E \dot{E}(y,t) &= -E(y,t) + (1 - E(y,t))S_E(J_E(y,t)), \\
\tau_I \dot{I}(y,t) &= -I(y,t) + (1 - I(y,t))S_I(J_I(y,t)), \\
S_E(J_E(y,t)) &= \exp\left(-\left(\tfrac{J_E(y,t)-E_\theta}{E_{sd}}\right)^2\right) - \exp\left(-\left(\tfrac{-E_\theta}{E_{sd}}\right)^2\right), \\
S_I(J_I(y,t)) &= \exp\left(-\left(\tfrac{J_I(y,t)-I_\theta}{I_{sd}}\right)^2\right) - \exp\left(-\left(\tfrac{-I_\theta}{I_{sd}}\right)^2\right), \\
J_E(y,t) &= \lambda_E \textstyle\int_0^L \left(w_{EE} e^{|y-z|/\sigma_{EE}} E(z,t) - w_{IE} e^{|y-z|/\sigma_{IE}} I(z,t)\right) dz + B(y,t), \\
J_I(y,t) &= \lambda_I \textstyle\int_0^L \left(w_{EI} e^{|y-z|/\sigma_{EI}} E(z,t) - w_{II} e^{|y-z|/\sigma_{II}} I(z,t)\right) dz,
\end{aligned} \tag{4.4}$$

where $w_{EE} = 2.0$, $w_{IE} = 1.65$, $w_{EI} = 1.5$, $w_{II} = 0.01$, $\sigma_{EE} = 70\ \mu$m, $\sigma_{IE} = 90\ \mu$m, $\sigma_{EI} = 90\ \mu$m, $\sigma_{II} = 70\ \mu$m, $E_\theta = 18$, $E_{sd} = 6.7$, $I_\theta = 10$, $I_{sd} = 3.2$ and the only replacement is that S_E and S_I are non-normalized Gaussian functions. When comparing these results to ones with a sigmoid firing function, we make the following replacements: $E_\theta = 12.41$, $E_{sd} = 2$, $I_\theta = 7.33$ and $I_{sd} = 0.95$. These parameters are similar to the neural mass model used above, but scaled as we do not have normalized connectivity weights due to the finite domain. In this setup, tissue near the boundary receives less input. Furthermore, we set the densities of excitatory or inhibitory neurons in homogeneous and isotropic tissue as $\lambda_E = \lambda_I = 1\ \mu m^{-1}$. The input $B(y,t)$ consists of a constant background of 1 and a 100 μm wide, 10 ms square-wave pulse with amplitude 10.

4.3.3 Simulation of network

Now, we simulate the model mentioned in the previous section. The results are found in Figure 4.8. On the top row, the network with a sigmoid firing rate function produces transient

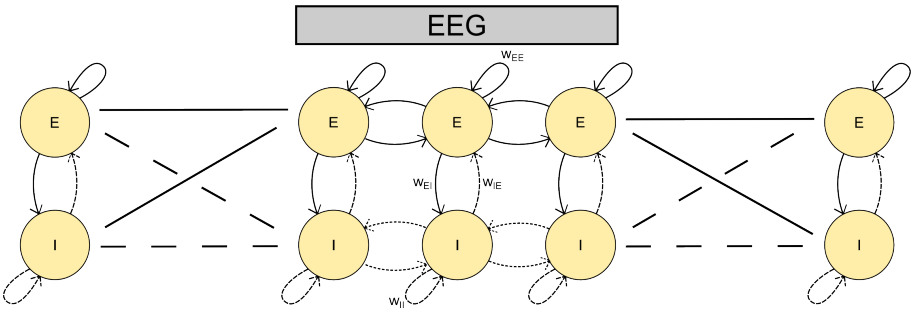

Figure 4.7: Overview of the network under consideration. All excitatory and inhibitory populations are connected but the synaptic strengths are modulated by distance and a particular space constants. Excitatory connections are solid lines and inhibitory connections are dashed lines.

behavior but no traveling pulse. With the introduction of a Gaussian activation function, we see, in the middle and bottom rows, a propagating wave. Here, we can clearly see activity originating in the middle, where the stimulation occurs, and propagating to the edges. The main takeaway point from this is that the excitatory activity (blue) has provided sufficient input to the inhibitory neurons, which have a smaller activation threshold, to drive them into depolarization block and, thus, the inhibitory activity (red) is not strong enough to keep the activity localized as seen by the spreading behavior. This is why, in the middle and bottoms rows of Figure 4.8, whenever excitation is large, inhibition is small and the activity moves outward.

Thus, we may conclude that our formalism provides a mechanism for dynamic disinhibition arising from depolarization block which the sigmoid firing rate function cannot reproduce without including additional variables. Another thing to notice is that, while the input is only to the excitatory neurons here, the excitatory pulse of excitation lags behind inhibition, a finding consistent with detailed recordings of epileptiform activity, [4]. It should be mentioned as well that we have found similar behavior when both kinds of neurons receive the same input. Lastly, in [96], the speed of the wave was estimated around 0.8 mm/s. We varied the strength of the excitatory coupling to match the wave speed in the model with this experimental value.

It should be mentioned that a full bifurcation analysis is possible on the space-clamped

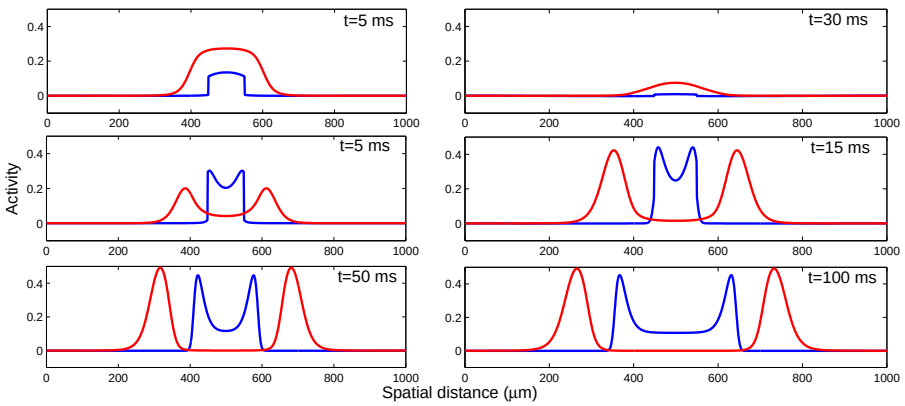

Figure 4.8: Propagation. Top row: Excitatory (blue) and inhibitory (red) activity with sigmoidal population activation function. Activity is extinguished by 100 ms. No propagation is present. Middle row: Population activities with Gaussian firing rate function. Here, a traveling wave pulse forms and begins to propagate. Bottom row: same as middle but at later times. The traveling wave continues to propagate until it dies at the boundary. The wavespeed is approximately 1 mm/sec. Parameters are the same in each plot.

model, [77]. In that paper, we show from investigating the nullcline structure of the modified Wilson-Cowan equations that the new activation function introduces, an additional stable equilibrium with high excitatory and low inhibitory activity. An analysis of coupled local populations reveals that this high excitatory, low inhibitory state can spread or remain localized. Whenever a traveling wave is produced, the inhibitory wave of activity always precedes an excitatory one, which is consistent with the spatially-extended model found above and with experimental findings.

4.4 Discussion

In this chapter, we have investigated the dynamics of a neural network governed by the Wilson-Cowan equations. In particular, motivated by experimental and theoretical means, we have chosen to use a Gaussian activation function, rather than the default sigmoid. We have mentioned the existence of an additional high excitatory steady state due to the Gaussian and noted its consequences for network dynamics. Many of the other attractors in this system have been discussed in earlier studies such as [16] and [17]. With multiple

local populations connected, the high activity provided strong drive to the surrounding populations resulting in breather-like dynamics. Beyond critical parameter values of which there are too many to write down, the activity could spread through the whole network.

The Gaussian activation function was motivated by observations of ictal activity recorded using a Utah array. An experimental activation function could be determined using the low-frequency component of the LFP as a measure of synaptic input, and the high-frequency component as spike output. For some cases this showed a nonmonotonic relationship suggesting the choice of a Gaussian over a sigmoid. This relationship reflects multiple sources and also represents inhibitory and excitatory cells. As cortical networks consist of 80% large excitatory neurons and 20% small inhibitory interneurons, one would interpret the graph in Figure 4.1C as predominantly originating from the excitatory population. Also, the experimental curve in Figure 4.1C suggests that, beyond the maximum, a plateau is reached. One possibility is that some of the large excitatory cells still exhibit a sigmoidal relationship at these high L-LFP levels. Then, it is not unreasonable to assume that inhibitory cells exhibit depolarization block even earlier. For simplicity, we have modeled the activation functions for both populations as a Gaussian which approaches zero for high input, but the input may not even achieve such levels. Indeed, in our simulations the external input strength never went beyond the maximum for S_E, however the duration of the stimulus allowed the total input to reach above this maximum. If not for this, introducing the new firing function would have served no purpose. We then found that, for a suitable choice of model parameters, there is an additional stable equilibrium with high excitatory and low inhibitory activity. This steady state coexists with the typical low activity equilibrium and oscillations as discussed in [125] and [126]. For this equilibrium to exist, the precise form of the activation function is not important as long as the inhibitory firing rate function has a maximum and then drops sufficiently for high input, e.g. due to depolarization block.

The network dynamics seen here are consistent with the recent proposal that an epileptic focus consists of a core and penumbra, [111]. The border of the core has a lot of spike

activity, whereas the surrounding has less spiking activity. On the other hand, LFP recordings representing synaptic activity, show the reverse situation with high amplitude signals in the penumbra and low amplitudes in the core. In addition, recent experimental recordings of seizures showed that spikes from inhibitory cells were nearly absent, but still many spikes from excitatory cells were observed, [4]. If the core receives high levels of input with relatively little fluctuations, so that the LFP with the DC-offset filtered away shows little signal, the inhibitory cells may actually experience a depolarization block. Subsequently, the inhibitory neurons can no longer veto ongoing epileptiform activity similar to observations in experimental seizures, [111]. In our model, we find large model-EEG signals in the penumbra (where the spreading waveforms are located) and much smaller in the core (the region inside the traveling waves). Hence, our model supports the idea of core and penumbra of an epileptic focus with different levels of activity corresponding to large and small LFP amplitudes. Recent work by Jirsa, [63], argues that the DC component during a seizure is quite different from normal conditions yet we have only shown data from within the core. We have examined the activity of areas with less activity, but the dynamic range was so small that we could not interpret this data. Hence, it would be interesting to determine, in another way, the activation functions outside the areas with epileptiform activity.

In our spatially continuous model, we showed that such a seizure can spread as a traveling front where inhibition is leading, see Figure 4.8. In contrast, the recording in Figure 4.1A has been considered in a recent modeling paper, [122], using the same Wilson-Cowan model and a sigmoidal firing rate function. In that study, a parameter change was needed to decrease inhibition, whereas our use of a Gaussian firing rate function leads dynamically to decreased inhibition. Also, their simulations suggest excitatory activity is leading at the front. In contrast, our simulations agree with the identification of the inhibitory spikes at the front. (see [4] and [111].) There is also an experimental seizure model where a subset of the inhibitory cells enter depolarization block during epileptiform activity, [128]. Such experimentally well-controlled settings might allow the observation of distinct neural

populations during propagating seizures. In our model, the activity settles to the high steady state at the rear of the traveling front. A different dynamical mechanism for the propagation of epileptiform activity has been considered in [101], similarly modeled as in [122]. Their epileptiform activity invades surrounding tissue also as a traveling wave front, with multiple pulses emitted from a spatially homogeneously oscillating core. This oscillating core expands slower than the front. In this chapter we focus on the front, but it would be interesting to consider the rear of the front in future work. We note that we only simulated our spatially continous model using insights from coupled populations. By approximating the activation function as a product of Heaviside-step functions, i.e. a blockpulse, we expect that it is possible to find implicit equations for the various phases of the travelling wave and the speed, using techniques as in [91]. This could elucidate the range of thresholds for depolarization block where our traveling pulse exists.

We do not attempt to argue that our model describes transitions between normal and ictal activity. As in many other modeling studies there can be exogeneous parameter transitions causing these changes. (see [86], [115], and [124]). The most influential parameters are the background input strength and duration and the local connections such as w_{EI}. Various other parameters also play a role but these main ones are certainly interesting to investigate for further study.

CHAPTER 5

CONCLUSION

5.1 Summary of findings

In this study, we analyzed a multitude of spatiotemporal properties which all shed light on the dynamics of large-scale brain activity with a focus on how they maintain stability in the networks under consideration. The two models used were the mean-field deterministic population equations from Wilson and Cowan ([125], [126], and [36]) and the 2-state Markov process of single neurons and synapses ([34] and [35]). While the two models have a completely different fundamental basis, both were able to yield results without any contradiction.

In Chapter 2, based on [11] and [120], we introduced, and investigated the underlying principles behind both models and then studied generic population dynamics in neocortical activity. In particular, the stochastic model was able to reproduce much of the data, specifically random bursting in the form of avalanches, behind spontaneous or resting activity. With this model, we were also able to find pair-correlations for resting activity whose amplitudes decayed with distance in a manner consistent with experimental data. Additionally, this model found that pair-correlations for stimulated activity also decayed with distance but at a much faster rate. Again, the falloff was consistent with experimental findings. The last piece of this study showed that the mean-field deterministic model could account for the qualitative change in behavior when an external stimulus drives a 1-dimensional line of neurons. We found that for weak stimuli, damped traveling waves are seen and for strong stimuli, no spreading dynamics occur. Additionally, the damped traveling waves propagated with a speed in the neighborhood of what data suggests. This contrast in behavior is particularly useful for the neocortex's abillity to maintain stability with respect to an external stimulus because neuronal activity never explodes in an unstable manner. Of course, extreme activity patterns such as seizures do exist in animals and human beings, but the mechanism of generation is not expected to be due just to external inputs.

After studying the general population responses during resting and driven activity, in Chapter 3, we analyzed the statistical properties of two simple neural networks when the synaptic connections were plastic. The plasticity model based on [118] was first rederived in the case of a single anti-Hebbian excitatory synapse with nonlinear neurons between excitatory populations, one of which had a recurrent pathway. The result of this synpatic plasticity was to introduce a control parameter into the Wilson-Cowan (order parameter) equations, which combined with the external E-population, provided all of the necessary ingredients for self-organized criticality. With the help of the Gillespie algorithm, we found power-law avalanche statistics in both UP and DOWN states of the network, confirming our hypothesis that this network has the ability to self-organize around a critical point. Afterwards, the plasticity model was generalized to include a second anti-Hebbian excitatory synapse and two Hebbian inhibitory synapses in a full Wilson-Cowan $E-I$ network where all of the connections are plastic. Interestingly, when these conditions are met, the plasticity forces the system towards a marginally stable fixed point, which a previous study, [11], showed was near a critical point. Thus, the $E-I$ network combined with our plasticity model did not exhibit self-organized criticality. Instead, it showed signs of what we coined, self-organized near-criticality, a term of considerable theoretical interest in the neuroscience community recently. Both properties, SOC and SONC, of dynamical systems have important consequences, which were discussed in the chaper and will be elaborated on in the section that follows, for the stability of neural networks.

Finally, we studied the case of an unstable neural network in the form of focal epilepsy. This required us, based on detailed electrophysiological recordings, to modify the Wilson-Cowan equations to include a second neuronal threshold. This upper threshold gives us a theoretical mechanism to model saturation in neurons, which we explain is the underlying basis for how a seizure begins i.e. the traveling wave begins when inhibitory neurons in the core saturate. One of the outstanding results of this work was the generation of epileptiform activity where a wave of inhibition spreads outward before an excitation one, which we mo-

tivated earlier with experimental data. This finding cannot be reproduced with the standard Wilson-Cowan firing functions because of the properties of monotonically increasing functions; recall that the sigmoid belongs to this class of functions. However, the introduction of a recovery variable or threshold adaption may be a way to generate results consistent with experimental data and a monotonic activation function. Our work in Chapter 4 naturally has extensions to non-seizure-like traveling waves that experiments have detected and theoretical neuroscientists have studied for the past few decades.

5.2 Future directions

Science is a never-ending search for knowledge and, by this point, it should be clear that more work needs to be done. Because our computational power continues to grow, it is becoming easier and easier to simulate more realistic neural networks. However, we feel that the immediate focus on the results mentioned in parts of this work needs to be theoretical. In particular, a mathematical analysis showing that the spatially inhomogenous Wilson-Cowan equations support damped traveling waves is of great importance. This is by no means a simple task considering the complex nature of integro-differential equations. However, if we could show a one-to-one correspondence between the Wilson-Cowan equations and another set of differential equations which have analytic solutions in the form of damped traveling waves, then that should be enough to prove the simulated results found in Chapter 2. Of course, a bifurcation analysis is also needed to interpret the change in behavior between transient responses and spreading dynamics seen in this thesis and experiments. The problem will not be solved until both of those are completed as well as an understanding of how these modes serve in the overall functioning of the neocortex. This last part will involve delving into much more experimental data.

With regard to self-organized criticality and near-criticality, the obvious next step is to build up the network until it becomes completely plastic, more realistic, and shows additional behavior consistent with critical dynamics. Clearly, the simple $E-E$ and $E-I$ networks

studied in Chapter 3 are not true representations of actual neural networks. At the very least, the network should ultimately carry the same complexity as the canonical Douglas-Martin microcircuit, [41]. Making all of the connections plastic will require a lot more computational power because the number of Markov particles will be on the order of N^2, where N is the number of neurons in the network, for all-to-all connectivity. Some of this worry, however, could be assuaged by introducing a cutoff for the connectivity, for example, by utilizing nearest-neighbor connections. Additionally, a significant way to strengthen the argument for self-organized criticality would be to measure the correlation length and susceptibility since both are measures which are infinite at a critical point. It would be very interesting to build a realistic network, compute these for some realistic set of parameters, measure those statistical quantities, and compare them to data. If theory matches experiment, we would have something very significant to say about the computational power, information transmission and processing, and stability of the neocortex.

There is also additional work that must be done for the study of epileptic waves. Not only did we focus solely on the formation of seizure activity, but we only investigated focal epilepsy. The natural next move would be to look at these traveling waves as they move over large distances. The dynamics of spreading behavior here is much different than when the wave forms because the process is different. The beginning of the seizure is characterized by local inhibitory neurons reaching depolarization block but after the wave disperses outward, local effects in the core no longer dominate the system. Of course, how the epileptic waves cease to exist is also of great importance and remains an unanswered question. It is entirely possible that the mechanism is completely different than for both the spreading and dampening of seizure-like activity, but we believe that all three can be explained using the modified Wilson-Cowan equations introduced in Chapter 4. Because epilepsy is a prime example of the nervous system's loss of stability, it is so important to understand. Other types of epilepsy such as generalized epilepsy (where the whole brain seizes) are additional future avenues to be studied in the field. Lastly, the redefinition of the firing function has many

further directions. It remains to be seen if the results mentioned in Chapter 2 and Chapter 5 are congruous but initial evidence suggests they are. If supplementary, more conclusive, tests show this too, we will have produced a biophysically-justified model that fits data ranging from tens of neurons all the way to millions of neurons.

APPENDIX A

APPENDIX TO CHAPTER 3

A.1 Deriving the synaptic plasticity update equation

In order to derive a mean-field update rule, we begin with the same energy function as in [118], but include an extra nonlinear term (g_E) in the potential

$$\Psi(w_{H,j}) = \frac{1}{2} < (\rho_0 - n_E(t))^2 >_t - \frac{1}{2}\kappa_{E,S} g_E \Sigma_j \bar{n}_{H,j}(t) w_{H,j}^2 \tag{A.1}$$

and so

$$\frac{d\Psi(w_{H,j})}{dw_{H,j}} = - < \rho_0 - n_E(t) >_t \frac{n_E}{\partial w_{H,j}} - \frac{1}{2}\kappa_{E,S}\frac{\partial g_E}{\partial w_{H,j}}\Sigma_j \bar{n}_{H,j}(t) w_{H,j}^2 - \kappa_{E,S} g_E \Sigma_j \bar{n}_{H,j}(t) w_{H,j} \tag{A.2}$$

where the minus sign in the potential comes from the fact that $\kappa_{E,S} < 0$ for anti-Hebbian synapses. If we can solve for g_E, then our plasticity update equation will be given by gradient descent just as in [118]. Now, we make the assumption that neural dynamics are much faster than plasticity changes so that (using the notation in Equation 3.32)

$$\frac{\partial < n >}{\partial t} = 0 \rightarrow < n >^* = \frac{\rho f(I)}{\alpha + f(I)} = \rho F[\alpha, \rho, f] \tag{A.3}$$

where I is the current to the E population. Because plasticity effects still occur, they slowly move the fixed point. Hence,

$$\frac{1}{\rho}\frac{\partial < n >^*}{\partial w_H} = F'(w_0 \frac{\partial < n >^*}{\partial w_H} + n_H) \rightarrow \frac{\partial < n >^*}{\partial w_H} = \frac{F'}{1/\rho - F' w_0} n_H \tag{A.4}$$

Thus, $g_E = \frac{F'}{1/\rho - F' w_0} \rightarrow \frac{\partial < n >^*}{\partial w_H} = g_E n_H$ and to leading order $\frac{\partial g_E}{\partial w_{H,j}} = g_E^2 + ...$ and we can now use gradient descent to find the weight update equation, noting that we switch notation

from $< n >^*$ to n_E. From gradient descent, it follows that

$$\begin{aligned} \frac{dw_{H,j}}{dt} &= -T\eta \frac{d\Psi(w_{H,j})}{dw_{H,j}} \\ &= T\eta[< \rho_0 - n_E(t) >_t g_E n_{H,j} + \frac{1}{2}\kappa_{E,S} g_E^2 \Sigma_j \bar{n}_{H,j}(t) w_{H,j}^2 + \kappa_{E,S} g_E \Sigma_j \bar{n}_{H,j}(t) w_{H,j}] \end{aligned} \tag{A.5}$$

Because g_E is a small term, the middle term can be neglected and the result is a learning rule given by

$$\frac{dw_{H,j}}{dt} = -\eta g_E (n_E(t) - \rho_0 - \kappa_{E,S} w_{H,j}) n_{H,j} \tag{A.6}$$

where η is the learning rule rate. Note that here I have neglected some of the density terms but placed them in the update equation found in Chapter 3.

A.2 Expanding the weighting function

We can approximate the convolution operator as the truncation of an expansion in the moments

$$\mu_k = \int d^d x x^k w(\mathbf{x}) \tag{A.7}$$

so

$$w\star = \int d^d x' w(\mathbf{x} - \mathbf{x}') \approx w_0 + \frac{1}{2!} w_2 \nabla^2 + \cdots \equiv L \tag{A.8}$$

where

$$w(\mathbf{x}) \to w(r) = \frac{b}{\sigma^d} e^{-r/\sigma}, \quad \sigma = r_0 \tag{A.9}$$

and

$$w_0 = \int d^d x \, w(\mathbf{x}) = b \frac{d\Gamma(d)}{\Gamma(d/2+1)} \pi^{d/2}, \quad w_2 = \int d^d x \, x^2 \, w(\mathbf{x}) = b\sigma^2 \frac{d\Gamma(d+2)}{\Gamma(d/2+1)} \pi^{d/2} \tag{A.10}$$

A.3 Renormalizing the neural action

We expand n_E about its mean value $\langle n_E \rangle = n_{\mathrm{E,cl}}$, which satisfies Equation 3.32 in the form

$$\partial_t n_{\mathrm{E,cl}} = -\alpha n_{\mathrm{E,cl}} + (\rho - n_{\mathrm{E,cl}}) f[s(n_{\mathrm{E,cl}})] \tag{A.11}$$

where

$$s(n_{\mathrm{E,cl}}) = k(w \star n_{\mathrm{E,cl}} + b_H \star n_{\mathrm{H,cl}}) \tag{A.12}$$

Thus, $n_E \to n_E + n_{\mathrm{E,cl}}, \tilde{n_E} \to \tilde{n_E}$, since $\tilde{n}_{\mathrm{E,cl}} = 0$. So, $s(n_E) \to s(n_E + n_{\mathrm{E,cl}})$ and $f[s(n_E)] \to f[s(n_E + n_{\mathrm{E,cl}})]$. If follows that $s(n_E + n_{\mathrm{E,cl}}) = k(w \star (n_E + n_{\mathrm{E,cl}}) + b_H \star (n_H + n_{\mathrm{H,cl}})) = k(w \star n_{\mathrm{E,cl}} + b_H \star n_{\mathrm{H,cl}}) + k(w \star n + b_H \star n_H)) = s(n_{\mathrm{E,cl}}) + s(n_E)$, and therefore $f[s(n_E)] = f[s(n_{\mathrm{E,cl}}) + s(n_E)]$. We next expand $f[s(n_E)]$ in a Taylor expansion about the mean-field value $n_{\mathrm{E,cl}}$, noting that from Equation A.8, $s(n_E) = k(w \star n_E + b_H \star n_H))) = k(Ln_E + b_H \star n_H))$.

In what immediately follows, we assume that the external stimulus $n_H(\mathbf{x}, t) = 0$. It follows that

$$\begin{aligned} f[s(n_E)] = f[kL(n_{\mathrm{E,cl}} + n_E)] = f[kLn_{\mathrm{E,cl}}] \quad &+ \quad f^{(1)}[kLn_{\mathrm{E,cl}}]kLn_E \\ &+ \quad \frac{1}{2} f^{(2)}[kLn_{\mathrm{E,cl}}](kLn_E)^2 + \cdots \end{aligned} \tag{A.13}$$

However, because of normal ordering, Equation A.13 leads to the expression

$$f[s(n_E)] = \sum_m g_m (kLn_E)^m, \quad \text{where} \quad g_m = \sum_{l=m} \frac{f^{(l)}}{l!} s_{l,m} \tag{A.14}$$

Since the leading terms of g_m are proportional to $f^{(m)}$, and given the assumed form for $f[s(n)]$ to be such that $f^{(1)} > 0$ and $f^{(2)} < 0$, then $g_m > 0$ for m odd, and $g_m < 0$ for m even.

In similar fashion, we expand the function $n_E f[s(n_E)]$ as

$$n_E f[s(n_E)] = g[s(n_E)] = \sum_m h_m (kLn_E)^m, \quad \text{where} \quad h_m = \sum_{l=m} \frac{g^{(l)}}{l!} s_{l,m} \tag{A.15}$$

But, we note that since $g^{(l)} = d^{(l)}g/ds^{(l)}$, $g^{(l)} = lf^{(l-1)} + f^{(l)}$ so that $h_m = g_m + g'_m$ where

$$g'_m = \sum_{l=m} \frac{f^{(l-1)}}{(l-1)!} s_{l,m} \tag{A.16}$$

so we have

$$(\rho - n_E) f[s(n_E)] = (\rho - \bar{k}) \sum_m g_m (kLn_E)^m - \bar{k} \sum_m g'_m (kLn_E)^m = \bar{\rho} f[s(n_E)] - \bar{k} g[s(n_E)] \tag{A.17}$$

where $\bar{k} = (kL)^{-1}$, $\bar{\rho} = \rho - \bar{k}$, and

$$g[(s(n_E)] = \sum_m g'_m (kLn_E)^m \tag{A.18}$$

We also expand the functions $\exp(\pm\tilde{n}_E)$. The resulting action $S(n_E)$ takes the form

$$\begin{aligned} S(n_E) = \quad & \int\int d^d x dt \left[\tilde{n}_E(\partial_t + \alpha - \bar{g}_1 kL) n_E - \frac{1}{2}\tilde{n}_E^2(\alpha + \bar{g}_1 kL) n_E + \tilde{n}_E |\bar{g}_2| (kL)^2) n_E^2 \right. \\ & \left. + \frac{1}{2}\tilde{n}_E^2 |\bar{g}_2| (kL)^2 n_E^2 + \cdots \right] \end{aligned} \tag{A.19}$$

where $\bar{g}_m = \bar{\rho} g_m - \bar{k} g'_m$.

It follows that for functions $n_E(\mathbf{x}, t)$ that vary slowly in space $\frac{1}{2} w_2 \nabla^2 n_E$ is small compared to $w_0 n_E$, so that in most expressions the terms proportional to $\nabla^{2m} n_E^m$ can be neglected. However this is not always the case for $m = 1$. Thus the first term can be written approximately as $\tilde{n}_E(\partial_t + \alpha - \bar{g}_1 k w_0 + \frac{1}{2}\bar{g}_1 k w_2 \nabla^2) n_E = \tilde{n}_E(\partial_t + \mu_E - D_E \nabla^2) n_E$ where $\mu_E = \alpha - \bar{g}_1 k w_0$ and $D_E = \frac{1}{2}\bar{g}_1 k w_2$.

Therefore, the expression for the action is now reduced to the form

$$S(n_E) = \int\int d^d x dt \left[\tilde{n}_E(\partial_t + \mu_E - D_E\nabla^2)n_E - \tilde{n}_E^2 G_1 n_E + \tilde{n}_E G_2 n_E^2 + \frac{1}{2}\tilde{n}_E^2 G_2 n_E^2 + \cdots\right] \tag{A.20}$$

where $G_1 = \frac{1}{2}(\alpha + \bar{g}_1 k w_0)$, $G_2 = |\bar{g}_2|k^2 w_0^2$. We need to demonstrate that the last term in $S(n_E)$, i.e., $\frac{1}{2}\tilde{n}_E^2 G_2 n_E^2$, and all higher order terms, are *irrelevant* in the sense of the renormalization group.

The renormalization group (RG) analysis is carried out via dimensional analysis. It can be shown that all the terms in $S(n_E)$ are zero-dimensional when integrated over d-dimensional space and over time, i.e., $[d^d x\, dt] = L^{-(d+2)}$ and (any term in the integrand) $= L^{d+2}$. However, as it stands $[n_E] = L^d$, but $[\tilde{n}_E] = L^0$, so that $[\tilde{n}_E n_E] = L^{0+d} = L^d$. This is not suitable for the scaling analysis implemented in the RG process. We therefore introduce a new *scaling*,

$$\tilde{s}_E = \sqrt{\frac{G_1}{G_2}}\tilde{n}_E, \quad s_E = \sqrt{\frac{G_2}{G_1}}n_E \tag{A.21}$$

such that $\tilde{s}_E s_E = \tilde{n}_E n_E$ where $[G_2/G_1] = L^{-d}$. The effect of this scaling is that both $\tilde{s}_E$ and s_E have dimension $L^{d/2}$. Let

$$\sqrt{G_1 G_2} = u_E \tag{A.22}$$

The net effect of this scaling transformation is that

$$S(s_E) = \int\int d^d x dt \left[\tilde{s}_E(\partial_t + \mu_E - D_E\nabla^2)s_E + u_E\tilde{s}_E(s_E - \tilde{s}_E)s_E + \cdots\right] \tag{A.23}$$

The constants of all higher-order terms all have dimensions such that the dimension of their ratio to the coupling constant u scales as $L^{-\beta d}$, where $\beta > 0$, so they become *irrelevant* as $L \to \infty$. It follows that

$$S(s_E) = \int\int d^d x dt \left[\tilde{s}_E(\partial_t + \mu_E - D_E\nabla^2)s_E + u_E\tilde{s}_E(s_E - \tilde{s}_E)s_E\right] \tag{A.24}$$

is the *renormalized action* of the large-scale neural activity of a single neural population.

A.4 Renormalizing the synaptic plasticity action

We now proceed to renormalize the action $S(b_H)$ just as we renormalized $S(n_E)$. We therefore expand the exponential term in Equation 3.44 and rewrite $S(b_H)$ in the form:

$$\begin{aligned} S(b_H) = \quad & \iint d^d x dt \left[\tilde{b}_H \partial_t b_H + H_1 \tilde{b}_H b_H n_H - \frac{1}{2} H_1 \tilde{b}_H^2 b_H n_H \right. \\ & \left. + H_2 (n_E - n_{E,0}) \tilde{b}_H \frac{n_H}{\rho_S} + H_2 (n_E - n_{E,0}) \tilde{b}_H^2 \frac{n_H}{\rho_S} \right] \end{aligned} \tag{A.25}$$

where $H_1 = \beta g_E |\kappa_{E,S}| / \rho_S$, and $H_2 = \beta g_E$.

We now introduce the scaling

$$\tilde{s}_H = \sqrt{\frac{H_2}{H_1}} \tilde{b}_H, \quad s_H = \sqrt{\frac{H_1}{H_2}} b_H \tag{A.26}$$

such that $\tilde{s}_H s_H = \tilde{b}_H b_H$, and $[H_1/H_2] = L^{-d}$. This scaling is analogous to the scaling of n and $\tilde{n}$ which we carried out earlier for neural activities. As before, the effect of this scaling is that both $\tilde{s}_H$ and s_H have dimension $L^{d/2}$.

Let

$$\sqrt{H_1 H_2} = u_H, \quad H_1 = 2\tau_H \tag{A.27}$$

and recall that Equation A.21 scales n_E to $\sqrt{G_1/G_2} s_E$.

Following the procedure outlined earlier we can calculate which terms in the transformed action $S(s_H)$ become irrelevant under scaling transformations. The resulting renormalized synaptic plasticity action takes the form:

$$S(s_H) = \int \int d^d x dt \left[\tilde{s}_H \partial_t s_H + u_H \tilde{s}_H s_H m_H + v_H (s_E - s_{E,0}) \tilde{s}_H m_H \right] \tag{A.28}$$

where

$$v_H = \sqrt{\frac{G_1}{G_2}}\frac{H_2}{\rho_S} \quad \text{and} \quad m_H = \sqrt{\frac{H_1}{H_2}}n_H \tag{A.29}$$

so that v_H has the same scaling dimension as u_H.

A.5 Renormalizing the driven neural action

We now assume that $n_H(\mathbf{x}, t) \neq 0$, so that the function s_E now takes the form

$$s(n_E, n_H) = k(Ln_E + b_H\frac{n_H}{\rho_S}) \tag{A.30}$$

It follows that the function $(\rho - n)f[s(n_E, n_H)]$ can now be expanded in the normal ordered form

$$(\rho - n)f[s(n_E, n_H)] = \sum_m \bar{g}_m \left((kLn_E)^m + (kb_H\frac{n_H}{\rho_S})^m \right) + \bar{h}_2 kLn_E b_H \frac{n_H}{\rho_S} + \cdots \tag{A.31}$$

where $\bar{h}_2 = \bar{\rho}f^{(2)}$. The effect of this is to generate additional terms in the neural action. We therefore expand Equation A.31 and retain only the first few terms because all the terms which give rise to 4-vertices or higher will not survive the renormalization group procedure. (see [109]) The extra terms we include in the action are

$$(\tilde{n}_E + \frac{1}{2}\tilde{n}_E^2)\left(\bar{g}_1(kb_H\frac{n_H}{\rho_S}) - |\bar{g}_2|(kb_H\frac{n_H}{\rho_S})^2 - |\bar{h}_2|(kLn_E kb_H\frac{n_H}{\rho_S}) \right) \tag{A.32}$$

However, only the term $\tilde{n}_E\bar{g}_1 kb_H n_H/\rho_S$ survives the RG process as $v_E\tilde{s}_E s_H m_H$, where v_E is a constant with the same scaling dimension as v_H and u_H.

A.6 Renormalizing the combined action

To renormalize the combined action is now simple, we simple add together the renormalized actions for the driven neural action, and that for synaptic plasticity. The result is

$$\begin{aligned} S(s_E, s_H) = \quad & \iint d^d x dt \, [\tilde{s}_E(\partial_t + \mu_E - D_E \nabla^2) s_E + u_E \tilde{s}_E (s_E - \tilde{s}_E) s_E \\ & + v_E \tilde{s}_E s_H m_H + \tilde{s}_H \partial_t s_H + u_H \tilde{s}_H s_H m_H + v_H (s_E - s_{E,0}) \tilde{s}_H m_H] \end{aligned} \quad \text{(A.33)}$$

where u_E, v_E and u_H, v_H are renormalized constants, all with the scaling dimension $L^{2-d/2}$.

APPENDIX B

MATLAB CODE FOR SIMULATIONS

B.1 Code used in Chapter 2 and 4

B.1.1 Simulation of traveling waves using spatial WC equations

```
%Simulations of spatiotemporal Wilson-Cowan equations
clear all
%close all

%for y=1:100
%for z=1:10

%Parameter settings
%wee=2.0;wie=1.65;wei=1.5;wii=.01;
%see=70;sie=90;sei=90;sii=70;
c=1;d=1;
%a=10;
%wee=16*c;wie=14.675*d;wei=37*d;wii=3*c; %%DWPs
wee=16*c;wie=91*d;wei=27*d;wii=20*c;
see=2.5;sie=2.7;sei=2.7;sii=2.5;    %%%sei>see
%betaE=1;betaI=1;tauE=1;tauI=3.22;  %%DWPs
betaE=1.1;betaI=1.1;tauE=0.1;tauI=0.18;
alphaE=1.5;alphaI=1;
aE=1.2;aI=1;
thetaE=2.6;thetaI=8;
inputstrength=1.2*8;%+2.5*(z-1)/9;
E_t=4.9105;E_sd=2.775182;I_t=10.77258872;I_sd=3.3302184463;
% E_t=18;E_sd=45;I_t=10;I_sd=10;
```

```
%Spatial discretization of connectivity using trapezoidal rule
L=100;N=101;dx=L/(N-1);
WEE=nan(N);WEI=nan(N);WIE=nan(N);WII=nan(N);
for i=1:N
    %W70(:,i) = exp(-abs(dx*((1:N)-i))/70)*dx;
    %W90(:,i) = exp(-abs(dx*((1:N)-i))/90)*dx;
    %W70(:,i) = exp(-abs(dx*((1:N)-i))/2.100)*dx/2.100;
    %W90(:,i) = exp(-abs(dx*((1:N)-i))/2.5)*dx/2.5;
    %WEE(:,i) = abs(dx*((1:N)-i)+a).*exp(-abs(dx*((1:N)-i))/see)
    %           *dx/(2*a*see+2*see^2*exp(-a/see));
    WEE(:,i) = exp(-abs(dx*((1:N)-i))/see)*dx/(2*see);
    WEI(:,i) = exp(-abs(dx*((1:N)-i))/sei)*dx/(2*sei);
    WIE(:,i) = exp(-abs(dx*((1:N)-i))/sie)*dx/(2*sie);
    WII(:,i) = exp(-abs(dx*((1:N)-i))/sii)*dx/(2*sii);
end
WEE(:,[1 end])=WEE(:,[1 end])/2;
WEI(:,[1 end])=WEI(:,[1 end])/2;
WIE(:,[1 end])=WIE(:,[1 end])/2;
WII(:,[1 end])=WII(:,[1 end])/2;

%Initialize and simulate using Forward-Euler
M=281;dt=.01;% simulation time is M*dt;
E=zeros(N,M);I=zeros(N,M);
maxwave=zeros(1,M);maxwaveindex=zeros(1,M);
maxwaveintime=zeros(N,1);maxwaveindexintime=zeros(N,1);
%Enoise=zeros(N,M);Inoise=zeros(N,M);
%for k=1:25
%    E(k,1)=0;
%    E(50+k,1)=0;
%    I(k,1)=0;
%    I(k+50,1)=0;
%end
%IL=ceil(1/dx);IR=floor(5/dx);
```

```
for i=2:M
    B=zeros(N,1);
    if (i<55)
        B(45:55)=B(45:55)+inputstrength;
    end
    %JE = wee*W70*E(:,i-1)-wie*W90*I(:,i-1)+B;
    %JI = wei*W90*E(:,i-1)-wii*W70*I(:,i-1);

    %JE = wee*WEE*E(:,i-1)-0.2*wie*WIE*I(:,i-1)+B+0.0;%+1.5;%+B;
    %JEnoise=awgn(JE,80);
    %Ecurr=JE+JEnoise;

    %JI = wei*WEI*E(:,i-1)-0.2*wii*WII*I(:,i-1)+B+0.0;%+0;%+B;
    %JInoise=awgn(JI,80);
    %Icurr=JI+JInoise;

    JE=wee*WEE*E(:,i-1)+B;
    JEnoise=awgn(JE,80);

    JI = -0.2*wii*WII*I(:,i-1)+B;
    JInoise=awgn(JI,80);

%Gaussian
    %FE = exp(-((JEnoise-E_t)/E_sd).^2)-exp(-((-E_t)/E_sd).^2);
    %FI = exp(-((JInoise-I_t)/I_sd).^2);%-exp(-((-I_t)/I_sd).^2);
    %FE=max(0,FE);FI=max(0,FI);
%Sigmoid
    %FE=1./(1+exp(-(JE-12.41)/2))-1./(1+exp(12.41/2));
    %FI=1./(1+exp(-(JI-7.33)/.95))-1./(1+exp(7.33/.95));
    %FE=1./(1+exp(-1.3*(JE-4)));%-1./(1+exp(1.3*4));   %% Decaying wave
    %parameters (DWPs)
    %FI=1./(1+exp(-1*(JI-10)));%-1./(1+exp(2*3.7));    %% DWPs
```

```
    FE=1./(1+exp(-aE*(JEnoise-thetaE)))-1./(1+exp(aE*thetaE));
    FI=1./(1+exp(-aI*(JInoise-thetaI)));%-1./(1+exp(1*8));
    FE=max(0,FE);FI=max(0,FI);

    %FEnoise=1./(1+exp(-aE*(Ecurr-thetaE)))-1./(1+exp(aE*thetaE));
    %FInoise=1./(1+exp(-aI*(Icurr-thetaI)));%-1./(1+exp(aI*thetaI));
    %FEnoise=max(0,FEnoise);FInoise=max(0,FInoise);

    E(:,i)= E(:,i-1)+dt*(-(alphaE*E(:,i-1))+(1-E(:,i-1)).*betaE.*FE)/tauE;
    I(:,i)= I(:,i-1)+dt*(-(alphaI*I(:,i-1))+(1-I(:,i-1)).*betaI.*FI)/tauI;

    %E(:,i)= E(:,i-1)+dt*(-(alphaE*E(:,i-1))+betaE.*FE)/tauE;  %%No 1-E
    %I(:,i)= I(:,i-1)+dt*(-(alphaI*I(:,i-1))+betaI.*FI)/tauI; %%No 1-I

    %Enoise(:,i)= Enoise(:,i-1)+dt*(-(1.5*Enoise(:,i-1))
    %             +(1-Enoise(:,i-1)).*betaE.*FEnoise)/tauE;
    %Inoise(:,i)= Inoise(:,i-1)+dt*(-(1*Inoise(:,i-1))
    %             +(1-Inoise(:,i-1)).*betaI.*FInoise)/tauI;

    [maxwave(1,i),maxwaveindex(1,i)]=max(E(:,i)-I(:,i));
end
for j=1:N
   [maxwaveintime(j,1),maxwaveindexintime(j,1)]=max(E(j,:)-I(j,:));
end

%figure(1);imagesc(E-I);
%%%%FOR E AND I SIM
%figure(1);
%for i=1:3:M;pause(0.05);plot(dx*(0:N-1),E(:,i)+I(:,i),
%dx*maxwaveindex(1,i),maxwave(1,i),'r--o',dx*(0:N-1),E(:,i),dx*(0:N-1),
%I(:,i));ylim([-0.1 1.0]);xlim([0 L]);drawnow;
%str=sprintf('Time= %g',i);
%title(str)
```

```
%end; %pause(0.001);

%figure(2);
%for i=1:3:M;pause(0.05);plot(dx*(0:N-1),E(:,i),dx*(0:N-1),I(:,i));
%ylim([-0.1 1.0]);xlim([0 L]);drawnow;
%str=sprintf('Time= %g',i);
%title(str)
%end; %pause(0.001);

figure(3);
subplot(2,2,1)
plot(dx*(0:N-1),E(:,5));ylim([-0.1 0.5]);xlim([0 L]);
subplot(2,2,2)
plot(dx*(0:N-1),E(:,40));ylim([-0.1 0.5]);xlim([0 L]);
subplot(2,2,3)
plot(dx*(0:N-1),E(:,80));ylim([-0.1 0.5]);xlim([0 L]);
subplot(2,2,4)
plot(dx*(0:N-1),E(:,120));ylim([-0.1 0.5]);xlim([0 L]);

figure(4);
subplot(2,2,1)
plot(dx*(0:N-1),I(:,20));ylim([-0.1 0.5]);xlim([0 L]);
subplot(2,2,2)
plot(dx*(0:N-1),I(:,40));ylim([-0.1 0.5]);xlim([0 L]);
subplot(2,2,3)
plot(dx*(0:N-1),I(:,80));ylim([-0.1 0.5]);xlim([0 L]);
subplot(2,2,4)
plot(dx*(0:N-1),I(:,120));ylim([-0.1 0.5]);xlim([0 L]);

%figure(3);
%for i=1:3:M;pause(0.05);plot(dx*(0:N-1),I(:,i));ylim([-0.1 1.0]);
%xlim([0 L]);drawnow;
%str=sprintf('Time= %g',i);
```

```
%title(str)
%end; %pause(0.001);

%globalmax=max(maxwave);
%n=20;
%figure(2);plot(dx*(0:N-1),E(:,n)-I(:,n),dx*maxwaveindex(1,n),maxwave(1,n),
%           'b--o',dx*(0:N-1),E(:,n+5)-I(:,n+5),dx*maxwaveindex(1,n+5),
%           maxwave(1,n+5),'g--o',dx*(0:N-1),E(:,n+10)-I(:,n+10),
%           dx*maxwaveindex(1,n+10),maxwave(1,n+10),'r--o',dx*(0:N-1),
%           E(:,n+15)-I(:,n+15),dx*maxwaveindex(1,n+15),maxwave(1,n+15),
%           'c--o',dx*(0:N-1),E(:,n+20)-I(:,n+20),dx*maxwaveindex(1,n+20),
%           maxwave(1,n+20),'m--o',dx*(0:N-1),E(:,n+25)-I(:,n+25),
%           dx*maxwaveindex(1,n+25),maxwave(1,n+25),'y--o',dx*(0:N-1),
%           E(:,n+30)-I(:,n+30),dx*maxwaveindex(1,n+30),maxwave(1,n+30),
%           'k--o',dx*(0:N-1),E(:,n+35)-I(:,n+35),dx*maxwaveindex(1,n+35),
%           maxwave(1,n+35),'b--o',dx*(0:N-1),E(:,n+40)-I(:,n+40),
%           dx*maxwaveindex(1,n+40),maxwave(1,n+40),'g--o');xlim([50 75]);
%           ylim([0 0.5])
%figure(2);plot(dx*(0:N-1),(E(:,n)+I(:,n))./maxwave,dx*maxwaveindex(1,n),
%           maxwave(1,n),'b--o',dx*(0:N-1),(E(:,n+5)+I(:,n+5))./maxwave,
%           dx*maxwaveindex(1,n+5),maxwave(1,n+5),'g--o',dx*(0:N-1),
%           (E(:,n+10)+I(:,n+10))./maxwave,dx*maxwaveindex(1,n+9),
%           maxwave(1,n+10),'r--o',dx*(0:N-1),
%           (E(:,n+15)+I(:,n+15))./maxwave,dx*maxwaveindex(1,n+15),
%           maxwave(1,n+15),'c--o',dx*(0:N-1),
%           (E(:,n+20)+I(:,n+20))./maxwave,dx*maxwaveindex(1,n+20),
%           maxwave(1,n+20),'m--o',dx*(0:N-1),
%           (E(:,n+25)+I(:,n+25))./maxwave,dx*maxwaveindex(1,n+25),
%           maxwave(1,n+25),'y--o',dx*(0:N-1),
%           (E(:,n+30)+I(:,n+30))./maxwave,dx*maxwaveindex(1,n+30),
%           maxwave(1,n+30),'k--o',dx*(0:N-1),
%           (E(:,n+35)+I(:,n+35))./maxwave,dx*maxwaveindex(1,n+35),
%           maxwave(1,n+35),'b--o',dx*(0:N-1),
```

```
%           (E(:,n+40)+I(:,n+40))./maxwave,dx*maxwaveindex(1,n+40),
%           maxwave(1,n+40),'g--o');
%l=100;
%figure(3);plot(dt*(0:M-1),E(l,:)-I(l,:),dt*(maxwaveindexintime(l,1)),
%            maxwaveintime(l,1),'b--o',dt*(0:M-1),E(l+5,:)-I(l+5,:),
%            dt*maxwaveindexintime(l+5,1),maxwaveintime(l+5,1),'g--o',
%            dt*(0:M-1),E(l+10,:)-I(l+10,:),
%            dt*(maxwaveindexintime(l+10,1)-1),maxwaveintime(l+10,1),
%            'r--o',dt*(0:M-1),E(l+15,:)-I(l+15,:),
%            dt*maxwaveindexintime(l+15,1),maxwaveintime(l+15,1),'c--o',
%            dt*(0:M-1),E(l+20,:)-I(l+20,:),dt*maxwaveindexintime(l+20,1),
%            maxwaveintime(l+20,1),'m--o',dt*(0:M-1),E(l+25,:)-I(l+25,:),
%            dt*maxwaveindexintime(l+25,1),maxwaveintime(l+25,1),'y--o',
%            dt*(0:M-1),E(l+30,:)-I(l+30,:),dt*maxwaveindexintime(l+30,1),
%            maxwaveintime(l+30,1),'k--o',dt*(0:M-1),E(l+35,:)-I(l+35,:),
%            dt*maxwaveindexintime(l+35,1),maxwaveintime(l+35,1),'b--o',
%            dt*(0:M-1),E(l+40,:)-I(l+40,:),dt*maxwaveindexintime(l+40,1),
%            maxwaveintime(l+40,1),'g--o');xlim([15*dt (M*dt)/2]);
%            %ylim([-0.1 0.5])
%expf=fit((dx*maxwaveindex(1,55:85))',
%           (maxwave(1,55:85)/globalmax)','exp1');
%figure(3);plot(expf,dx*maxwaveindex(1,55:2:80),
%               maxwave(1,55:2:85)/globalmax,'predobs');
%expf=fit((dx*maxwaveindex(1,40:185))',
%              (maxwave(1,40:185)/globalmax)','exp1')
%figure(4);plot(expf,dx*maxwaveindex(1,40:185),
%               maxwave(1,40:185)/globalmax,'predobs');%xlim([55 65])
%max(dx*maxwaveindex(1,40:M))
%linff=fit((dx*maxwaveindex(1,55:85))',
%          (maxwave(1,55:85)/globalmax)','poly1');
%figure(4);plot(dx*maxwaveindex(1,15:2:65),maxwave(1,15:2:65)/globalmax,
%           'd','MarkerFaceColor','b','MarkerSize',4);xlim([45 55])
%linf=fit((dx*maxwaveindex(1,40:185))',(dt*(40:185))','poly1')
```

```
%figure(5);plot(linf,dx*maxwaveindex(1,40:185),dt*(40:185),'predobs');
%xlim([55 65])
%figure(5);plot(dx*maxwaveindex(1,40:2:105),dt*(40:2:105),'d',
%'MarkerFaceColor','b','MarkerSize',4);xlim([45 55])

%figure(2);for i=1:3:M; pause(0.05);plot(dx*(0:N-1),E(:,i)+I(:,i));
%                   ylim([-0.25 1.0]);xlim([0 L]);drawnow;end;
%figure(2);for i=1:3:M; pause(0.02);plot(dx*(0:N-1),E(:,i),dx*(0:N-1),
%                    I(:,i),dx*(0:N-1),(E(:,i)+I(:,i)));ylim([-0.25 1.0]);
%                    xlim([0 L]);drawnow;end;
%figure(2);for i=1:3:M; pause(0.02);plot(dx*(0:N-1),E(:,i),dx*(0:N-1),
%                    Enoise(:,i),dx*(0:N-1),I(:,i),dx*(0:N-1),Inoise(:,i),
%                    dx*(0:N-1),(E(:,1)+I(:,i)));ylim([-0.25 1.0]);
%                    xlim([0 L]);drawnow;end;

% Correlation across distance plots
%reference=(N-1)/2;
%for i=1:20
%    correlations=corrcoef((E(reference,15:M)+I(reference,15:M))',
%                 (E(reference+3+i,15:M)+I(reference+3+i,15:M))');
%    corrcoefs(i,z)=correlations(1,2);   %%column needs to be z
                                         %%if running many times
%    distance(i,z)=dx*i;                 %%column needs to be z
                                         %%if running many times
%end

%corrlinfit=fit(distance',corrcoefs','poly1');
%figure(11);hold;plot(corrlinfit,distance,corrcoefs);ylim([0 1]);
%xlim([0 20])

%figure(11);hold;plot(distance,corrcoefs,'-o','MarkerFaceColor',[0 0 0]);
%ylim([0 1])
%end
```

```
%figure(1);for i=1:3:M; pause(0.05);plot(dx*(0:N-1),E(:,i)+I(:,i),
% dx*maxwaveindex(1,i),maxwave(1,i),'r--o');ylim([-0.1 2.0]);
% xlim([0 L]);drawnow;end; %pause(0.001);
%meancorrcoefs=mean(corrcoefs,2);

%figure(20);hold on;
%C={[0 0 1],'g','r','k','y','c','m',[.5 .6 .6],[.5 .6 .8],[.5 .6 1]};
%for ii=1:z
%    plot(distance(:,ii),corrcoefs(:,ii),'color',C{ii},'marker','o');
%    ylim([0 1])
%end
%legend({'0';'';'';'';'';'';'';'';'';'2.5'})
%plot(distance(:,z),meancorrcoefs,'-o','MarkerFaceColor',[0 0 0])

%averagemeancorrcoefsnoise(y,1)=mean(meancorrcoefs);
%end
%figure(14);
%plot(1:y,averagemeancorrcoefsnoise);
%str=sprintf('Ensemble & distance-averaged corr coef vs signal/noise,
%stimulus= %g',inputstrength);
%title(str)

%close all;A=rand(1,5);[maxA(1),maxAindex(1)]=max(A(1,:));
%for i=2:25; A(i,:)=A(i-1,:)+2*rand(1,5)-1;
%[maxA(i),maxAindex(i)]=max(A(i,:));
%end;figure(1);
%for i=1:25; pause(0.05);plot(1:5,A(i,:),maxAindex(i),maxA(i),'r--o');
%drawnow;
%end
```

B.1.2 Simulation of traveling waves using Gillespie algorithm

```
% This program simulates the spatially-extended Wilson-Cowan equations. It
% clumps N_cells neurons into N_EI modules (80% E 20% I per module).
% Neurons in a given population all receive the same input. Weights decay
% exponentially with distance. Rows correspond to modules in space. Columns
% correspond to modules in time.

% Jeremy Neuman 3/15

clear all;
%close all
starttime=tic;
for z=1:1
%clearvars -except starttime z
for y=1:1
clearvars -except meancorrcoefs starttime distance corrcoefs z y
blocks=1;
block_size=500000;
% Parameters and initial values (all initial activity is set to 0)
N_cells=8080;                       % number of cells in population
L=100;N_EI=101;dx=L/(N_EI-1);       % N_EI are number of pieces on line
NE_cells_per=0.8*N_cells/N_EI;
NI_cells_per=0.2*N_cells/N_EI;
%NE=zeros(NE_cells_per,1);
%NI=zeros(NI_cells_per,1);
%for i=1:(0.3*NE_cells)
%    NE(i)=1;
%end
%for j=1:(0.3*NI_cells)
%    NI(j)=1;
%end
%N=repmat([NE;NI],N_EI,1);                    % Activity vector
N=zeros(N_cells,1);rands=rand(N_cells,1);
i=1;
```

```
for i=1:N_cells
    if rands(i)>0.5                              % Make % of neurons 1
        N(i)=0;                                  % Initial value of network
    end
end
Nvec=repmat([ones(NE_cells_per,1);zeros(NI_cells_per,1)],N_EI,1);
% Vector of neuron type - 1 if neuron is E, 0 if neuron is I
%EAD(1) = 0;%sum(NE)/NE_cells;
%IAD(1) = 0;%sum(NI)/NI_cells;
%EAS=zeros(N_EI,block_size);
%IAS=zeros(N_EI,block_size);
for i=1:N_EI                % Update activity matrices of E and I modules
    EAS(i,1)=mean(N((i-1)*(NE_cells_per+NI_cells_per)+1:(i-1)*
    (NE_cells_per+NI_cells_per)+NE_cells_per));
    IAS(i,1)=mean(N((i-1)*(NE_cells_per+NI_cells_per)+1+NE_cells_per:
    (i-1)*(NE_cells_per+NI_cells_per)+NE_cells_per+NI_cells_per));
end
tauE=0.1;tauI=0.18;              % times constants
alphaE=1.5/tauE;alphaI=1/tauI;   % decay rate a -> q (set around 1/100 ms)
betaE=1.1/tauE;betaI=1.1/tauI;   % amplitude of firing rate functions
wee=16;wie=91;wei=27;wii=20;     % initial feedback weight between neurons
see=2.5;sie=2.7;sei=2.7;sii=2.5; % space constants, sei>see always
H=0.4;Q=0.4;                     % input
aE=1.2;aI=1;                     % slopes of firing rate functions
thetaE=2.6;thetaI=8;             % thresholds of firing rate functions
inputstrength=2.8+(z-1)*1.0;
xES=zeros(N_EI,1);xIS=zeros(N_EI,1);
f_tildeES=betaE./(1+exp(-aE*(xES-thetaE)))-betaE./(1+exp(aE*thetaE));
f_tildeIS=betaI./(1+exp(-aI*(xIS-thetaI)));%-betaI./(1+exp(aI*thetaI));
f_tildeS=zeros(N_cells,1);
T=3;                                    % Epoch (in s)

%Spatial discretization of connectivity using trapezoidal rule
```

```
WEE=nan(N_EI);WEI=nan(N_EI);WIE=nan(N_EI);WII=nan(N_EI);
for i=1:N_EI
    WEE(:,i) = exp(-abs(dx*((1:N_EI)-i))/see)*dx/(2*see);
    WEI(:,i) = exp(-abs(dx*((1:N_EI)-i))/sei)*dx/(2*sei);
    WIE(:,i) = exp(-abs(dx*((1:N_EI)-i))/sie)*dx/(2*sie);
    WII(:,i) = exp(-abs(dx*((1:N_EI)-i))/sii)*dx/(2*sii);
end
WEE(:,[1 end])=WEE(:,[1 end])/2;
WEI(:,[1 end])=WEI(:,[1 end])/2;
WIE(:,[1 end])=WIE(:,[1 end])/2;
WII(:,[1 end])=WII(:,[1 end])/2;

% Stochastic model
count=1;                            % counter for the AS array
cum_t=0;                            % initial time
times(count)=cum_t;                 % stochastic time base

while cum_t < T                     % Main LOOP
    if count==length(EAS)
            EAS=[EAS zeros(N_EI,block_size)];
            IAS=[IAS zeros(N_EI,block_size)];
            blocks=blocks+1;
    end
    B=zeros(N_EI,1);
    if (cum_t<1.5)
       B(48:52)=B(48:52)+inputstrength;
    end
    xES=wee*WEE*EAS(:,count)-0.2*wie*WIE*IAS(:,count)+H+B;
    % Define/update current
    xIS=wei*WEI*EAS(:,count)-0.2*wii*WII*IAS(:,count)+Q+B;
    % These vectors are N_EI by 1
    f_tildeES=betaE./(1+exp(-aE*(xES-thetaE)))-betaE./(1+exp(aE*thetaE));
    % N_EI by 1
```

```
f_tildeIS=betaI./(1+exp(-aI*(xIS-thetaI)));%-betaI./(1+exp(aI*thetaI));
% N_EI by 1
f_tildeES=max(0,f_tildeES);f_tildeIS=max(0,f_tildeIS);
% Eliminate negative firing rate values. Doesn't change dynamics
% but is necessary for Gillespie
for i=1:N_EI              % vector made here will be N_cells by 1
    f_tildeS((i-1)*(NE_cells_per+NI_cells_per)+1:
    i*(NE_cells_per+NI_cells_per),1)=
    [repmat(f_tildeES(i),NE_cells_per,1);
        repmat(f_tildeIS(i),NI_cells_per,1)];
end
% compute the overall rates in the variables a#
a1=sum(N.*Nvec.*alphaE+N.*(-Nvec+1).*alphaI); % sum of decay rates
a2=dot(-N(:)+1,f_tildeS);                    % sum of activation rates
a0=a1+a2;                                    % total sum of rates
% pick a two random # from uniform distribution
%(following Gillespie's algorithm)
r=rand(1,2);

% compute timestep tau (based on exponential distribution)
tau=(1/a0)*log(1/r(1));         % Gillespie (1977) Eq (21a)

% Now we compute the cumulative distribution of all cells
% this could be done more efficient here in the all-to-all connection
% case; here we only have two variables to update Q and A
% However, the following approach of updating individual cells is
% more general.
P=N.*Nvec.*alphaE+N.*(-Nvec+1).*alphaI;  % all active cells multiplied
                                         % by alphaE if E neuron,
                                         % alphaI if I neuron
for i=1:length(P)
    if P(i)==0;
        P(i)=f_tildeS(i);
```

```
        end;   % all inactive cells become correspond f_tildeS
    end;
    %plot(P)
    P=P./sum(P);                          % normalize P
    F=cumsum(P);                          % cumulative function F of all
                                          % probabilities associated with
                                          % the cells in N

    % pick a cell # using the cumulative distribution
    pick=0;
    i=0;
    while pick == 0
        i=i+1;
        if (F(i)>=r(2));mu=i;pick=1;end; % (Gillespie, (1977), Eq (21b)
    end;

    % Update time, cell and counter
    if N(mu)==1;N(mu)=0;else N(mu)=1;end;   % Update cell
    count=count+1;                        % update the counter
    cum_t=cum_t+tau;                      % update the time
    times(count)=cum_t;                   % and stochastic timebase
    for i=1:N_EI                          % Update activity matrices
                                          % of E and I modules
        EAS(i,count)=mean(N((i-1)*(NE_cells_per+NI_cells_per)+1:(i-1)*
        (NE_cells_per+NI_cells_per)+NE_cells_per));
        IAS(i,count)=mean(N((i-1)*(NE_cells_per+NI_cells_per)+1+
        NE_cells_per:(i-1)*(NE_cells_per+NI_cells_per)+NE_cells_per+
        NI_cells_per));
    end
end;
%difftimes=diff(times);

% Deterministic model
```

```
% -------------------
% this simulation based on kinetic rate equation
% note that equilibrium is at dA=0
% --> A_equilibrium = f/alpha
%{
M=501;dt=.01;% simulation time is M*dt;
E=zeros(N_EI,M);I=zeros(N_EI,M);
%E=zeros(N_EI,length(times));I=zeros(N_EI,length(times));
maxwave=zeros(1,M);maxwaveindex=zeros(1,M);
%maxwave=zeros(1,length(times));maxwaveindex=zeros(1,length(times));
maxwaveintime=zeros(N_EI,1);maxwaveindexintime=zeros(N_EI,1);

%for k=1:25
%    E(k,1)=0;
%    E(50+k,1)=0;
%    I(k,1)=0;
%    I(k+50,1)=0;
%end
%IL=ceil(1/dx);IR=floor(5/dx);
for i=2:M
    B=zeros(N_EI,1);
    if (i<15)
        B(48:52)=B(48:52)+inputstrength;
    end
    %JE = wee*W70*E(:,i-1)-wie*W90*I(:,i-1)+B;
    %JI = wei*W90*E(:,i-1)-wii*W70*I(:,i-1);
    JE = wee*WEE*E(:,i-1)-0.2*wie*WIE*I(:,i-1)+B;%+1.5;%+B;
    %JEnoise=awgn(JE,1000);
    JI = wei*WEI*E(:,i-1)-0.2*wii*WII*I(:,i-1)+B;%+0;%+B;
    %JInoise=awgn(JI,1000);

%Gaussian
    %FE = exp(-((JE-E_t)/E_sd).^2)-exp(-((-E_t)/E_sd).^2);
```

```
    %FI = exp(-((JI-I_t)/I_sd).^2)-exp(-((-I_t)/I_sd).^2);
%Sigmoid
    %FE=1./(1+exp(-(JE-12.41)/2))-1./(1+exp(12.41/2));
    %FI=1./(1+exp(-(JI-7.33)/.95))-1./(1+exp(7.33/.95));
    %FE=1./(1+exp(-1.3*(JE-4)));%-1./(1+exp(1.3*4));   %% Decaying wave
    %parameters (DWPs)
    %FI=1./(1+exp(-1*(JI-10)));%-1./(1+exp(2*3.7));    %% DWPs

    FE=1./(1+exp(-aE*(JE-thetaE)))-1./(1+exp(aE*thetaE)); %%Terry params
    FI=1./(1+exp(-aI*(JI-thetaI)));%-1./(1+exp(1*8));     %%Terry params
    FE=max(0,FE);FI=max(0,FI);

    E(:,i)= E(:,i-1)+dt*(-(alphaE*E(:,i-1))+(1-E(:,i-1)).*betaE.*FE);%%1-E
    I(:,i)= I(:,i-1)+dt*(-(alphaI*I(:,i-1))+(1-I(:,i-1)).*betaI.*FI);%%1-I

    [maxwave(1,i),maxwaveindex(1,i)]=max(E(:,i)+I(:,i));
end
for j=1:N
   [maxwaveintime(j,1),maxwaveindexintime(j,1)]=max(E(j,:)+I(j,:));
end
%figure(1);imagesc(E-I);
figure(1);
for i=1:3:M; pause(0.05);plot(dx*(0:N_EI-1),E(:,i)+I(:,i),
% dx*maxwaveindex(1,i),maxwave(1,i),'r--o');ylim([-0.1 2.0]);
% xlim([0 L]);drawnow;end; %pause(0.001);
%for i=1:3:(count-1); plot(dx*(0:N_EI-1),E(:,i)+I(:,i),
% dx*maxwaveindex(1,i),maxwave(1,i),'r--o');ylim([-0.1 2.0]);
% xlim([0 L]);drawnow;end; %pause(0.001);
globalmax=max(maxwave);
%}

%{
% Avalanche Distributions
```

```
difftimes = diff(times);
spikes=0;
for j=1:length(AS)-1
    if AS(j+1)>AS(j)
        spikes=spikes+1;
    end
end
delta_t = times(end)/spikes;
sizeaval=0;
duraval=0;
counter=1;
spikecount=0;
duravalbegin=0;
i=1;
for i=1:length(difftimes)
if (i==1 && difftimes(i)<delta_t)
    if AS(i+1)>AS(i)
    spikecount=spikecount+1;
    end
end
if (i==1 && difftimes(i)>delta_t)
    sizeaval=0;
end
if i>1 && difftimes(i)<delta_t
    if AS(i)>AS(i-1)
        spikecount = spikecount+1;
    end
else
    if i>1 && AS(i)>AS(i-1)
        spikecount=spikecount+1;
    end
    duravalend=(times(i+1)+times(i))/2;
    sizeaval(counter) = spikecount;
```

```
    duraval(counter) = duravalend-duravalbegin;
    spikecount=0;
    duravalbegin=duravalend;
    counter=counter+1;
end
end
sizeaval=sizeaval(2:length(sizeaval));   %eliminating the first avalanche
duraval(2)=duraval(1)+duraval(2);
duraval=duraval(2:length(duraval));
[freqsize, size] = hist(sizeaval,15);
[freqdur, dur] = hist(duraval,15);
figure
subplot(2,2,1)
plot(size,log(freqsize),'o')
title('Avalanche Size Distribution')
xlabel('Size of Avalanche')
ylabel('Log Frequency')
subplot(2,2,2)
plot(dur,log(freqdur),'o')
title('Avalanche Duration Distribution')
xlabel('Duration of Avalanche')
ylabel('Log Frequency')
% plot results
%figure;hold
subplot(2,2,[3 4])
%}

EAS(:,count:end)=[];
IAS(:,count:end)=[];

% Plotting total activity
%figure(15);
for i=1000:1000:50000; figure(i); plot(dx*(0:N_EI-1),EAS(:,i)+IAS(:,i),
```

```
    dx*(0:N_EI-1),EAS(:,i)-IAS(:,i),dx*(0:N_EI-1),EAS(:,i),dx*(0:N_EI-1),
    IAS(:,i));ylim([-0.2 1.5]);xlim([0 L]);drawnow;end;%pause(0.05)

% Comparing determinstic with stochastic
%figure(3);hold
%for i=1:3:M; pause(0.05);plot(dx*(0:N_EI-1),E(:,i)+I(:,i),
% dx*maxwaveindex(1,i),maxwave(1,i),'r--o');ylim([-0.1 2.0]);
% xlim([0 L]);drawnow;end; %pause(0.001);
%for i=1:3:(count-1); plot(dx*(0:N_EI-1),EAS(:,i)+IAS(:,i));
% xlim([0 L]);ylim([-0.1 2.0]);drawnow;end;

%plot(timeD,EAD,'b',timeD,IAD,'k')
%plot(times(1:length(EAS)),EAS,'g',times(1:length(IAS)),IAS,'r')
%title ('Deterministic model (E blue I black); stochastic (E green I red)')
%xlabel('time (ms)')
%ylabel(' # of Active Cells')
% Power spectrum
%figure(6);
%power=abs(fft(EAS+IAS))/(count/2);power=power(1:count/2).^2;
%freq=[0:count/2-1]/T;semilogy(freq,power);axis([0 40 0 1]);

% Correlation across distance plots
reference=(N_EI-1)/2;
for i=1:20
    correlations=corrcoef((EAS(reference,1:count-1)-
    IAS(reference,1:count-1))',(EAS(reference+2+i,1:count-1)-
    IAS(reference+2+i,1:count-1))');
    corrcoefs(i,y,z)=correlations(1,2);
    distance(i,y)=dx*(i+2);
    %corrcoefs(i)=correlations(1,2);
    %distance(i)=dx*i;
end
corrcoefs(isnan(corrcoefs))=0;
```

```
%corrlinfit=fit(distance',corrcoefs','poly1')
%figure(17+z);plot(corrlinfit,distance,corrcoefs,'predobs');ylim([-0.1 1])
%str=sprintf('Input strength = %g, Number of cells = %g, Background = %g',
%             inputstrength,N_cells,H);
%title(str)
end
%meancorrcoefs=mean(corrcoefs,2);
%meancorrcoefs=reshape(meancorrcoefs,[i y])

%figure(z);hold on;
%for ii=1:y
%    plot(distance(:,ii),corrcoefs(:,ii),'-o','MarkerFaceColor',
%     [1 ii/21 0]);%,'o',distance(:,2),corrcoefs(:,2),'o',distance(:,3),
%     corrcoefs(:,3),'o',distance(:,4),corrcoefs(:,4),'o',distance(:,5),
%     corrcoefs(:,5),'o',distance(:,6),corrcoefs(:,6),'o',distance(:,7),
%     corrcoefs(:,7),'o',distance(:,8),corrcoefs(:,8),'.',distance(:,9),
%     corrcoefs(:,9),'.',distance(:,10),corrcoefs(:,10),'.',distance(:,11),
%     corrcoefs(:,11),'.',distance(:,12),corrcoefs(:,12),'.',
%     distance(:,13),corrcoefs(:,13),'.',distance(:,14),corrcoefs(:,14),
%     '.',distance(:,15),corrcoefs(:,15),'+',distance(:,16),
%     corrcoefs(:,16),'+',distance(:,17),corrcoefs(:,17),'+',
%     distance(:,18),corrcoefs(:,18),'+',distance(:,19),corrcoefs(:,19),
%     '+',distance(:,20),corrcoefs(:,20),'+',distance(:,21),
%     corrcoefs(:,21),'+');xlim([0 10]);ylim([0 1])
%end
%plot(distance(:,y),meancorrcoefs,'-o','MarkerFaceColor',[0 0 0])
%str=sprintf('E+I, Input strength = %g, Number of cells = %g,
%               Background = %g',inputstrength,N_cells,H);
%title(str)
%end
end
meancorrcoefs=mean(corrcoefs,2);
```

```
meancorrcoefs=reshape(meancorrcoefs,[i z]);

figure(31);
plot(distance(:,1),meancorrcoefs(:,1:z),'-o','MarkerFaceColor',[0 0 0]);
%str=sprintf('E-I, Input str. up as BlGRCPYBk, # cells = %g,
%            Background = %g, T = %g ',N_cells,H,T);
title(str)

endtimes=toc(starttime)
```

B.2 Code used in Chapter 3

B.2.1 Simulation of E network using space-clamped WC equations and Gillespie algorithm

```
for comp=1

    % Parameters model
    N_cells=900+(comp-1)*(6400-900);       % number of cells in population
    NH=0.45;                               % number of cells in external
                                           % population
    W=3.5;                                 % initial feedback weight
                                           % between neurons
    We=W;
    a=250;                                 % slope of sigmoid curve
    theta=20;                              % threshold of sigmoid curve
    alpha=0.2;                             % decay rate a -> q (set
                                           % around 1/100 ms)
    g=0.002;                               % f'/(Ith-W*f'), held to be
                                           % constant right now
    k=1;                                   % wH = k*bH
```

```
pE0=0.2;                                % Vogels' target rate
pES=0.001;                              % Window function amplitude
s=1/(1+exp(a*theta));
NHperc=0.0;
nearestneighbortorus=false;
nearestneighborreflex=false;
%Q=1.2;

% Parameters computation
dt=0.01;                                % Deterministic timestep for
                                        % the deterministic
                                        % computation(set at 1 ms)
T=500000;                               % Epoch (in s)
steps=floor(T/dt);                      % # of timesteps in
                                        % deterministic case
blocks=1;                               % Counts the number of zero
                                        % blocks added
block_size=3000000;
perc=1;

%N=round((rand(1)/2+.5)*rand(1,N_cells));   % randomized inital state
                                            % of vector N
i=1; %0.8*N_cells;                          % # of cells
N=[ones(i,1);zeros(N_cells-i,1)];           % not randomized initial
                                            % state of vector N
N=N(randperm(N_cells))';                    % randomized initial state
                                            % of vector N
%for i=1:450                                % make the first 8000 of
%    N(:,i)=1;                              % the 10,000 cells active
%end

%Allocate Memory
timeD=0:dt:T;                               % determinsitic timebase
```

```
AD=zeros(1,steps+1);                        % Deterministic
bHD=zeros(1,steps+1);                       % Deterministic
f_tildeD=zeros(1,steps+1);                  % Deterministic
Nones=ones(1,length(N));
AS=zeros(1,block_size);                     % Stochastic
avgbH=zeros(1,block_size);                  % Stochastic
time_steps=zeros(1,block_size);             % Stochatic time of events
f_tilde=zeros(1,N_cells);
variam=zeros(1,block_size);
variap=zeros(1,block_size);
variab=zeros(1,block_size);
P=zeros(1,3*N_cells);
count=1;                                    % timestep counter for
                                            % the AS array
cum_t=0;                                    % initial time
x=zeros(1,block_size);


% Initial values
AD(1)=sum(N)/N_cells;                       % initial value for the
                                            % deterministic case
bHD(1)=38.4;                                % initial external weight
                                            % value for the deter
bH=bHD(1)*ones(1,length(N));                % initial modifiable
                                            % weight Stochastic case
avgbH(1) = sum(bH)/N_cells;                 % initial average weights


%DETERMINISTIC Case
%     Deterministic model
%     -------------------
%     this simulation based on kinetic rate equation
%     note that equilibrium is at dA=0
```

```
%     --> A_equilibrium = f/alpha
%
%          for i=1:steps
%             x=AD(i)*W+NH*bHD(i);                        % current
%             f_tildeD(i)=1/(1+exp(-a*(x-theta)))-s;
%             dAD = f_tildeD(i)*(1-AD(i))-alpha*AD(i);
%             dbHD = -g*(AD(i)-pE0+pES*k*bHD(i))*NH;
%             AD(i+1)=AD(i)+dAD*dt;
%             bHD(i+1)=bHD(i)+dbHD*dt;
%          end;
    %plot(x,f_tildeD)
    % figure(1);hold
    % plot(timeD,AD,'k')
    % title ('Deterministic model (black); stochastic (blue)')
    % xlabel('time (s)')
    % ylabel(' % of Active Cells')
    % drawnow

    % Computing time help, also see marktime script
    exectimes=zeros(1,100);         % Calculating times between 2 marktimes
    tic;
    starttime=tic;                  % Starting time of the stochastic
                                    % calculation
    lasttime=tic;                   % Initializing lasttime

    % Equivalent Stochastic model
    % ---------------------------
    % this simulation based on stochastic model
    % Specific parameters and initial values
    % background of the method can be found in Gillespie (1976, 1977)

    if nearestneighbortorus==true;
        W=zeros(N_cells);
```

```
for m=0:(sqrt(N_cells)-1)
    for  l=m*sqrt(N_cells)+1:(m+1)*sqrt(N_cells)
    %^lattice site index number moving from left to right
    % (next row starts at left at l->l+1)
        i=m+1;              %x-coord of lattice site
        j=l-m*sqrt(N_cells); %y-coord of lattice site
        if i==1             %Boundary condition on the top
            x=sqrt(N_cells)*(sqrt(N_cells)-1)+j;
            W(l,x)=We;
        else
            top_near_neigh = sqrt(N_cells)*(i-2)+j;
            W(l,top_near_neigh)=We;
        end
        if i==sqrt(N_cells)  %Boundary condition on the bottom
            W(l,j)=We;
        else
            bottom_near_neigh = sqrt(N_cells)*i+j;
            W(l,bottom_near_neigh)=We;
        end
        if j==1             %Boundary condition on the left
            y=(m+1)*sqrt(N_cells);
            W(l,y)=We;
        else
            left_near_neigh = sqrt(N_cells)*(i-1)+(j-1);
            W(l,left_near_neigh)=We;
        end
        if j==sqrt(N_cells)  %Boundary condition on the right
            z=m*sqrt(N_cells)+1;
            W(l,z)=We;
        else
            right_near_neigh = sqrt(N_cells)*(i-1)+(j+1);
            W(l,right_near_neigh)=We;
        end
```

```
        end
    end
    W=sparse(W);

end

if nearestneighborreflex==true;
    W=zeros(N_cells);
    for m=0:(sqrt(N_cells)-1)                          %row#-1
        for  l=m*sqrt(N_cells)+1:(m+1)*sqrt(N_cells)
            %^lattice site index number moving from left to right
            % (next row starts at left at l->l+1)
            i=m+1;              %x-coord of lattice site
            j=l-m*sqrt(N_cells);%y-coord of lattice site
            if i==1             %Boundary condition on the top
                if j==1         %Reflective top left corner
                    W(l,l)=2*We;
                elseif j==sqrt(N_cells)  %Reflective top right corner
                    W(l,l)=2*We;
                else
                    W(l,l)=We;
                end
            else
                top_near_neigh = sqrt(N_cells)*(i-2)+j;
                W(l,top_near_neigh)=We;
            end
            if i==sqrt(N_cells) %Boundary condition on the bottom
                if j==1         %Reflective bottom left corner
                    W(l,l)=2*We;
                elseif j==sqrt(N_cells) %Reflective bottom right corner
                    W(l,l)=2*We;
                else
                    W(l,l)=We;
```

```
                end
            else
                bottom_near_neigh = sqrt(N_cells)*i+j;
                W(l,bottom_near_neigh)=We;
            end
            if j==1             %Boundary condition on the left
                if i>j && i~=sqrt(N_cells)
                    W(l,l)=We;
                end
            else
                left_near_neigh = sqrt(N_cells)*(i-1)+(j-1);
                W(l,left_near_neigh)=We;
            end
            if j==sqrt(N_cells) %Boundary condition on the right
                if i<j && i~=1
                    W(l,l)=We;
                end
            else
                right_near_neigh = sqrt(N_cells)*(i-1)+(j+1);
                W(l,right_near_neigh)=We;
            end
        end
    end
    W=sparse(W);

end
% W=ones(sqrt(N_cells),sqrt(N_cells));

while cum_t < T % Main LOOP
    execslot=1;
    if count==length(AS)
        AS=[AS,zeros(1,block_size)];
        avgbH=[avgbH,zeros(1,block_size)];
```

```
    avgf=[avgf,zeros(1,block_size)];
    time_steps=[time_steps,zeros(1,block_size)];
    blocks=blocks+1;
end

NHrand=rand(1,N_cells);
indexNH=find(NHrand>NHperc);
NHselect=zeros(1,N_cells);
NHselect(indexNH)=NH;

AS(count)=sum(N)/N_cells;% Stochastic value of A; # of active cells

if nearestneighborreflex==true
    x=N*W+bH.*NHselect;            % Define/update current
else
    for i=1:N_cells
        if N(i)==1
            x=We*(AS(count)-1/N_cells)+bH.*NHselect;
        else
            x=We*(AS(count))+bH.*NHselect;
        end
    end
end

[exectimes,execslot,res]=marktime(exectimes,execslot,lasttime);
lasttime=res;

for i=1:N_cells
    f_tilde(i)=1/(1+exp(-a*(x(i)-theta)))-s;
end

% Deterministic update dbH = -g*(AD(i)-pE0+pES*k*bH(i))*NH;
t_plus=g*(pE0-pES*k*bH).*NHselect;
```

```
t_minus=g*NHselect.*N;
%{
mintminus=min(t_minus);
minftilde=min(f_tilde);
minbH=min(bH);
if mintminus <0
    mintminus
    break
end
%if minftilde<0
%    minftilde
%    break
%end
if minbH<0
    minbH
    break
end
%}
% compute the overall rates in the variables a#
a1=sum(N*alpha);                    % rate for the decay
a2=dot(-N+1,f_tilde);               % rate for cells becoming active
a3=sum(t_minus);                    % rate for weights to increase
a4=sum(t_plus);                     % rate for weights to decrease
a0=a1+a2+a3+a4;
% pick a two random # from uniform distribution
r=rand(1,2);

% compute timestep tau (based on exponential distribution)
tau=(1/a0)*log(1/r(1));          % Gillespie (1977) Eq (21a)
% Now we compute the cumulative distribution of all cells
% this could be done more efficient here in the all-to-all
% connection case; here we only have two variables to update
% Q and A. However, the following approach of updating individual
```

```
% cells is more general.

% Now make a PDF size 3 x N:
% first part has alpha's and f's
% 2nd part t+ and 3rd part t-
% then make a cumulative distribution for picking what to update

P=N*alpha;                  % all active cells multiplied by alpha

for i=1:N_cells
    if P(i)==0;
        P(i)=f_tilde(i);    % all inactive cells become f
    end
end
P=[P t_minus t_plus];       % concatenate the vectors in one
                            % PDF of 1x3N vector
P=P./sum(P);                % normalize P
F=cumsum(P);                % cumulative function F of all

% probabilities associated with
% the cells in N
% now pick a cell # using the cumulative distribution
pick=0;
i=0;
while pick == 0
    i=i+1;
    if (F(i)>=r(2));mu=i;pick=1;end;
end;
% Update time, cell and counter
if mu <= length(N)
    if N(mu)==1;
        N(mu)=0;
    else N(mu)=1;
```

```
    end;    % Update cell

end
if (mu > length(N) && mu <= 2*length(N))
    bH(mu-length(N)) = bH(mu-length(N))-1;

    % should be t+
    % ------------------------------------------------------
    %t_minus(mu-length(N))=g*(pE0+pES*k*bH(mu-length(N)))*NH;
    %



end
if (mu > 2*length(N) && mu <= 3*length(N))
    bH(mu-2*length(N)) = bH(mu-2*length(N))+1;

    % should be t-
    % ------------------------------------------------
    %t_plus(mu-2*length(N))=g*AS(count)*NH;
    %------------------------------------------------



end
count=count+1;                          % update the counter
cum_t=cum_t+tau;                        % update the time
time_steps(count)=cum_t;
%times(count)=cum_t;                     % stochastic timebase
avgbH(count)=sum(bH)/N_cells;           % and average weight
avgf(count)=sum(f_tilde)/N_cells;
%         marktime;
%         if cum_t/T > perc*0.1
%             disp(cum_t);
%             perc=perc+1;
```

```
        %         end
        %                          if (count>1000000) ,break, end

    end;
    execcum=0;
    %     for i=1:(execslot-1)
    %
    %         [i,exectimes(i)/count]
    %         execcum=execcum+exectimes(i);
    %     end
    %     [count,execcum/count]

    final=toc(starttime)

    AS(count:end)=[];
    avgbH(count:end)=[];
    avgf(count:end)=[];
    time_steps(count:end)=[];
    save (sprintf('outputmodified weight%d.mat',comp),'-v7.3')
end



% figure(2);
% plot(times(1:length(AS)),AS)
% title ('stochastic (blue)')
% xlabel('time (s)')
% ylabel(' # of Active Cells')


% function marktime
```

B.2.2 Avalanche Size and Duration Distributions

Avalanche Distributions for an entire data set

```
difftimes = diff(times);
spikes=0;
for j=1:length(AS)-1
    if AS(j+1)>AS(j)
        spikes=spikes+1;
    end
end
delta_t = times(end)/spikes;
sizeaval=0;
duraval=0;
counter=1;
spikecount=0;
duravalbegin=0;
i=1;
for i=1:length(difftimes)
if (i==1 && difftimes(i)<delta_t)
    if AS(i+1)>AS(i)
    spikecount=spikecount+1;
    end
end
if (i==1 && difftimes(i)>delta_t)
    sizeaval=0;
end
if i>1 && difftimes(i)<delta_t
    if AS(i)>AS(i-1)
        spikecount = spikecount+1;
    end
else
```

```
    if i>1 && AS(i)>AS(i-1)
        spikecount=spikecount+1;
    end
    duravalend=(times(i+1)+times(i))/2;
    sizeaval(counter) = spikecount;
    duraval(counter) = duravalend-duravalbegin;
    spikecount=0;
    duravalbegin=duravalend;
    counter=counter+1;
end
end
sizeaval=sizeaval(2:length(sizeaval));   %eliminating the first avalanche
duraval(2)=duraval(1)+duraval(2);
duraval=duraval(2:length(duraval));
[freqsize, size] = hist(sizeaval,23);
[freqdur, dur] = hist(duraval,23);
logsize = log(size);
logfreqsize = log(freqsize);
logdur = log(dur);
logfreqdur = log(freqdur);
figure
subplot(2,1,1)
plot(logsize,logfreqsize,'o')
title('Avalanche Size Distribution')
xlabel('Log Size of Avalanche')
ylabel('Log Frequency')
subplot(2,1,2)
plot(logdur,logfreqdur,'o')
title('Avalanche Duration Distribution')
xlabel('Log Duration of Avalanche (ms)')
ylabel('Log Frequency')
```

UP and DOWN State Avalanche Distributions

```
close all
index=find(time_steps>180000 & time_steps<500000);
newAS=AS(index);
newtimes=time_steps(index);
newavgbH=avgbH(index);
hold
plot(newtimes,newAS);
title('Activity versus Time')
xlabel('Time')
ylabel('% of Active Cells')
figure;
plot(newtimes,newavgbH);
title('Average Weight versus Time')
xlabel('Time')
ylabel('Average Weight')
figure;
plot(newavgbH,newAS);
title ('Phase plot')
xlabel('Average Synaptic Weight')
ylabel('% of Active Cells')


%avalanche_code(newtimes,newAS);


highindex=find(newAS>0.32);
highnewAS=newAS(highindex);
highnewtimes=newtimes(highindex);
figure;hold
plot(highnewtimes,highnewAS);
```

```
title ('High activity states versus Time')
xlabel('Time')
ylabel('% of Active Cells')
[highsize, highfreqsize,highdur,highfreqdur] =
                                    avalanche_code(highnewtimes,highnewAS);
plothighsize=log(highsize);
plothighfreqsize=log(highfreqsize);
hindex0 = find(highfreqsize == 0);
highsize(hindex0)=[];
highfreqsize(hindex0)=[];
loghighsize=log(highsize);
loghighfreqsize=log(highfreqsize);
hindex1 = find(loghighfreqsize == 0);
loghighsize(hindex1)=[];loghighfreqsize(hindex1)=[];
hindex2 = find(loghighsize>9);
loghighsize(hindex2)=[];loghighfreqsize(hindex2)=[];

lowindex=find(newAS<0.09);
lownewAS=newAS(lowindex);
lownewtimes=newtimes(lowindex);
figure;
plot(lownewtimes,lownewAS);
title ('Low activity states versus Time')
xlabel('Time')
ylabel('% of Active Cells')
[lowsize,lowfreqsize,lowdur,lowfreqdur] =
                                     avalanche_code(lownewtimes,lownewAS);

plotlowsize=log(lowsize);
plotlowfreqsize=log(lowfreqsize);
figure;hold
plot(plotlowsize,plotlowfreqsize,'.')
plot(plothighsize,plothighfreqsize,'o')
```

```
lindex0 = find(lowfreqsize == 0);
lowsize(lindex0)=[];lowfreqsize(lindex0)=[];
loglowsize=log(lowsize);loglowfreqsize=log(lowfreqsize);
lindex1 = find(loglowfreqsize == 0);
loglowsize(lindex1)=[];
loglowfreqsize(lindex1)=[];
lindex2 = find(loglowsize>6);
loglowsize(lindex2)=[];
loglowfreqsize(lindex2)=[];
[lowslope,lowintercept,lowcorrcoef,highslope,highintercept,highcorrcoef]=
Regression(loghighsize,loghighfreqsize,loglowsize,loglowfreqsize)

%{
freqsize=sum(lowfreqsize)+sum(highfreqsize)
a=lowfreqsize/freqsize;b=highfreqsize/freqsize;
loga=log(a);logb=log(b); loglsize=log(lowsize);loghsize=log(highsize);
hold;plot(loglsize,loga,'o');plot(loghsize,logb,'.');
index0 = find(loglowfreqsize == 0); loglowsize(index0)=[];
lowfreqsize(index0)=[];
%}
```

B.2.3 Simulation of $E-I$ network using space-clamped WC equations

```
%clear all
%close all

%EEend=82.9427;
%IIend=76.1754;
%EIend=74.4614;
%IEend=81.4749;
```

```
%for param1=1:25
%for param2=1:10
%for param3=1:10

clear all
%close all

% Parameters
N_cells_E=40;               % number of cells in E population
N_cells_I=40;               % number of cells in I population
N_cells=N_cells_E+N_cells_I;

NH=0.1;                     % number of cells in external population

a_E=1.5;%.1;%/3;            % slope of E sigmoid curve
a_I=6;%2.0;%/3;

theta_E=2.5;%*3;%+0.1*(param1-1);           % threshold of sigmoid curve
theta_I=4.3;%0.2;%*3;%+0.1*(param2-1);

alpha_E=1;%0.1;             % decay rate a -> q (set around 1/100 ms)
alpha_I=1;%0.1;

g_E=0.1;%0.5;%*3;           % f'/(Ith-W*f'), held to be constant right now
g_I=0.1;%0.5;%*3;           % Since only WEI changes, no g_I

k=1;                        % WEI = k*bE
pE0=0.2;%+0.05*(param3-1);  % Vogels' target rate
pI0=0.2;
pES=0.000001;               % Window function amplitude
pIS=0.000001;

s_E=1/(1+exp(a_E*theta_E));
```

```
s_I=1/(1+exp(a_I*theta_I));


% Weights
WEE=16;%EEend;%22%16;   %decrease
WII=12;%IIend;%36
WEI=15;%EIend; %22
WIE=12;%IEend;%36%22;   %increase
WEH=0;
WIH=0;

dt=0.01;                    % Deterministic timestep for the
                            % deterministic computation(set at 1 ms)
T=250000;%00;%1500000;      % Epoch (in s)
steps=floor(T/dt);          % # of timesteps in deterministic case

timeD=0:dt:T;               % Determinsitic timebase
EAD=zeros(1,steps+1);       % Deterministic
IAD=zeros(1,steps+1);       % Deterministic
bEID=zeros(1,steps+1);      % Deterministic
bIED=zeros(1,steps+1);      % Deterministic
bEED=zeros(1,steps+1);      % Deterministic
bIID=zeros(1,steps+1);      % Deterministic
Ex=zeros(1,steps+1);        % Deterministic
Ix=zeros(1,steps+1);        % Deterministic
Ef_tildeD=zeros(1,steps+1); % Deterministic
If_tildeD=zeros(1,steps+1); % Deterministic
Ex=zeros(1,steps+1);        % Deterministic
Ix=zeros(1,steps+1);        % Deterministic
delta=zeros(1,steps+1);     % Deterministic

% Initial values
EAD(1)=0.5;%0.3;            % initial value for E-pop
```

```
IAD(1)=0.5;%0.3;              % initial value for I-pop
bEID(1)=WEI/k;                % initial external weight value for the deter
bIED(1)=WIE/k;
bEED(1)=WEE/k;
bIID(1)=WII/k;
%delta(1)=1+g_E*g_I*bIED(1)*bEID(1);

tic

    for i=1:steps
        %Ex(i)=((EAD(i)*bEED(1)*(N_cells_E-1)-IAD(i)*bEID(1)
        %      *N_cells_I)+1.25)/40;%+NH*WEH);          % E current
        %Ix(i)=((EAD(i)*bIED(1)*N_cells_E-IAD(i)*bIID(1)*
        %      (N_cells_I-1))-0)/40;%+NH*WIH);          % I current
        Ex(i)=((EAD(i)*bEED(i)-IAD(i)*bEID(i))+0.3)/1;
        Ix(i)=((EAD(i)*bIED(i)-IAD(i)*bIID(i))-0)/1;
        Ef_tildeD(i)=1/(1+exp(-a_E*(Ex(i)-theta_E))); %-s_E;
        If_tildeD(i)=1/(1+exp(-a_I*(Ix(i)-theta_I))); %-s_I;

        dEAD = Ef_tildeD(i)*(1-EAD(i))-alpha_E*EAD(i);
        dIAD = If_tildeD(i)*(1-IAD(i))-alpha_I*IAD(i);
        dbEID = g_E*(EAD(i)-pE0-pES*k*bEID(i))*IAD(i);
        dbIED =-g_I*(IAD(i)-pI0+pIS*k*bIED(i))*EAD(i);
        dbEED =-g_E*(EAD(i)-pE0+pES*k*bEED(i))*EAD(i);
        dbIID = g_I*(IAD(i)-pI0-pIS*k*bIID(i))*IAD(i);

        EAD(i+1)=EAD(i)+dEAD*dt;
        IAD(i+1)=IAD(i)+dIAD*dt;
        bEID(i+1)=bEID(i)+dbEID*dt;
        bIED(i+1)=bIED(i)+dbIED*dt;
        bEED(i+1)=bEED(i)+dbEED*dt;
        bIID(i+1)=bIID(i)+dbIID*dt;
        %delta(i)=1+g_E*g_I*bIED(i)*bEID(i);
```

```
        %if bEID(i)<0 || bIED(i)<0 || bEED(i)<0 || bIID(i)<0
        %    break
        %end
    end;

toc
%if param1==10
figure;subplot(3,2,[5 6])
hold
plot(timeD,EAD,'k','Linewidth',2)
plot(timeD,IAD,'r--')
%title ('Deterministic model E-pop(black), I-pop(blue)')
xlabel('time (s)')
ylabel(' % of Active Cells')

subplot(3,2,1)
plot(timeD,bEID,'k')
title('Deterministic weight I->E')
xlabel('time (s)')
ylabel('WEI')

subplot(3,2,2)
plot(timeD,bIED,'k')
title('Deterministic weight E->I')
xlabel('time (s)')
ylabel('WIE')

subplot(3,2,3)
plot(timeD,bEED,'k')
title('Deterministic weight E->E')
xlabel('time (s)')
ylabel('WEE')
```

```
subplot(3,2,4)
plot(timeD,bIID,'k')
title('Deterministic weight I->I')
xlabel('time (s)')
ylabel('WII')

%figure;hold
%plot(timeD,Ex,'k')
%plot(timeD,Ix,'r')
%end
EAD(end)
IAD(end)
EEend=bEED(end)
IIend=bIID(end)
EIend=bEID(end)
IEend=bIED(end)
%if EAD(end)<0.15 && IAD(end)<0.15
%save (sprintf('outputmodified weight%d.mat',comp),'-v7.3')
%end

%end
%end
%end
```

B.2.4 Simulation of $E-I$ network using Gillespie algorithm

```
%%%%%%%%%%%%%%%%%%%%%%%%%%%%%%%%%%%%%%%%%%%%%%%%%%%%%%%%%%%%%%%%%%%%%%%%%%%%
% This simulation is designed to simulate an EI network with all weights
% plastic.
% J Neuman 8/2013
%%%%%%%%%%%%%%%%%%%%%%%%%%%%%%%%%%%%%%%%%%%%%%%%%%%%%%%%%%%%%%%%%%%%%%%%%%%%
clear all
```

```
close all
for comp=7

    % Parameters
    N_cells_E=56+8*(comp-7);            % number of cells in E population
    N_cells_I=64+8*(comp-7);            % number of cells in I population
    N_cells=N_cells_E+N_cells_I;

    %N will now be a 2xN_cells matrix. The first row will be activity
    %vector. The second row will be E/I marker
    %{
    i=0.25*N_cells;                       % # of initial active cells
    N=[ones(i,1);zeros(N_cells-i,1)];     % not randomized initial state
                                            of vector N
    N=N(randperm(N_cells))';              % randomized initial state
                                            of vector N
    j=1;
    for j=1:N_cells_E
        EI(1,j)=1;
    end
    for j=N_cells_E+1:N_cells
        EI(1,j)=0;
    end
    EIrand=EI(randperm(N_cells))';
    N=[N' EIrand];
    N=N';
    %}

    i_E=0.125*N_cells_E;
    E=[ones(i_E,1);zeros(N_cells_E-i_E,1)];
    E=E(randperm(N_cells_E))';
    E(2,:)=1;
```

```
i_I=0.5*N_cells_I;
I=[ones(i_I,1);zeros(N_cells_I-i_I,1)];
I=I(randperm(N_cells_I))';
I(2,:)=0;

N=[E I];
NE=N(1,:).*N(2,:);
NI=N(1,:).*(-N(2,:)+1);

NH=0.1;                         % number of cells in external population

a_E=0.3;%1.3%/3;                % slope of E sigmoid curve
a_I=0.3;%1.3%2.0;%/3;

theta_E=0.5;%3.5;               % threshold of sigmoid curve
theta_I=0.5;%3.5;

alpha_E=0.1;                    % decay rate a -> q (set around 1/100 ms)
alpha_I=0.1;

g_E=0.005;%0.5;%*3;             % f'/(Ith-W*f'), held to be constant
g_I=0.005;%0.5;%*3;             % right now

k=1;
pE0=0.25;                       % Vogels' target rate
pI0=0.25;
pES=0.000001;                   % Window function amplitude
pIS=0.000001;

s_E=1/(1+exp(a_E*theta_E));
s_I=1/(1+exp(a_I*theta_I));

% Weights
```

```
WEE=80;%16
WII=60;%33;
WIE=3010;%25%17;
WEI=60;%22;
WEH=0;
WIH=0;

%nearestneighbor=false;

% Parameters computation
dt=0.05;                  % Deterministic timestep for the
                          % deterministic computation(set at 1 ms)
T=1000000;                % Epoch (in s)
steps=floor(T/dt);        % # of timesteps in deterministic case
blocks=1;                 % Counts the number of zero blocks added
block_size=8000000;
perc=1;

%Allocate Memory
timeD=0:dt:T;             % Determinsitic
EAD=zeros(1,steps+1);
IAD=zeros(1,steps+1);
bEID=zeros(1,steps+1);
bIED=zeros(1,steps+1);
bEED=zeros(1,steps+1);
bIID=zeros(1,steps+1);
Ef_tildeD=zeros(1,steps+1);
If_tildeD=zeros(1,steps+1);
Ex=zeros(1,steps+1);
Ix=zeros(1,steps+1);
%deltaD=zeros(1,steps+1);

time_steps=zeros(1,block_size);              % Stochastic
```

```
EAS=zeros(1,block_size);
IAS=zeros(1,block_size);
%avgbEI=zeros(1,block_size);
avgbIE=zeros(1,block_size);
%avgbEE=zeros(1,block_size);
%avgbII=zeros(1,block_size);
listmu=zeros(1,block_size);
deltaS=zeros(1,block_size);
f_tilde=zeros(1,N_cells);

%NEVE=zeros(1,N_cells_E*N_cells_E);
%NIVE=zeros(1,N_cells_E*N_cells_I);
NEVI=zeros(1,N_cells_E*N_cells_I);
%NIVI=zeros(1,N_cells_I*N_cells_I);

NIrepmatIE=zeros(N_cells_E,N_cells_I);
NI_tminus_IE=zeros(1,N_cells_E*N_cells_I);
%NErepmatEI=zeros(N_cells_I,N_cells_E);
%NE_tplus_EI=zeros(1,N_cells_I*N_cells_E);
%NErepmatEE=zeros(N_cells_E-1,N_cells_E);
%NE_tminus_EE=zeros(1,N_cells_E*(N_cells_E-1));
%NIrepmatII=zeros(N_cells_I-1,N_cells_I);
%NI_tplus_II=zeros(1,N_cells_I*(N_cells_I-1));

%t_plusEI= zeros(1,N_cells_E*N_cells_I);
%t_minusEI=zeros(1,N_cells_E*N_cells_I);
t_plusIE= zeros(1,N_cells_I*N_cells_E);
t_minusIE=zeros(1,N_cells_I*N_cells_E);
%t_plusEE= zeros(1,N_cells_E*(N_cells_E-1));
%t_minusEE=zeros(1,N_cells_E*(N_cells_E-1));
%t_plusII= zeros(1,N_cells_I*(N_cells_I-1));
%t_minusII=zeros(1,N_cells_I*(N_cells_I-1));
LN=length(N(1,:));
```

```
%LbEI=length(t_minusEI);
LbIE=length(t_plusIE);
%LbEE=length(t_plusEE);
%LbII=length(t_minusII);
%DO NOT INITIALIZE THIS
P=zeros(1,LN+2*LbIE);%+2*LbEI+2*LbIE+2*LbEE+2*LbII);

count=1;                        % timestep counter for the EAS/IAS array
cum_t=0;                        % initial time

% Initial values
EAD(1)=sum(NE)/N_cells_E;       % initial excitatory value for the
                                % deterministic case
IAD(1)=sum(NI)/N_cells_I;       % initial inhibitory value for the
                                % deterministic case
EAS(1)=sum(NE)/N_cells_E;       % Stochastic value of EAD; Proportion
                                % of active excitatory cells
IAS(1)=sum(NI)/N_cells_I;       % Stochastic value of IAD; Proportion
                                % of active inhibitory cells
bEID(1)=WEI/k;                  % initial I->E weight for the deter
bIED(1)=WIE/k;
bEED(1)=WEE/k;
bIID(1)=WII/k;
bEI=bEID(1).*ones(1,N_cells_E*N_cells_I);  % initial modifiable weight
                                           % for stochastic case
bIE=bIED(1).*ones(1,N_cells_I*N_cells_E);
bEE=bEED(1).*ones(1,N_cells_E*(N_cells_E-1));
bII=bIID(1).*ones(1,N_cells_I*(N_cells_I-1));
%avgbEI(1)=sum(bEI)/length(bEI);           % initial average weights
avgbIE(1)=sum(bIE)/length(bIE);            % initial average weights
%avgbEE(1)=sum(bEE)/length(bEE);           % initial average weights
%avgbII(1)=sum(bII)/length(bII);           % initial average weights
%EAD(1)=0.2;                               % initial value for E-pop
```

```
 %IAD(1)=0.25;                                % initial value for I-pop
 %deltaD=1+g_E*g_I*bIED(1)*bEID(1);
 %deltaS(1)=1+g_E*g_I*avgbIE(1)*avgbEI(1);
 %{
 tic;
 %DETERMINISTIC Case
 %     Deterministic model
 %     -------------------
 %     this simulation based on kinetic rate equation

for i=1:steps
Ex=((EAD(i)*bEED(1)*(N_cells_E-1)-IAD(i)*bEID(1)*N_cells_I+NH*WEH))/100;
Ix=((EAD(i)*bIED(1)*N_cells_E-IAD(i)*bIID(i)*(N_cells_I-1)+NH*WIH))/100;
Ef_tildeD(i)=0.5/(1+exp(-a_E*(Ex-theta_E))); %-s_E;
If_tildeD(i)=0.5/(1+exp(-a_I*(Ix-theta_I))); %-s_I;
%deltaD(i)=1+g_E*g_I*bIED(i)*bEID(i);
%deltaD(1)=1;
dEAD = Ef_tildeD(i)*(1-EAD(i))-alpha_E*EAD(i);
dIAD = If_tildeD(i)*(1-IAD(i))-alpha_I*IAD(i);
%dbEID = (g_E/deltaD(1))*(EAD(i)-pE0-pES*k*(bEID(i)/deltaD(1)))*IAD(i);
%dbIED =-(g_I/deltaD(1))*(IAD(i)-pI0+pIS*k*(bIED(i)/deltaD(1)))*EAD(i);
%dbEED =-(g_E/deltaD(1))*(EAD(i)-pE0+pES*k*bEED(i))*EAD(i);
%dbIID = (g_I/deltaD(1))*(IAD(i)-pI0-pIS*k*bIID(i))*IAD(i);

%dbEID = g_E*(EAD(i)-pE0-pES*k*bEID(i))*IAD(i);
dbIED  =-g_I*(IAD(i)-pI0+pIS*k*bIED(i))*EAD(i);
%dbEED =-g_E*(EAD(i)-pE0+pES*k*bEED(i))*EAD(i);
%dbIID = g_I*(IAD(i)-pI0-pIS*k*bIID(i))*IAD(i);
EAD(i+1)=EAD(i)+dEAD*dt;
IAD(i+1)=IAD(i)+dIAD*dt;
%bEID(i+1)=bEID(i)+dbEID*dt;
bIED(i+1)=bIED(i)+dbIED*dt;
%bEED(i+1)=bEED(i)+dbEED*dt;
```

```
%bIID(i+1)=bIID(i)+dbIID*dt;
%deltaD(i+1)=1+g_E*g_I*bIED(i)*bEID(i);
%if bEID(i)<0 || bIED(i)<0 || bEED(i)<0 || bIID(i)<0
%    break
%end
end;

 finalD=toc
 %}
 % Computing time help, also see marktime script
 exectimes=zeros(1,100);  % Calculating times between 2 marktimes
 tic;
 starttime=tic;           % Starting time of the stochastic calculation
 lasttime=tic;            % Initializing lasttime

 % Equivalent Stochastic model
 % ---------------------------
 % This simulation based on stochastic model
 % Specific parameters and initial values
 % background of the method can be found in Gillespie (1976, 1977)

 %%%%%%%%%%%%%%%%%%%%%%%%%%%%%%%%%%%%%%%%%%%%%%%%
 % MAIN LOOP BEGINS HERE
 %%%%%%%%%%%%%%%%%%%%%%%%%%%%%%%%%%%%%%%%%%%%%%%%
 b=1;
 while cum_t < T
     execslot=1;
     if count==length(EAS)
         EAS=[EAS,zeros(1,block_size)];
         IAS=[IAS,zeros(1,block_size)];
         %avgbEE=[avgbEE,zeros(1,block_size)];
         %avgbEI=[avgbEI,zeros(1,block_size)];
         avgbIE=[avgbIE,zeros(1,block_size)];
```

```
    %avgbII=[avgbII,zeros(1,block_size)];
    avgx=[avgx,zeros(1,block_size)];
    avgf=[avgf,zeros(1,block_size)];
    time_steps=[time_steps,zeros(1,block_size)];
    listmu=[listmu,zeros(1,block_size)];
    %deltaS=[deltaS,zeros(1,block_size)];
    blocks=blocks+1;
end

NE=N(1,:).*N(2,:);     % 1 in entry means active excitatory neuron
NI=N(1,:).*(-N(2,:)+1) % 1 in entry means active inhibitory neuron

NEmatrix=N(1:2,1:N_cells_E);
NImatrix=N(1:2,N_cells_E+1:N_cells);

%NEVE=repmat(NEmatrix(1,:),1,N_cells_E);
NEVI=repmat(NEmatrix(1,:),1,N_cells_I);
%NIVE=repmat(NImatrix(1,:),1,N_cells_E);
%NIVI=repmat(NImatrix(1,:),1,N_cells_I);

%NEVEE=reshape(NEVE,N_cells_E,N_cells_E);
%NEVEE(1:N_cells_E+1:N_cells_E*N_cells_E)=[];

%NIVII=reshape(NIVI,N_cells_I,N_cells_I);
%NIVII(1:N_cells_I+1:N_cells_I*N_cells_I)=[];

NIrepmatIE=repmat(NImatrix(1,:),N_cells_E,1);
NI_tminus_IE=reshape(NIrepmatIE,N_cells_E*N_cells_I,1)';

%NErepmatEI=repmat(NEmatrix(1,:),N_cells_I,1);
%NE_tplus_EI=reshape(NErepmatEI,N_cells_I*N_cells_E,1)';

%NErepmatEE=repmat(NEmatrix(1,:),N_cells_E-1,1);
```

```
%NE_tminus_EE=reshape(NErepmatEE,N_cells_E*(N_cells_E-1),1)';

%NIrepmatII=repmat(NImatrix(1,:),N_cells_I-1,1);
%NI_tplus_II=reshape(NIrepmatII,N_cells_I*(N_cells_I-1),1)';

%if nearestneighbor==true
%      xE=N(1,:)*WE+bEH*NH.*ones(1,N_cells_E)+WIE*AS(count);
%      xI=N(1,:)*WI+bIH.*NH+WEI.*AS(count);
%else
    %x=zeros(1,N_cells);
    m=1;                    %Counter for excitatory cells
    n=1;                    %Counter for inhibitory cells
    for i=1:length(N)
        if N(2,i)==1
            NES=NEmatrix;
            NES(:,n)=[];
            x(i)=(dot(bEE((n-1)*(N_cells_E-1)+1:n*(N_cells_E-1)),
            NES(1,:))-dot(bEI((n-1)*N_cells_I+1:n*N_cells_I),
            NImatrix(1,:))+NH*WEH)/200;
            f_tilde(i)=0.5/(1+exp(-a_E*(x(i)+theta_E)));  %-10*s_E;
            n=n+1;
        else
            NIS=NImatrix;
            NIS(:,m)=[];
            x(i)=(dot(bIE((m-1)*N_cells_E+1:m*N_cells_E),
            NEmatrix(1,:))-dot(bII((m-1)*(N_cells_I-1)+
            1:m*(N_cells_I-1)),NIS(1,:))+NH*WIH)/200;
            f_tilde(i)=0.5/(1+exp(-a_I*(x(i)+theta_I)));  %-10*s_I;
            m=m+1;
        end
    end
%end
```

```
[exectimes,execslot,res]=marktime(exectimes,execslot,lasttime);
lasttime=res;

%dbEI = (g_E/deltaD)*(E(i)-pE0-pES*k*bEI(i)/deltaD)*I(i);
%t_plusEI=g_E*NE_tplus_EI.*NIVE;
%t_minusEI=g_E*(pE0+pES*k*bEI).*NIVE;

%dbIE =-(g_I/deltaD)*(I(i)-pI0+pIS*k*bIE(i)/deltaD)*E(i);
t_plusIE =g_I*pI0.*NEVI;
t_minusIE=g_I*(NI_tminus_IE.*bIE.^(-1)+pIS).*NEVI;

%dbEE =-(g_E/deltaD)*(E(i)-pE0+pES*k*bEE(i))*E(i);
%t_plusEE=g_E*pE0.*NEVEE;
%t_minusEE=g_E*(NE_tminus_EE+pES*k*bEE).*NEVEE;

%dbII = (g_I/deltaD)*(I(i)-pI0-pIS*k*bII(i))*I(i);
%t_plusII=g_I*NI_tplus_II.*NIVII;
%t_minusII=g_I*(pI0*bII.^(-1)+pIS).*NIVII;
%{
minbEI=min(bEI);
minbIE=min(bIE);
minbEE=min(bEE);
minbII=min(bII);
if minbEI<0 || minbIE<0 || minbEE<0 || minbII<0
    minbEI
    minbIE
    minbEE
    minbII
    break
end
%}
% compute the overall rates in the variables a#
a1=sum(NE*alpha_E)+sum(NI*alpha_I);% rate for the E decay
```

```
a2=dot(-N(1,:)+1,f_tilde);          % rate for cells becoming active
%a3=sum(t_minusEI);
%a4=sum(t_plusEI);
a5=sum(t_minusIE);
a6=sum(t_plusIE);
%a7=sum(t_minusEE);
%a8=sum(t_plusEE);
%a9=sum(t_minusII);
%a10=sum(t_plusII);
%a0=a1+a2+a3+a4+a5+a6+a7+a8+a9+a10;
a0=a1+a2+a5+a6;

% pick a two random # from uniform distribution
% (following Gillespie's algorithm)
r=rand(1,2);

% compute timestep tau (based on exponential distribution)
tau=(1/a0)*log(1/r(1));          % Gillespie (1977) Eq (21a)
% Now we compute the cumulative distribution of all cells
% this could be done more efficient here in the all-to-all
% connection case; here we only have two variables to update Q
% and A. However, the following approach of updating individual
% cells is more general.

% Now make a PDF size 3 x N:
% first part has alpha's and f's
% 2nd part t+ and 3rd part t-
% then make a cumulative distribution for picking what to update
%{
P=zeros(1,N_cells);
for i=1:N_cells       % THIS WORKS FOR ALL CONFIGS. METHOD
    if N(2,i)==1      % BELOW DOESN'T WORK FOR NEAREST
        if N(1,i)==1  % NEIGHBOR BECAUSE N(2,:) WILL BE RANDOM.
```

```
                P(i)=alpha_E;
            else
                P(i)=f_tilde(i);
            end
        else
            if N(1,i)==1
                P(i)=alpha_I;
            else
                P(i)=f_tilde(i);
            end
        end
    end
    %}
    PNE=alpha_E*NEmatrix(1,:)+f_tilde(1:N_cells_E).*(-NEmatrix(1,:)+1);

PNI=alpha_I*NImatrix(1,:)+f_tilde(N_cells_E+1:N_cells).*(-NImatrix(1,:)+1);

    %P=[P t_minusEI t_plusEI t_minusIE t_plusIE
    %   t_minusEE t_plusEE t_minusII t_plusII];
    % concatenate the vectors in one PDF of 1x3N vector
    P=[PNE PNI t_minusIE t_plusIE];

    normP=P./sum(P);
    F=cumsum(normP);          %Cumulative function F of all trans rates

    %Now pick a reaction using the cumulative distribution
    pick=0;
    q=0;
    while pick == 0
        q=q+1;
        if (F(q)>=r(2));mu=q;pick=1;end; % (Gillespie, (1977), Eq (21b)
    end;
    if (mu>length(F))
```

```
    break
end;

% Update cell
if mu <= LN
    if N(1,mu)==1;
        N(1,mu)=0;
    else
        N(1,mu)=1;
    end;
NE=N(1,:).*N(2,:); % 1 in entry means active excitatory neuron
NI=N(1,:).*(-N(2,:)+1);% 1 in entry means active inhibitory neuron
end
%{
if (mu > LN && mu <= LN+LbEI)
    bEI(mu-LN) = bEI(mu-LN)-1;
end

if (mu > LN+LbEI && mu <= LN+2*LbEI)
    bEI(mu-LN-LbEI) = bEI(mu-LN-LbEI)+1;
end
%}
%if (mu > LN+2*LbEI && mu <= LN+2*LbEI+LbIE)
if (mu > LN && mu <= LN+LbIE)
    bIE(mu-LN)=bIE(mu-LN)-1;
    %bIE(mu-LN-2*LbEI) = bIE(mu-LN-2*LbEI)-1;
end

%if (mu > LN+2*LbEI+LbIE && mu <= LN+2*LbEI+2*LbIE)
if (mu > LN+LbIE && mu <= LN+2*LbIE)
    bIE(mu-LN-LbIE)=bIE(mu-LN-LbIE)+1;
    %bIE(mu-LN-2*LbEI-LbIE) = bIE(mu-LN-2*LbEI-LbIE)+1;
end
```

```
%{
if (mu > LN+2*LbEI+2*LbIE && mu <= LN+2*LbEI+2*LbIE+LbEE)
    bEE(mu-LN-2*LbEI-2*LbIE) = bEE(mu-LN-2*LbEI-2*LbIE)-1;
end

if (mu > LN+2*LbEI+2*LbIE+LbEE && mu <= LN+2*LbEI+2*LbIE+2*LbEE)
    bEE(mu-LN-2*LbEI-2*LbIE-LbEE) =
    bEE(mu-LN-2*LbEI-2*LbIE-LbEE)+1;
end

%if (mu > LN+2*LbEI+2*LbIE+2*LbEE &&
%    mu <= LN+2*LbEI+2*LbIE+2*LbEE+LbII)
if (mu > LN && mu <= LN+LbII)
    %bII(mu-LN-2*LbEI-2*LbIE-2*LbEE) =
    %bII(mu-LN-2*LbEI-2*LbIE-2*LbEE)-1;
    bII(mu-LN) = bII(mu-LN)-1;
end
if (mu > LN+LbII && mu <= LN+2*LbII)
%if (mu > LN+2*LbEI+2*LbIE+2*LbEE+LbII &&
%    mu <= LN+2*LbEI+2*LbIE+2*LbEE+2*LbII)
    %bII(mu-LN-2*LbEI-2*LbIE-2*LbEE-LbII) =
    %bII(mu-LN-2*LbEI-2*LbIE-2*LbEE-LbII)+1;
    bII(mu-LN-LbII) = bII(mu-LN-LbII)+1;
end
%}
listmu(count)=mu;
count=count+1;                          % update the counter
cum_t=cum_t+tau;                        % update the time
time_steps(count)=cum_t;                % stochastic timebase
EAS(count)=sum(NE)/N_cells_E;% Stochastic value of EAD;
                            %Proportion of active excitatory cells
IAS(count)=sum(NI)/N_cells_I;% Stochastic value of IAD;
                            %Proportion of active inhibitory cells
```

```
        %avgbEI(count)=sum(bEI)/length(bEI);      % and average weight
        avgbIE(count)=sum(bIE)/length(bIE);
        %avgbEE(count)=sum(bEE)/length(bEE);
        %avgbII(count)=sum(bII)/length(bII);
        avgx(count)=sum(x)/N_cells;
        avgf(count)=sum(f_tilde)/N_cells;
        %deltaS(count)=1+g_E*g_I*avgbIE(count)*avgbEI(count);
        %         marktime;
        %         if cum_t/T > perc*0.1
        %             disp(cum_t);
        %             perc=perc+1;
        %         end
        %                         if (count>1) ,break, end

    end;
    execcum=0;


    finalS=toc(starttime)


    listmu(count:end)=[];
    EAS(count:end)=[];
    IAS(count:end)=[];
    %avgbEI(count:end)=[];
    avgbIE(count:end)=[];
    %avgbEE(count:end)=[];
    %avgbII(count:end)=[];
    avgx(count:end)=[];
    avgf(count:end)=[];
    time_steps(count:end)=[];
    save (sprintf('outputonlybIE%d.mat',comp),'-v7.3')
end
```

REFERENCES

[1] Abarbanel H, Broznan J. Structure of the Vacuum Singularity in Reggeon Field Theory. *Phys. Lett. B*, 48: 345-348, 1974.

[2] Abarbanel H, Broznan J, Schwimmer A, Sugar R. Intercept of the Pomeron. *Phys. Rev. D*, 14(2): 636-646, 1976.

[3] Abarbanel H, Broznan J, Sugar R, White A. Reggeon Field Theory: Formulation and Use. *Phys. Reports*, 21(3): 119-182, 1975.

[4] Ahmed O, Kramer M, Truccolo W, Naftulin J, Potter N, Eskandar E, Cosgrove G, Blum A, Hochberg L, Cash S. Inhibitory single neuron control of seizures and epileptic traveling waves in humans. *BMC Neurosci.*, 15(Suppl 1): 3, 2014.

[5] Alstrom P. Mean-field exponents for self-organized critical phenomena. *Phys. Rev. A*, 38(9): 4905-4906, 1988.

[6] Amati D, Marchesini G, Ciafoloni M, Parisi G. Expanding disc as a dynamical vacuum instability in Reggeon field theory. *Nuclear Physics B*, 114: 483-504, 1976.

[7] Bak P. *How Nature Works: the science of self-organized criticality.* Springer. New York. 1996.

[8] Bak P, Tang C, Wiesenfeld K. Self-organized criticality. *Phys. Rev. A*, 38(1): 364-374, 1988.

[9] Beggs J, Plenz D. Neuronal Avalanches in Neocortical Circuits. *J. Neurosci.*, 23(35): 11167-11177, 2003.

[10] Benayoun M. *Network Dynamics and Epilepsy.* PhD thesis, University of Chicago, 2010.

[11] Benayoun M, Cowan J, van Drongelen W, Wallace E. Avalanches in a stochastic model of spiking neurons. *PLoS Comput. Biol.*, 6(7): e1000846, 2010.

[12] Benucci A, Frazor RA, Carandini M. Standing waves and traveling waves distinguish two circuits in visual cortex. *Neuron*, 55: 103-117, 2007.

[13] Berg AT, Berkovic SF, Brodie MJ, Buchhalter J, Cross JH, Van Emde Boas W, Engel J, French J, Glauser TA, Mathern GW, Moshé SL, Nordli D, Plouin P, and Scheffer IE. Revised terminology and concepts for organization of seizures and epilepsies: Report of the ILAE Commission on Classification and Terminology, 2005–2009. *Epilepsia*, 51(4): 676-685, 2010.

[14] Berger H. Über das Elektroenzenkephalogram des Menschen. *Arch. für Psychiat.*, 87: 527-570, 1929.

[15] Beurle RL. Properties of a Mass of Cells Capable of Regenerating Pulses. *Phil. Trans. Roy. Soc. Lond. B*, 240(669): 55-94, 1956.

[16] Borisyuk GN, Borisyuk RM, Khibnik AI, Roose D. Dynamics and bifurcations of two coupled neural oscillators with different connection types. *Bull. Math. Biol.*, 57(6): 809-840, 1995.

[17] Borisyuk RM, Kirillov AB. Bifurcation analysis of a neural network model.*Biol. Cybernetics*, 66(4): 319-325, 1992.

[18] Bressloff, P. Stochastic neural field theory and the system-size expansion. *SIAM J. Appl. Math.*, 70(5): 1488-1521, 2009.

[19] Buice M, Cowan J. Field Theoretic Approach to fluctuation effects for neural networks. *Phys. Rev. E*, 75: 051919, 2007.

[20] Buice M, Cowan J. Statistical mechanics of the neocortex. *Prog. Biophys. Theor. Biol.*, 99(2-3): 53-86, 2009.

[21] Buice M, Cowan J. Unpublished, 2007.

[22] Burns BD. Some Properties of the Isolated Cerebral Cortex in the Unanaesthetized Cat. *J. Physiol.*, 112: 156-175, 1951.

[23] Burns BD. The mechanism of after-bursts in cerebral cortex. *J. Physiol.*, 127: 168-188, 1955.

[24] Butler T, Benayoun M, Wallace E, van Drongelen W, Goldenfeld N, Cowan J. Evolutionary constraints on visual cortex architecture from the dynamics of hallucinations. *PNAS*, 109(2): 606-609, 2012.

[25] Buzsáki G, Anastassiou CA, Koch C. The origin of extracellular fields and currents–EEG, ECoG, LFP and spikes. *Nat. Rev. Neurosci.*, 13(6): 407-420, 2012.

[26] Cai D, Tao L, Shelley M, McLaughlin. An effective kinetic representation of fluctuation-driven neuronal networks with application to simple and complex cells in visual cortex. *Proc. Nat. Acad. Sci.*, 101(20): 7757-7762, 2004.

[27] Cardy J, Sugar R. Directed percolation and Reggeon field theory. *J. Phys. A: Math. Gen.*, 13: L423-L427, 1980.

[28] Caton R. The electric currents of the brain. *Brit. Med. J.*, 2: 278, 1875.

[29] Chu PH, Milton J, Cowan JD. Connectivity and the Dynamics of Integrate-and-Fire Neural Networks. *Int. J. Bifurc. Chaos*, 4(1): 237-243, 1994.

[30] Churchland, MM, Yu BM, Cunningham JP, Sugrue LP, Cohen MR, Corrado GS, Newsome WT, Clark AM, Hosseini P, Scott BB, Bradley DC, Smith MA, Kohn A, Movshon JA, Armstrong KM, Moore T, Chang SW, Snyder LH, Lisberger SG, Priebe NJ, Finn IM, Ferster D, Ryu SI, Santhanam G, Shenoy KV. Stimulus onset quenches neural variability: a widespread cortical phenomenon. *Nature Neurosci.*, 13(3): 369-378, 2010.

[31] Cowan JD. A personal account of the development of the field theory of large-scale brain

activity from 1945 onward, in *Neural Fields: Theory and Applications*, ed. Coombes S, biem Graben P, Potthast R, Wright JJ. Springer. New York. p. 47-99, 2013.

[32] Cowan JD. Statistical mechanics in nervous nets, in *Neural Networks*, ed. E.R. Caianiello. Springer. Berlin. p. 181-188, 1968.

[33] Cowan JD. Stochastic Neurodynamics, in *Advances in Neural Information Processing Systems 3*, ed. Touretzsky DS, Lippman RP, Moody JE. Morgan-Kaufmann. San Mateo, CA. p. 62-68, 1991.

[34] Cowan JD, Neuman J, Kiewiet B, van Drongelen W. Self-organized criticality in a network of interacting neurons. *J. Stat. Mech.*, P04030, 2013.

[35] Cowan JD, Neuman J, van Drongelen W. Self-organized criticality and near-criticality in neural networks, in *Criticality in Neural Systems*, ed. Niebur E, Plenz D. Wiley-VCH Verlag GmbH & Co. KGaA. Weinheim, Germany. p. 465-484, 2014.

[36] Cowan JD, Neuman J, van Drongelen W. Wilson-Cowan equations for Neocortical Dynamics. *J. Math. Neurosci.*, in press.

[37] Destexhe A, Sejnowski TJ. The Wilson-Cowan model, 36 years later. *Biol. Cybern.*, 101(1): 1-2, 2009.

[38] Dhooge A, Govaerts W, Kuznetsov YA, Meijer HGE, Sautois B. New features of the software MatCont for bifurcation analysis of dynamical systems. *Math. Comput. Model. Dyn. Syst.*, 14(2): 147-175, 2008.

[39] Doi M. Second quantization representation for classical many-particle system. *J. Phys. A: Math. Gen.*, 9(9): 1465-1477, 1976.

[40] Doi M. Stochastic theory of diffusion controlled reaction. *J. Phys. A: Math. Gen.*, 9(9): 1479-1495, 1976.

[41] Douglas R, Martin K. Neuronal circuits of the neocortex. *Annu. Rev. Neurosci.*, 27: 419-451, 2004.

[42] Ermentrout GB, Cowan JD. A mathematical theory of visual hallucinations. *Biol. Cybern.*, 34: 137, 1979a.

[43] Ermentrout GB, Cowan JD. Temporal oscillations in neuronal nets. *J. Math. Biol.*, 7: 265-280, 1979b.

[44] Ermentrout GB, Cowan JD. Large scale spatially organized activity in neural nets. *SIAM J. Appl. Math.*, 38(1): 1-21, 1980.

[45] Ermentrout GB, Kleinfeld D. Traveling electrical waves in cortex: insights from phase dynamics and speculation on a computational role. *Neuron*, 29(1): 33-44, 2001.

[46] Fitzhugh R. Impulses and physiological states in theoretical models of nerve membrane. *Biophys. J.*, 1: 445-466, 1961.

[47] Frazer W, Moshe M. Representations of Reggeon Green's functions: Their scaling form and the approach to scaling. *Phys. Rev. D*, 12(8): 2370-2384, 1975.

[48] Gil L, Sornette D. Landau-Ginzburg Theory of Self-Organized Criticality. *Phys. Rev. Lett.*, 76(21): 3991-3994, 1996.

[49] Gillespie DT. Exact stochastic simulation of coupled chemical reactions. *J. Phys. Chem.*, 81(25): 2340-2361, 1977.

[50] Gillespie DT. The chemical Langevin equation. *J. Chem. Phys.*, 113(1): 297-306, 2000.

[51] Ginzburg V. Some remarks about second-order phase transitions and the microscopic nature of ferroelectrics. *Sov. Phys. Solid State*, 2: 1824-1834, 1960.

[52] Glauber R. Photon Correlations. *Phys. Rev. Lett.*, 10(3): 84-86, 1963.

[53] Haimovici A, Tagliazucchi E, Balenzuela P, Chialvo D. Brain organization into resting state networks emerges at criticality on a model of the human connectome. *Phys. Rev. Lett.*, 110: 178101, 2013.

[54] Han VZ. Grant K, Bell C. Reversible Associative Depression and Nonassociative Potentiation at a Parallel Fiber Synapse. *Neuonr*, 24: 611-622, 2000.

[55] Henrie JA, Shapley R. LFP Power Spectra in V1 Cortex: The Graded Effect of Stimulus Contrast. *J. Neurophysiol.*, 94: 479-490, 2005.

[56] Hinrichsen H. Non-equilibrium critical phenomena and phase transitions into absorbing states. *Advances in Physics*, 49(7): 815-958, 2000.

[57] Homburg AJ, Sandstede B. Homoclinic and heteroclinic bifurcations in vector fields, in *Handbook of Dynamical Systems*, ed. Broer H, Takens F, Hasselblatt B. Elsevier. Amsterdam. p. 379-524, 2010.

[58] Hoppensteadt FC, and Izhikevich EM. *Weakly Connected Neural Networks*. MIT Press. Cambridge, Mass, 1997.

[59] Huang X, Troy W, Yang Q, Ma H, Laing C, Schiff S, Wu J. Spiral Waves in Disinhibited Mammalian Neocortex. *J. Neurosci.*, 24(44): 9897-9902, 2004.

[60] Izhikevich EM. *Dynamical Systems in Neuroscience: the geometry of excitability and bursting*. MIT Press. Cambridge, Mass. 2007.

[61] Janssen, H. Directed percolation with colors and flavors. *J. Stat. Phys.*, 103(5-6): 801-839, 2001.

[62] Janssen HK, Täuber UC. The field-theory approach to percolation processes. *Ann. Phys.*, 315: 147-192, 2005.

[63] Jirsa VK, Stacey WC, Quilichini PP, Ivanov AI, Bernard C. On the nature of seizure dynamics. *Brain*, 137(8): 2210-2230, 2014.

[64] Johnston D, Brown TH. Giant synpatic potential hypothesis for epileptiform activity. *Science*, 211(4479): 294-297, 1981.

[65] Jung P, Mayer-Kress G. Noise controlled spiral growth in excitable media. *Chaos*, 5(2): 458-462, 1955.

[66] Kilman V, van Rossum M, Turrigiano G. Activity Deprivation Reduces Miniature IPSC Amplitude by Decreasing the Number of Postsynaptic $GABA_A$ Receptors Clustered at Neocortical Synapses. *J. Neurosci.*, 22(4): 1328-1337, 2002.

[67] Kohn A, Zandvakili, Smith MA. Correlations and brain states: from electrophysiology to functional imaging. *Curr. Opin. Neurobiol.*, 19: 434-438, 2009.

[68] Korolev K, Nelson D. Competition and Cooperation in one-dimensional stepping-stone models. *Phys. Rev. Lett.*, 107(8): 88-103, 2011.

[69] Kuo C-C, Bean BP. Na^+ channels must deactivate to recover from inactivation. *Neuron*, 12(4): 819-829, 1994.

[70] Kuznetsov YA. *Elements of Applied Bifurcation Theory*. Springer. New York. 2004.

[71] Kwan P and Brodie MJ. Early Identification of Refractory Epilepsy. *N. Engl. J. Med.*, 342(5): 314-319, 2000.

[72] Lampl I, Reichova I, Ferster D. Synchronous membrane potential fluctuations in neurons of the cat visual cortex. *Neuron*, 22: 361-374, 1999.

[73] Levina A, Herrmann J, Geisel T. Dynamical synapses causing self-organized criticality in neural networks. *Nature Phys.*, 3(12): 857-860, 2007.

[74] Magnasco M, Piro O, Cecchi G. Self-tuned critical anti-hebbian networks. *Phys. Rev. Lett.*, 102: 258102, 2009.

[75] Marcuccilli CJ, Tryba AK, van Drongelen W, Koch H, Viemari JC, Peña-Ortega F, Doren EL, Pytel P, Chevalier M, Mrejeru A, Kohrman MH, Lasky RE, Lew SM, Frim DM, Ramirez J-M. Neuronal Bursting Properties in Focal and Parafocal Regions in Pediatric Neocortical Epilepsy Stratified by Histology. *J. Clin. Neurophysiol.*, 27(6): 387-397, 2010.

[76] McCulloch WS, Pitts WH. A logical calculus of the ideas immanent in nervous activity. *Bull. Math. Biophys.*, 5: 115-133, 1943.

[77] Meijer HGE, Eissa T, Kiewiet B, Neuman J, Schevon C, Emerson R, Goodman R, McKhann G Jr., Marcuccilli CJ, Tryba AK, Cowan J, van Gils S, van Drongelen W. Modeling Focal Epileptic Activity in the Wilson-Cowan Model with Depolarization Block. *J. Math. Neurosci.* 5(7), 2015. doi:10.1186/s13408-015-0019-4,.

[78] Millman D, Mihalas S, Kirkwood A, Niebur E. Self-organized criticality occurs in non-conservative neuronal networks during 'up' states. *Nature Phys.*, 6(10): 801-805, 2010.

[79] Muller L, Reynaud A, Chavane F, Destexhe A. The stimulus-evoked population response in visual cortex of awake monkey is a propagating wave. *Nat. Commun.*, 5: 3675, 2014.

[80] Munoz M, Dickman R, Vespignani A, Zapperi S. Avalanche and spreading exponents in systems with absorbing states. *Phys. Rev. E*, 59(5): 6175-6179, 1999.

[81] Murphy B, Miller K. Balanced amplification: a new mechanism of selective amplification of neural activity patterns. *Neuron*, 61(4): 635-648, 2009.

[82] Nauhaus I, Busse L, Carandini M, Ringach DL. Stimulus contrast modulates functional connectivity in visual cortex. *Nature Neurosci.*, 12(1): 70-76, 2009.

[83] Nauhaus I, Busse L, Ringach DL, Carandini MN. Robustness of traveling waves in ongoing activity in visual cortex. *J. Neurosci.*, 32(9): 3088-3094, 2012.

[84] Neuman J, Kiewiet B, Cowan JD, van Drongelen W. *Observations of dynamical behavior in a stochastic Wilson-Cowan population with plasticity*. Poster session presented at the Twenty Second Annual Computational Neuroscience Meeting, Paris, France. 2013.

[85] Neuman J, Cowan JD, van Drongelen W. *Damped traveling waves and localized responses in a Wilson-Cowan network*. Poster session presented at the Twenty Fourth Annual Computational Neuroscience Meeting, Prague, Czech Republic. 2015.

[86] Nevado-Holgado AJ, Marten F, Richardson MP, Terry JR. Characterising the dynamics of EEG waveforms as the path through parameter space of a neural mass model: application to epilepsy seizure evolution. *NeuroImage*, 59: 2374-2392, 2012.

[87] Nunez PL. *Neocortical Dynamics and Human EEG Rhythms*. Oxford University Press. Oxford. 1995.

[88] Ohira T, Cowan J. Stochastic neurodynamics and the system size expansion, in *Proceedings of the First International Conference on the Mathematics of Neural Networks*, ed. Ellacort S, Anderson I. Academic Press, p. 290-294, 1997.

[89] Ohkubo J. Duality in interacting particle systems and boson representation. *J. Stat. Phys.*, 139(3): 454-465, 2010.

[90] Peliti L. Path integral approach to birth-death processes on a lattice. *J. Physique*, 46: 1469-1483, 1985.

[91] Pinto D, Ermentrout GB. Spatially Structured Activity in Synaptically Coupled Neuronal Networks: I. Traveling Fronts and Pulses. *SIAM J. Appl. Math.*, 62(1): 206-255, 2001.

[92] Polking JC. *Ordinary Differential Equations Using MATLAB*. Prentice Hall. New York. 2004.

[93] Priesemann V, Wibral M, Valderama M, Pröpper R, Le Van Quyen M, Geisel T, Triesch J, Nikolić D, Munk MHJ. Spike avalanches *in vivo* suggest a driven, slightly subcritical brain state. *Front. Sys. Neurosci.*, 8: 1-17, 2014.

[94] Rowe DL., Robinson PA, Rennie CJ. Estimation of neurophysiological parameters from the waking EEG using a biophysical model of brain dynamics. *J. Theor. Biol.*, 231(3): 413-433, 2004.

[95] Rumsey C, Abbott L. Synaptic equalization by anti-STDP. *Neurocomputing*, 58-60: 359-364, 2004.

[96] Schevon CA, Weiss SA, McKhann G, Goodman RR,Yuste R, Emerson RG, Trevelyan AJ. Evidence of an inhibitory restraint of seizure activity in humans. *Nat. Commun.*, 3: 1060, 2012.

[97] Schrödinger E. Der stetige Übergang von der Mikro-zur Makromechanik. *Die Naturwissenschaften*, 14: 664-666, 1926.

[98] Schulz DPA, Carandini M. An uncorrelated state for the cortex? *F1000 Biol. Rep.*, 2: 43, 2010.

[99] Shimbel A, Rapoport A. A Statistical Approach to the Theory of the Central Nervous System. *Bull. Math. Biophys.*, 10: 41–55, 1948.

[100] Sholl DA. *The Organization of the Cerebral Cortex*. London, Methuen. 1956.

[101] Shusterman V, Troy WC. From baseline to epileptiform activity: a path to synchronized rhythmicity in large-scale neural networks. *Phys. Rev. E*, 77(6): 061911, 2008.

[102] Smith DR, Davidson CH. Maintained activity in neural nets. *J. ACM*, 9(2): 268-279, 1962.

[103] Softky WR, Koch C. The highly irregular firing of cortical cells is inconsistent with temporal integration of random EPSPs. *J. Neurosci.*, 13(1): 334-350, 1993.

[104] Staff NP, Jung HY, Thiagarajan T, Yao M, Spruston N. Resting and active properties of pyramidal neurons in subiculum and CA1 of rat hippocampus. *J. Neurophysiol.*, 84(5): 2398-2408, 2000.

[105] Stevens C. How cortical interconnectedness varies with network size. *Neural Comp.*, 1: 473-479, 1989.

[106] Tagliazucchi E, Balenzuela P, Fraiman D, Chialvo D. Criticality in large-scale brain fMRI dynamics unveiled by a novel point process analysis. *Front. Physiol.*, 3: 1-12, 2012.

[107] Takano H, and Coulter DA. Imaging of Hippocampal Circuits in Epilepsy, in *Jasper's Basic Mechanisms of the Epilepsies [Internet]*, ed. Noebels JL Avoli M, Rogawski MA, Olsen RW, Delgado-Escueta AV. National Center for Biotechnology Information. Bethesda. p. 1-13, 2012.

[108] Täuber UC. Population oscillations in spatial stochastic Lotka-Volterra models: a field-theoretic perturbational analysis. *J. Phys. A: Math. and Theo.*, 45(40): 405002, 2012.

[109] Täuber UC, Howard M, Vollmayer-Lee BP. Applications of field-theoretic renormalization group methods to reaction-diffusion problems. *J. Phys. A: Math. Gen.*, 38: R79-R131, 2005.

[110] Thurner S, Windischberger C, Moser E, Walla P, Barth M. Scaling laws and persistence in human brain activity. *Physica A*, 326(3-4): 511-521, 2003.

[111] Trevelyan AJ, Sussillo D, Watson BO, and Yuste R. Modular Propagation of Epileptiform Activity: Evidence for an Inhibitory Veto in Neocortex. *J. Neurosci.*, 26(48): 12447-12455, 2006.

[112] Tsodyks M, Sejnowski T. Rapid state switching in balanced cortical network models. *Network: Computation in Neural Systems*, 6(2): 111-124, 1995.

[113] Uttley AM. The probability of neural connections. *Proc. Roy. Soc. Lond. B*, 144(915): 229-240, 1955.

[114] van Drongelen W, Koch H, Elsen FP, Lee HC, Mrejeru A, Doren E, Marcuccilli CJ, Hereld M, Stevens RL, Ramirez JM. Role of persistent sodium current in bursting activity of mouse neocortical networks in vitro. *J. Neurophysiol.*, 96(5): 2564-2577, 2006.

[115] van Drongelen W, Lee HC, Hereld M, Chen Z, Elsen FP, Stevens RL. Emergent epileptiform activity in neural networks with weak excitatory synapses. *IEEE Trans. Neural Syst. Rehabil. Eng.*, 13(2): 236-241, 2005.

[116] van Kampen NG. *Stochastic Processes in Physics and Chemistry*. North Holland, Amsterdam. 1981.

[117] van Wijland F. Field theory for reaction-diffusion processes with hard-core particles. *Phys. Rev. E*, 63: 022101, 2001.

[118] Vogels TP, Sprekeler H, Zenke F, Clopath C, Gerstner W. Inhibitory Plasticity Balances Excitation and Inhibition in Sensory Pathways and Memory Networks. *Science*, 334(6062): 1569-1573, 2011.

[119] Wallace E. *Noise and Synchrony in Neural Networks*. PhD thesis, University of Chicago, 2010.

[120] Wallace E, Benayoun M, van Drongelen W, Cowan JD. Emergent Oscillations in Networks of Stochastic Spiking Neurons. *PLoS One*, 6(5): e14804, 2011.

[121] Wang J, Kádár S, Jung P, Showalter K. Noise Driven Avalanche Behavior in Subexcitable Media. *Phys. Rev. Lett.*, 82(4): 855-858, 1999.

[122] Wang Y, Goodfellow M, Taylor PN, Baier G. Dynamic Mechanisms of Neocortical Focal Seizure Onset. *PLoS Comput. Biol.*, 10(8): 1003787, 2014.

[123] Wei Y, Ullah G, Ingram J, Schiff SJ. Oxygen and seizure dynamics: II. Computational modeling. *J. Neurophysiol.*, 112(2): 213-223, 2014.

[124] Wendling F, Hernandez A, Bellanger J-J, Chauvel P, Bartolomei F. Interictal to Ictal Transition in Human Temporal Lobe Epilepsy: Insights From a Computational Model of Intracerebral EEG. *J. Clin. Neurophysiol.*, 22(5): 343-356, 2005.

[125] Wilson HR, Cowan JD. A mathematical theory of the functional dynamics of cortical and thalamic nervous tissue. *Kybernetik*, 13: 55-80, 1973.

[126] Wilson HR, Cowan JD. Excitatory and Inhibitory Interactions in Localized Populations of Model Neurons. *Biophys. J.*, 12(1): 1-24, 1972.

[127] Wilson K. Renormalization Group and Critical Phenomena. I. Renormalization Group and the Kadanoff Scaling Picture. *Phys. Rev. B*, 4(9): 3174-3183, 1974.

[128] Yi F, DeCan E, Stoll K, Marceau E, Deisseroth K, Lawrence JJ. Muscarinic excitation of parvalbumin-positive interneurons contributes to the severity of pilocarpine-induced seizures. *Epilepsia*, 56: 297-309, 2015.